PB-236 928

ODOR REMOVAL FROM AIR BY ADSORPTION ON CHARCOAL

B. G. Kyle, et al

Kansas State University

Prepared for:

National Environmental Research Center

September 1974

DISTRIBUTED BY:

NTIS

National Technical Information Service
U. S. DEPARTMENT OF COMMERCE
5285 Port Royal Road, Springfield Va. 22151

TECHNICAL REPORT DATA
(Please read Instructions on the reverse before completing

PB 236 928

1. REPORT NO. EPA-650/2-74-084	2.
3. RECIPIENT'S ACCESSION NO.	
4. TITLE AND SUBTITLE: Odor Removal from Air by Adsorption on Charcoal	5. REPORT DATE: September 1974
	6. PERFORMING ORGANIZATION CODE
7. AUTHOR(S): B. G. Kyle and N. D. Eckhoff	8. PERFORMING ORGANIZATION REPORT NO.
9. PERFORMING ORGANIZATION NAME AND ADDRESS: Kansas State University, Manhattan, Kansas 66502	10. PROGRAM ELEMENT NO.: 1AB015; ROAP 21AXM-061
	11. CONTRACT/GRANT NO.: EHSD 71-4
12. SPONSORING AGENCY NAME AND ADDRESS: EPA, Office of Research and Development, NERC-RTP, Control Systems Laboratory, Research Triangle Park, NC 27711	13. TYPE OF REPORT AND PERIOD COVERED: Final; Through 12/31/73
	14. SPONSORING AGENCY CODE
15. SUPPLEMENTARY NOTES	

16. ABSTRACT: The report gives results of an evaluation of the efficacy of charcoal for removing odorous organic vapors from extremely low concentrations in air, at ambient conditions. Two systems were studied in detail: acetaldehyde--Pittsburgh PCB charcoal, and ethylmercaptan--Pittsburgh BPL charcoal. Fixed-bed breakthrough data were taken for the acetaldehyde--Pittsburgh PCB charcoal system at an acetaldehyde concentration of 28 ppm. These data were analyzed using a modeling approach that indicated that the rate-controlling step was intraparticle diffusion. Preliminary design calculations based on this work indicate that fixed-bed adsorption with charcoal is a feasible process for the 98% removal of small concentrations of acetaldehyde from polluted air. An integral reactor approach using Pittsburgh BPL charcoal was used in the study of the catalytic oxidation of ethylmercaptan in the concentration range 20-125 ppm. Diethyldisulfide was identified as a reaction product and the reaction was found to be one-half order in ethylmercaptan concentration. Preliminary design calculations show that 99% removal of ethylmercaptan from air by catalytic oxidation on charcoal appears to be feasible.

17. KEY WORDS AND DOCUMENT ANALYSIS

a. DESCRIPTORS	b. IDENTIFIERS/OPEN ENDED TERMS	c. COSATI Field/Group
Air Pollution	Air Pollution Control	13B
Odor Control	Stationary Sources	
Adsorption	Catalytic Oxidation	
Charcoal	Organic Vapors	
Activated Carbon	Ethylmercaptan	11G
Acetaldehyde		07C
Thiols		

18. DISTRIBUTION STATEMENT: Unlimited	19. SECURITY CLASS (This Report): Unclassified	21. NO. OF PAGES: 109
	20. SECURITY CLASS (This page): Unclassified	22. PRICE: 5.25

EPA Form 2220-1 (9-73)

Reproduced by
NATIONAL TECHNICAL
INFORMATION SERVICE
U S Department of Commerce
Springfield VA 22151

EPA-650/2-74-084

ODOR REMOVAL FROM AIR BY ADSORPTION ON CHARCOAL

by

B. G. Kyle and N. D. Eckhoff

Kansas State University
Manhattan, Kansas 66502

Contract No. EHSD 71-4
ROAP No. 21AXM-061
Program Element No. 1AB015

EPA Project Officer: Belur N. Murthy

Control Systems Laboratory
National Environmental Research Center
Research Triangle Park, North Carolina 27711

Prepared for

OFFICE OF RESEARCH AND DEVELOPMENT
U.S. ENVIRONMENTAL PROTECTION AGENCY
WASHINGTON, D.C. 20460

September 1974

ia

This report has been reviewed by the Environmental Protection Agency and approved for publication. Approval does not signify that the contents necessarily reflect the views and policies of the Agency, nor does mention of trade names or commercial products constitute endorsement or recommendation for use.

TABLE OF CONTENTS

CONCLUSIONS 1

RECOMMENDATIONS 2

INTRODUCTION 3

Background, Purpose and Scope of Project 3

Description of Project Phases 4

Theory 6

EXPERIMENTAL PHASE 16

Differential-Bed Adsorption Studies Using Radioactive Tracers . . 16

Fixed-Bed Adsorption Studies 27

Fixed-Bed Catalytic Studies 35

DISCUSSION 38

Acetaldehyde Adsorption Study 38

Fixed-Bed Catalytic Study 63

APPLICATION TO DESIGN 77

Acetaldehyde Removal 77

Ethylmercaptan Removal 79

REFERENCES 82

NOMENCLATURE 83

APPENDIX 85

LIST OF FIGURES

Figure		Page
1.	Charcoal Adsorption System	17
2.	Charcoal Sample Holder	18
3.	1st Test with Ar 41	20
4.	1st Test with Ar 41	21
5.	2nd Test with Ar 41	22
6.	2nd Test with Ar 41	23
7.	Test with Ethylmercaptan	25
8.	Ethylmercaptan Presaturation Test	28
9.	Ethylmercaptan Presaturation Test	29
10.	Experimental Adsorption System	31
11.	Diffusion Tube	32
12.	Gas Mixer	34
13.	Static Equilibrium Data for Acetaldehyde on Pittsburgh PCB Charcoal at 30°C	41
14.	Equilibrium Data for Acetaldehyde on Pittsburgh PCB Charcoal in Linear Form	42
15.	Test of the Freundlich Isotherm Equation	43
16.	Pressure Drop Through Beds of Charcoal	46
17.	Relation Between Mean Residence Time and Effective Distribution Ratio for Particle-Phase Diffusion Model	53
18.	Relation Between Mean Residence Time and Effective Distribution Ratio for Pore Diffusion Model	54
19.	Relation Between Mean Residence Time and Effective Distribution Ratio for External Diffusion Model	55
20.	Relation Between Mean Residence Time and Effective Distribution Ratio for Reaction Kinetics Model	56

LIST OF FIGURES (Continued)

Figure		Page
21.	Number of Mass Transfer Units versus Residence Time for Particle-Phase Diffusion Model	57
22.	Number of Mass Transfer Units versus Residence Time for Pore Diffusion Model	58
23.	Number of Mass Transfer Units versus Residence Time for External Diffusion Model	59
24.	Number of Mass Transfer Units versus Residence Time for Reaction Kinetics Model	60
25.	Comparison of Particle-Phase Modeling Break Times with Experimental Values	62
26.	Comparison of Pore Diffusion Modeling Break Time with Experimental Values	67
27.	Comparison of External Diffusion Modeling Break Times with Experimental Values	68
28.	Comparison of Reaction Kinetics Model Break Time Data with Experimental Values	69
29.	A Plot of Conversion versus W/F	71
30.	Typical Effluent History Curve	73
31.	Test of 0.5 Order Reaction	74
A-1.	Fixed-Bed Test APC-14	86
A-2.	Fixed-Bed Test APC-18	87
A-3.	Fixed-Bed Test APC-19	88
A-4.	Fixed-Bed Test APC-20	89
A-5.	Fixed-Bed Test APC-21	90
A-6.	Fixed-Bed Test APC-22	91
A-7.	Fixed-Bed Test APC-26	92
A-8.	Fixed-Bed Test APC-29	93

LIST OF FIGURES (Continued)

Figure		Page
A-9.	Fixed-Bed Test APC-30	94
A-10.	Fixed-Bed Test APC-31	95
A-11.	Fixed-Bed Test APC-32	96
A-12.	Fixed-Bed Test APC-38	97
A-13.	Fixed-Bed Test APC-39	98
A-14.	Gas Chromatograph Calibration Curve for Ethylmercaptan	99
A-15.	Chromatographic Calibration Curve for Acetaldehyde	100

LIST OF TABLES

Table		Page
1.	Results of Fixed-Bed Tests with Acetaldehyde Adsorbed on Pittsburgh PCB Charcoal	39
2.	Results of Static Equilibrium Tests with Acetaldehyde and Pittsburgh PCB Charcoal at 30°C	40
3.	Parameters Obtained from Model Equation for Particle-Phase Diffusion Model	49
4.	Parameters Obtained from Model Equation for Pore Diffusion Model	50
5.	Parameters Obtained from External Diffusion Model Equation	51
6.	Parameters Obtained from Reaction Kinetics Model Equation	52
7.	Comparison of Calculated N_{pore} Values with Modeling Values	64
8.	Results of Calculated N_f Values Compared with the Modeling N_f	65
9.	Results of Fixed-Bed Tests with Ethylmercaptan and Pittsburgh BPL Charcoal	66
10.	Elements Present in Charcoal Samples as Determined by Neutron Activation Analysis	76
11.	Amount of Charcoal Required to Remove Various Percentages of Ethylmercaptan from Various Concentrations in Air at 30°C	80

CONCLUSIONS

ACETALDEHYDE REMOVAL

1. Preliminary design calculations show that fixed-bed adsorption appears to be a feasible process for removing up to 98% of acetaldehyde from air in the 10 to 35 PPM concentration range.
2. Equilibrium data for the adsorption of acetaldehyde vapor onto Pittsburgh PCB charcoal at 30°C can be represented by the Langmuir Isotherm Equation over the range 1 to 35 PPM of acetaldehyde in air.
3. Fixed-bed breakthrough data for the acetaldehyde vapor - Pittsburgh PCB charcoal system can be represented with constant - pattern, internal-diffusion models. The parameters in these models behave realistically. The rate of adsorption appears to be controlled by intraparticle diffusion.

ETHYLMERCAPTAN REMOVAL

1. Preliminary design calculations show that 99% removal of ethylmercaptan from air in the 20 to 125 PPM concentration range by catalytic oxidation on charcoal appears to be a feasible process.
2. Diethyldisulfide has been identified as a product of the catalytic oxidation of ethylmercaptan with air during adsorption on Pittsburgh BPL charcoal.
3. The catalytic reaction was found to be one-half order in ethylmercaptan concentration.

RECOMMENDATIONS

ABSORPTION

1. It is recommended that the study involving adsorption of Acetaldehyde on Pittsburg PCB charcoal be expanded to include concentrations of Acetaldehyde as high as 10 mole percent. The aim of such a study would be to determine whether the rate-controlling processes are the same for all concentration levels or change as extremely low levels are reached. If the former condition is obtained, it might be possible to extrapolate the information available in the literature, the bulk of which applies to much higher concentration levels.
2. It is recommended that the adsorption equilibrium and kinetic behavior of other members of the aldehyde family be studied. Such a study could lead to systematic parameter correlations which would allow the adsorption behavior of any member of a family of compounds to be predicted from the parameters of a few members.
3. In order to provide all of the information needed for design of adsorption systems the regeneration behavior of charcoal, especially at low levels of adsorbate loading, should be studied.

MERCAPTAN CATALYTIC OXIDATION

It is recommended that the study begun here be expanded to include other members of the mercaptan family and other types of charcoal. The effect of temperature and the long term stability of the catalyst should also be investigated. Identification of the reaction products should also be a major part of this study.

INTRODUCTION

BACKGROUND, PURPOSE, AND SCOPE OF THE PROJECT

Background

The Division of Process Control Engineering (now Control Systems Laboratory) started the odor control project in 1968. A survey of the existing control technology for odors revealed the urgent need for the development of suitable adsorption systems as one of the control devices. The present plans for odor control research call for detailed investigations of odor adsorption mechanisms using known odorants and activated charcoal and/or other suitable adsorbents. This contract is to develop useful information on the design data needed for the construction of efficient odor control adsorption units.

Purpose

The contract is expected to accomplish the following: (a) development of suitable experimental techniques so that reliable adsorption equilibrium and kinetic data may be obtained, (b) provide data for several homologous series of adsorbates, (c) from data gathered and analyzed, acquire an understanding of the thermodynamics and kinetics of adsorption at low adsorbate concentrations. The data and conclusions resulting from these studies will be used in the scale-up and development of package adsorption devices for industrial odor control.

Scope

The scope of the original contract consisted of the following: (a) Conduct a literature survey on the existing data on adsorption equilibrium and kinetics relating to odors and activated charcoal, (b) Standardize suitable analytical techniques like application of radioactive tracers and ionization detectors for the system selected for study, (c) Derive mathematical expressions relating adsorption efficiencies and operating process variables from adsorption equilibrium and kinetic data collected in the laboratory, and (d) Conclusions should include design data for scale-up, as well as recommendations for further R & D in the field of Adsorption Mechanisms.

Upon extension of the contract the following items were added to the scope of the project: (a) Modify the analytical equipment to increase the capability for analyzing all the components of the reaction mixture involved in the adsorption/desorption of mercaptans on activated charcoal, (b) Construct a differential or integral reactor and adsorption system suitable for determining the reaction mechanisms and scale-up parameters, (c) Expand the literature survey effort to include the related studies of catalysis and regeneration of adsorbents, (d) Conduct fixed bed studies with more than one type of activated charcoal to test the catalytic ability of other types of charcoal than the one being presently studied under the existing contract, (e) Identify and analyze all the reaction products involved in the absorption/desorption of mercaptans on activated charcoal, and (f) Study the reaction mechanism using the differential or integral reactor constructed and develop suitable design equations from the data, for the construction of reliable and low cost regenerable adsorption control devices for odor control.

DESCRIPTION OF PROJECT PHASES

Differential-Bed Adsorption Studies Using Radioactive Tracers

The intent of this study was to follow the adsorption kinetics using an experimental method which consisted essentially of recirculating a gas containing radioactivity-tagged adsorbate through a shallow bed of adsorbent while continuously monitoring the gas-phase concentration of the adsorbate with a radiation detector. A material balance would allow the adsorbent loading to be calculated for any adsorbate concentration, thus permitting the determination of instantaneous values of gas-phase adsorbate concentration and corresponding values of adsorbent loading. The instantaneous rate of adsorption could then be determined from the time dependence of the adsorbent loading. This then would provide the rate as a function of gas-phase adsorbate concentration and is the major advantage to the differential bed method. Unfortunately, this experimental technique could not be successfully implemented because of adsorption of the radioactive component on the radiation detector. An integral or fixed-bed approach was then adopted.

Fixed-Bed Adsorption Studies

This experimental technique involves passing a gas stream containing a known and constant concentration of adsorbate through a bed packed with

adsorbent. Initially, the adsorbent is fresh and practically all of the adsorbate is adsorbed so that the effluent stream from the bed contains very little adsorbate. With the passage of more fluid the adsorbent in the bed begins to saturate thus causing the concentration of adsorbate in the effluent stream to rise. A plot of effluent adsorbate concentration versus time, or volume of fluid processed, is called a breakthrough curve. The shape and position of the breakthrough curve are dependent on the adsorption kinetics, however, because of the complexity of the fixed-bed process, it is necessary to employ a modeling approach which only allows the kinetic behavior to be determined indirectly.

The technique of modeling as applied to fixed-bed operations seeks to simplify the mathematical description of these highly complex systems by approximating the actual flow patterns with idealized representations and by specifying a rate-controlling step for the transport of mass between the fluid and solid phase. A solution of these simplified descriptive equations, referred to here as the model equation, takes the form of an expression relating concentration to time and position within the bed. The results predicted by the model equation are then compared with experiment and the validity of the model is judged by its ability to fit the experimental breakthrough data. The nature of the flow patterns and the rate-controlling mass transport mechanism are thus deduced by determining which of several models best fits the experimental results. Each model will contain one or two parameters which can be evaluated by fitting the model equation to the experimental data. A further test of the model is whether these parameters are physically realistic; with a realistic model it is possible to correlate these model parameters with the system variables so that behavior of similar systems can be predicted.

Fixed-Bed Catalytic Studies

The experimental apparatus and technique for the study of solid-fluid catalytic reactions in fixed-beds are similar to those for fixed-bed adsorption studies, but these studies have the advantage that because the catalytic fixed-bed system operates at steady state the data are easier to analyze. An influent stream containing a known and constant concentration of reactant is passed at a constant flow rate through a packed bed of catalyst particles. The effluent stream from this bed is monitored and when steady state is attained the concentrations of reactants and products are determined. Thus

for a single run the conversion is determined for a given ratio of catalyst weight to influent flow rate. A differential material balance relationship allows the reaction rate to be determined from the slope of a curve obtained from plotting conversion versus this ratio. It is therefore required that enough runs be made so that this curve can be established. Alternately, one may assume a rate expression, integrate the differential material balance relationship with this rate expression, and obtain an algebraic equation relating conversion to the catalyst to feed ratio. This corresponds to the modeling approach described earlier as each rate expression yields a different integrated rate equation. As before, the validity of a rate expression is determined by how well its corresponding integrated rate equation fits the conversion versus catalyst to feed ratio data.

THEORY

Fixed-Bed Adsorption

The development of model breakthrough equations presented here closely follows that of Vermeulen (1) and begins with a material balance applied over an infinitesimally small time increment to an infinitesimally thin cross sectional slice of the bed containing dv volume of adsorbate. As the fluid moves through this slice of adsorbent bed the concentration of adsorbate in the fluid decreases an infinitesimally small quantity dC and the adsorbent loading in the slice increases by dq. Therefore, from the principle of conservation of mass it follows that

$$\begin{pmatrix}\text{Amount of adsorbate}\\ \text{entering the slice}\end{pmatrix} = \begin{pmatrix}\text{Amount of adsorbate}\\ \text{picked up by adsorbent}\end{pmatrix} + \begin{pmatrix}\text{Amount of adsorbate}\\ \text{leaving the slice}\end{pmatrix} + \begin{pmatrix}\text{Accumulation of adsorbate}\\ \text{within the void spaces}\end{pmatrix}$$

Written in mathematical language the material balance equation is

$$-\left(\frac{\partial C}{\partial v}\right)_V = \rho_b\left(\frac{\partial q}{\partial V}\right)_v + \varepsilon\left(\frac{\partial C}{\partial V}\right)_v \qquad (1)$$

Because C is a function of v and V, it can also be expressed as a function of v and V - vε. This change of variable produces the following simplified equation

$$-\left(\frac{\partial C}{\partial v}\right)_{V-v\varepsilon} = \rho_b\left(\frac{\partial q}{\partial V}\right)_v \qquad (2)$$

By introducing the following dimensionless concentration variables

$$X = C/C_o \tag{3}$$

$$Y = q/q_o^* \tag{4}$$

and a dimensionless through-put parameter

$$Z = \frac{C_o(V - v\varepsilon)}{q_o^* \rho_b v} = \frac{V - v\varepsilon}{v\varepsilon D} \tag{5}$$

equation 2 can be written

$$-\left(\frac{\partial X}{\partial v}\right)_{Zv} = \left(\frac{\partial Y}{\partial Zv}\right)_v \tag{6}$$

This is the material balance partial differential equation for a fixed-bed and is the starting point for most model breakthrough equations.

It is an experimental fact that for many systems the breakthrough curves retain a constant shape regardless of bed length. This is because of a constant rate of movement of all parts of the exchange zone. This can be stated mathematically as

$$\left(\frac{\partial t}{\partial v}\right)_x = \text{constant} \tag{7}$$

or in terms of the through-put parameter

$$\left(\frac{\partial\ Zv}{\partial v}\right)_x = \text{constant} \tag{8}$$

The right hand side of the material balance equation can be restated so that equation 6 can be written as follows

$$-\left(\frac{\partial X}{\partial v}\right)_{Zv} = \left(\frac{\partial X}{\partial\ Zv}\right)_v \left(\frac{\partial Y}{\partial X}\right)_v \tag{9}$$

rearrangement of equation 9 gives

$$\left(\frac{\partial Y}{\partial X}\right)_v = -\frac{(\partial X/\partial v)_{Zv}}{(\partial X/\partial Zv)_v} = \left(\frac{\partial\ Zv}{\partial v}\right)_x = \text{constant} \tag{10}$$

Equation 10 integrates to

$$Y = (\text{constant})X + C_1 \tag{11}$$

where C_1 is the constant of integration. Because X and Y are dimensionless variables and have the same limits equation 11 simplifies to

$$Y = X \tag{12}$$

which also leads to

$$dY = dX \tag{13}$$

Thus for the constant pattern case the material balance relationship results in the simple statements of equations 12 and 13. We will now develop breakthrough equations for the constant pattern case where different rate-controlling mechanisms obtain.

Fluid-phase Diffusion Model - For this model we assume that the slowest, and therefore rate-controlling, step involves the migration of adsorbate molecules from the bulk of the fluid phase to the surface of the adsorbent particle. Customarily, the rate in such situations is expressed in terms of a mass transfer coefficient and a characteristic concentration difference

$$\frac{dY}{dt} = \frac{k_f a}{\varepsilon D} (X - X^*) \tag{14}$$

The X* term is the fluid-phase concentration which would obtain if equilibrium existed at the solid-fluid interface. In order to obtain this term something must be said about the equilibrium relationship. For a great many systems it has been found that this can be accomplished in the following manner

$$Y^* = \frac{X}{R + (1-R)X} \tag{15}$$

or

$$X^* = \frac{RY}{1 + (R-1)Y} \tag{16}$$

where R is called the separation factor and is usually assumed to be constant over the full range of X and Y. If this equilibrium relationship is used along with the constant pattern conditions expressed by equations 12 and 13 it is possible after some simplification to write equation 14 as

$$\frac{dX}{dt} = \frac{k_f a}{\varepsilon D} \frac{X(X-1)(R-1)}{1 + (R-1)X} \tag{17}$$

It is more convenient to replace the time variable with the through-put parameter Z where the two are related by the following

$$Z = \frac{tF}{\varepsilon Dv} \tag{18}$$

This substitution results in

$$\frac{dX}{dZ} = N_f \frac{X(X-1)(R-1)}{1 + (R-1)X} \tag{19}$$

where N_f is the number of fluid-phase transfer units defined as

$$N_f = \frac{k_f a v}{F} \tag{20}$$

In equation 19 variables are separable and integration yields

$$\left(\frac{1}{1-R}\right)\ell n\ X - \left(\frac{R}{1-R}\right)\ell n\ (1-X) = N_f(Z-1) + \alpha_f \qquad (21)$$

where α_f is the sum of constant terms including the integration constant and can be evaluated by making a material balance for the entire column at saturation

$$\int_{Z=0}^{X=1} (1-X)dZ = 1 \qquad (22)$$

Equation 21 is the breakthrough equation for the constant-pattern, fluid-phase diffusion model; it relates the dimensionless effluent concentration, X, to the through-put parameter, Z, in terms of an equilibrium parameter, R, and a rate parameter N_f.

Solid-phase Diffusion Model - Diffusion arising from a concentration gradient within the individual adsorbent particles after the adsorbate arrives at the solid-fluid interface is called solid-phase diffusion. This includes diffusion through a homogeneous, permeable, non-porous solid, and diffusion in a mobile, adsorbed phase covering the pore surface of a porous solid whose crystalline portion is impermeable. This is assumed to be the rate-controlling step and by analogy with the more thoroughly studied phenomenon of fluid-phase diffusion the rate is expressed as

$$\frac{dY}{dt} = \frac{k_p a}{\varepsilon D}(Y^* - Y) \qquad (23)$$

where Y is the average adsorbed-phase concentration and Y* is the value of the average adsorbed-phase concentration which would obtain if equilibrium were established between the particle and the fluid. The solid-phase mass transfer coefficient is related to particle diameter and particle diffusivity in the following manner

$$k_p a = \frac{60\ D_p\ \varepsilon D}{d_p^2} \qquad (24)$$

There is little theoretical justification for equations 23 and 24; however, they are more tractable mathematically than the more rigorous expressions for solid-phase diffusion. They have been widely used with reasonable success.

Starting with equation 23, if one employs a derivation which closely follows that outlined for the fluid-phase diffusion model the breakthrough curve is

$$\left(\frac{R}{1-R}\right) \ln X - \left(\frac{1}{1-R}\right) \ln (1-X) = N_p(Z-1) + \alpha_p \qquad (25)$$

where N_p is the number of particle-phase transfer units defined as

$$N_p = \frac{k_p a v}{F} \qquad (26)$$

and α_p is a constant which can be evaluated from the separation factor, R.

Reaction Kinetics Model - Langmuir derived his famous isotherm equation by saying that the net rate of adsorption is equal to the rate at which molecules from the gas phase are adsorbed on the surface minus the rate at which molecules leave the surface.

$$\frac{dq}{dt} = k[p(q_m - q) - q/b] \qquad (27)$$

Here the adsorption rate is assumed proportional to the partial pressure of the gas and the amount of surface unoccupied by adsorbed molecules and the desorption rate is assumed proportional to the number of adsorbed molecules. At equilibrium the net rate is zero and equation 27 reduces to the familar Langmuir isotherm equation. The form of the Langmuir isotherm equation is such that it corresponds to equation 15 with the separation factor R constant with a value between zero and unity. Therefore, in terms of dimensionless concentrations equation 27 can be written

$$\frac{dY}{dt} = \left(\frac{k\ P_o}{1-R}\right) [X(1-Y) - RY(1-X)] \qquad (28)$$

We have also seen that the rate can be expressed in terms of fluid and solid phase resistances. Thus since the rate through each resistance is equal we can write from equations 14 and 23

$$\frac{dY}{dt} = \frac{k_f a}{\varepsilon D} (X - X^*) = \frac{k_p a}{\varepsilon D} (Y^* - Y) \qquad (29)$$

As before, the X* and Y* terms can be eliminated by using the separation factor. If this is followed by summing the numerators and denominators one obtains

$$\frac{dY}{dt} = \frac{\dfrac{X}{R + (1-R)X} - Y + X - \dfrac{RY}{1 + (R-1)Y}}{D\varepsilon\left(\dfrac{1}{k_p a} + \dfrac{1}{k_f a}\right)} \qquad (30)$$

When equations 28 and 30 are equated and the resulting equation simplified the familar reciprocal form for resistances in series results, but modified by a correction term β

$$\frac{\beta}{k} = \frac{1}{k_p a} + \frac{1}{k_f a} \qquad (31)$$

The correction term β is a function of X, Y, and R but has been evaluated and found to depend mainly on R (1). Therefore, for a given adsorption system the correction factor may be regarded as constant.

Except in rare cases, adsorption at the solid surface is usually found to be extremely rapid and the resistance due to this step will generally be negligible. However, this mechanism finds wide useage because with the correction term β the rate expression is equivalent to that written for combined particle-phase and fluid-phase resistances.

The development of the breakthrough equation for the reaction kinetics model begins with equation 28 and follows the same general procedure used for the two previously developed models. The result is

$$\left(\frac{1}{1-R}\right) \ell n \left(\frac{X}{1-X}\right) = N_R(Z-1) \qquad (32)$$

where N_R is the number of reaction units defined as

$$N_R = \frac{k\, p_o\, D\, v\epsilon}{F(1-R)} \qquad (33)$$

Pore Diffusion Model - Pore diffusion refers to the diffusion occurring within the fluid-filled pores of the solid; the driving force for this process is the concentration gradient existing in the fluid within the pores. If the fluid-phase concentration in the pores is assumed negligible compared to the solid-phase value, the equation of continuity can be written

$$\frac{D_{pore}}{r^2} \frac{\partial}{\partial r} \left(r^2 \frac{\partial C}{\partial r}\right) = \rho_b \frac{\partial q}{\partial t} \qquad (34)$$

In equation 34 the terms c and q represent point values of the fluid and solid-phase concentrations respectively. The average solid-phase concentration is

$$\bar{q} = \frac{3}{r_p^3} \int_0^{r_p} q r^2 \, dr \qquad (35)$$

Differentiation of equation 35 gives

$$\frac{\partial}{\partial r}\left(\frac{d\bar{q}}{dt}\right) = \frac{3r^2}{r_p^3}\left(\frac{\partial q}{\partial t}\right) \tag{36}$$

Combination of equation 36 with the continuity equation yields

$$\frac{d\bar{q}}{dt} = \frac{3\, D_{pore}\, r^2}{\rho_b r_p^3}\frac{\partial C}{\partial r} \tag{37}$$

The pore diffusion model has been worked out only for the case of irreversible adsorption (R = 0). This allows the assumption that the concentration wave penetrating the particle will saturate each spherical layer before it penetrates further. That is, C cannot exceed zero at a particular radius $r = r_i$ until q at that r has become equal to the saturation value q_m. Thus $q = q_m$ for $r_i < r < r_p$ and $q = 0$ for $r < r_i$. This simplifies equation 35 to

$$\frac{\bar{q}}{q_m} = Y = 1 - \left(\frac{r_i}{r_p}\right)^3 \tag{38}$$

From equation 38 we obtain

$$\frac{d\bar{q}}{dt} = -\frac{3\, q_m\, r_i^2}{r_p^3}\frac{dr_i}{dt} \tag{39}$$

substitution of this expression into equation 37 results in

$$\frac{dr_i}{dt} = -\left(\frac{D_{pore}}{q_m\, \rho_b\, r_i^2}\right) r^2 \frac{\partial C}{\partial r} \tag{40}$$

The term $r^2 \frac{\partial C}{\partial r}$ can now be evaluated from the original equation of continuity. If equation 34 is applied in the region $r_i < r < r_p$ where, according to the model, $\frac{\partial q}{\partial t} = 0$ we obtain

$$r^2 \frac{\partial C}{\partial r} = \text{constant} = C_1 \tag{41}$$

Equation 41 can be integrated subject to the following boundary conditions

$$C = C_f = C_o X \quad \text{at} \quad r = r_p \tag{42}$$

$$C = 0 \quad \text{at} \quad r = r_i \tag{43}$$

where C_f is the concentration in the fluid surrounding the particle. The $r^2 \frac{\partial C}{\partial r}$ term can now be written

$$r^2 \frac{\partial C}{\partial r} = \frac{C_o X r_i r_p}{r_p - r_i} \tag{44}$$

When equation 44 is substituted into equation 40 the resulting equation of continuity becomes

$$\frac{dr_i}{dt} = - \frac{C_o D_{pore} r_p}{q_m \rho_b} \frac{X}{r_i (r_p - r_i)} \tag{45}$$

Because X is the dimensionless concentration in the fluid surrounding the particle, the constant pattern condition can be applied and X replaced by Y as given by equation 38. On simplification, equation 45 can be expressed in terms of r_i and t

$$\frac{dr_i}{dt} = - \left(\frac{k_{pore}a}{15}\right)\left(\frac{r_p^2 + r_p r_i + r_i^2}{r_i}\right) \tag{46}$$

where

$$k_{pore}a = \frac{60 D_{pore} C_o}{\rho_b q_m d_p^2} \tag{47}$$

Integration of equation 46 gives r_i as a function of time. This can be followed by numerical evaluation of Y via equation 38, and application of the constant pattern condition (equation 12) yields X as a function of t or Z. The result fits the empirical relation

$$X = 0.557[N_{pore}(Z-1) + 1.15] - 0.0774[N_{pore}(Z-1) + 1.15]^2 \tag{48}$$

where

$$N_{pore} = \frac{k_{pore}a\, v}{F} \tag{49}$$

The four model breakthrough equations developed here (equations 21, 25, 32, and 48) are the ones applied to the experimental breakthrough data obtained for this project. There are many other models found in the literature which could be used, but these four cover the complete range of mechanisms and are widely used. Their popularity undoubtedly stems from their relative simplicity and the fact that the behavior of the two parameters is easily predicted qualitatively, if not quantitatively. These considerations are of paramount importance when design is the ultimate objective.

Fixed-Bed Catalysis

Because a fixed-bed catalytic reactor operates under steady state conditions the material balance equation is an ordinary differential equation rather than the partial differential equation as required for fixed-bed adsorption. If we focus our attention on a very thin cross-sectional slice of the catalyst bed which contains dW mass of catalyst a material balance for the reactant is

$$F_{Ao}dx_A = VC_{Ao}dx_A = r\ dW \tag{50}$$

The reaction rate based on a unit mass of catalyst, r, is expected to be a function of temperature and the various reactant and product concentrations, however here we will restrict our attention to isothermal operation.

There are two ways in which equation 50 can be applied to the analysis of data from a fixed-bed catalytic reactor.

Equation 50 can be applied in differential form. Rearrangement gives

$$\frac{dx_A}{d(W/F)} = \frac{C_{Ao}\ dx_A}{d(W/V)} = r \tag{51}$$

Thus, it is seen that the rate can be obtained from the slope of a curve of x_A versus W/F or W/V. The customary practice is to operate the reactor under various conditions and make a plot of x_A vs W/F or W/V for a constant C_{Ao}; the slope of this curve gives the rate at that particular conversion or reactant concentration. The concentration dependence of the rate is then determined by examining these data.

The alternate approach is to substitute various rate equations into equation 50 and integrate to obtain an expression involving x_A and W/F or W/V. Various curve fitting procedures are then used to test this integrated equation against the experimental data. The test of these integrated equations lies in how well they are able to fit the data. As an example of this approach, consider a 1/2 order and irreversible mechanism. The rate is

$$r = kC_{Ao}(1-x_A)^{1/2} \tag{52}$$

When this expression is substituted into equation 50 and integration is performed with the boundary condition that $x_A = 0$ when $W/F = 0$ the following integrated rate equation results

$$W/V = \frac{2C_{Ao}^{1/2}}{k} [1 - (1-x_A)^{1/2}] \qquad (53)$$

Thus, this proposed mechanism could be tested by plotting $[1 - (1-x_A)^{1/2}]$ versus W/V. If a straight line passing through the origin is obtained, the mechanism is said to be valid.

EXPERIMENTAL PHASE

DIFFERENTIAL-BED ADSORPTION STUDIES USING RADIOACTIVE TRACERS

Experimental Apparatus

The volumetric adsorption apparatus used radioactive tracers for measurement of the extremely low concentration of the adsorbate in the gas phase. A gas mixture consisting of air and the tagged adsorbate was circulated through a shallow bed of charcoal while the gas phase was continuously monitored with a radiation detector. The detector output allowed the instantaneous partial pressure of the adsorbate to be determined. If the assumption of perfect gas mixture behavior is made, a material balance allows the instantaneous asorbent loading to be calculated

$$q = \frac{V_s(p_o - p)}{ART} \qquad (54)$$

The instantaneous values of p and q allow a study of the adsorption kinetics to be made. When a constant value of adsorbate partial pressure is attained the equilibrium values of p and q can be determined from equation 54.

A schematic diagram of the proposed adsorption system is shown on Figure 1 and a drawing of the charcoal sample holder is shown in Figure 2. Gas flow could be routed through the charcoal sample holder or bypassed by proper positioning of the 4-way stopcock. The charcoal sample holder, cold trap, and coil were fabricated from pyrex glass. These pieces were connected by Teflon tubing with the exception of the piping adjacent to the diaphram circulating pump which consisted of copper tubing with brass valves and fittings. The volume of the system, V_s, could be varied depending on the diameter and length of pyrex tubing in the coil. A differential pressure transducer in conjunction with a pressure gauge was used to measure the pressure in the system to within ± 0.2 mm Hg. The pressure transducer was also used to monitor the flow of gas through the radiation detector by measuring the pressure drop. The entire apparatus, with the exception of the radiation detector and the pressure gauge was contained within a thermostated air bath. The radiation detector was a Packard TRI-CARB Scintillation Spectrometer initially equiped with a flow cell fabricated from plexiglass and packed with anthracene crystal scintillators.

CHARCOAL ADSORPTION SYSTEM

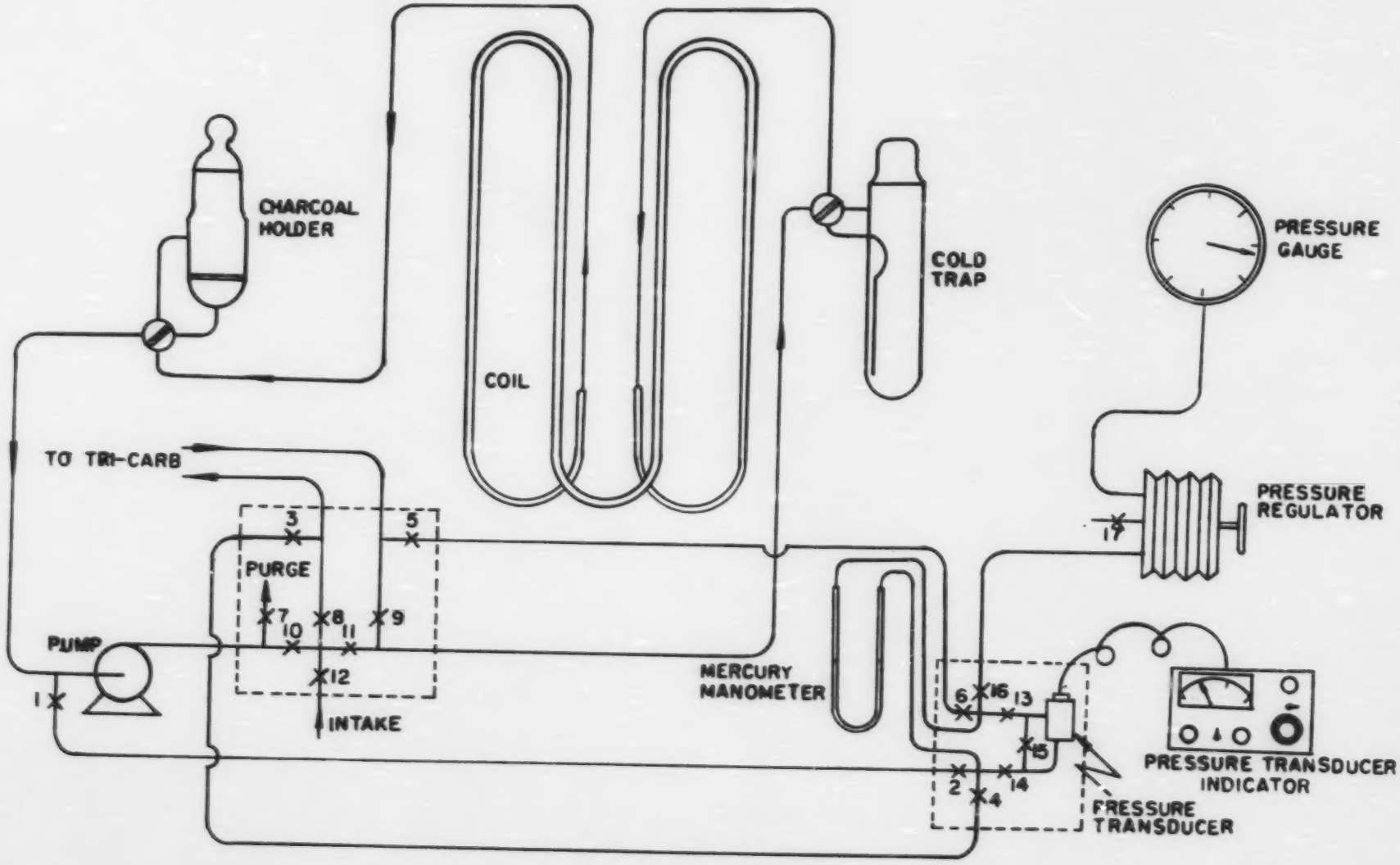

FIGURE 1

Fig. 2. Charcoal Sample Holder

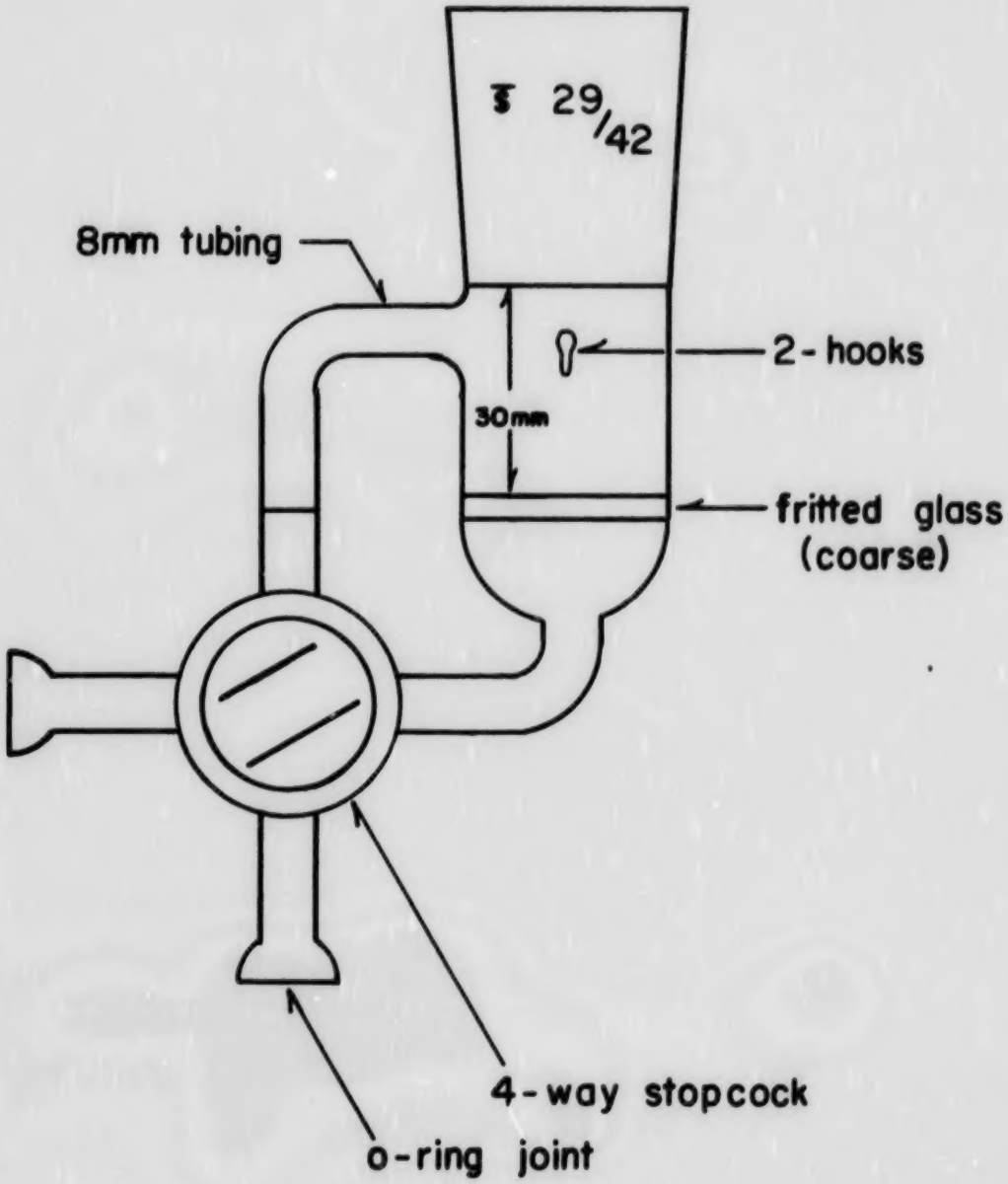

The following operating procedure was followed:

1. Using an analytical balance the desired quantity of charcoal (about 10 to 20 grams) was weighed into the charcoal sample holder.

2. With the charcoal sample holder stopcock in the bypass position the air pressure in the system was reduced to $[760-p_o]$ mm Hg. The air was then circulated through the cold trap containing charcoal at a lower temperature so that any adsorbable components were removed.

3. With the cold trap out of the system the gaseous adsorbate was admitted to the system through the intake valve until the pressure in the system reached 760 mm Hg. Pressure readings before and after introduction of the adsorbate were made. (p_o was in the range of 20 to 80 mm Hg.)

4. The gas mixture was then circulated through the system until a reliable initial reading was obtained from the radiation detector.

5. At time zero the charcoal sample holder was connected into the system and the output of the radiation detector continuously monitored.

6. After equilibrium had been attained the charcoal could be discarded or steps 2 through 5 could be repeated in order to obtain data at higher adsorbent loadings.

Argon 41 Tests

To test the feasibility of using the Packard TRI-CARB spectrometer system and to learn the mixing characteristics of the experimental adsorption apparatus, two tests with the radioactive isotope Argon 41 were performed under different operating conditions.

The results of the two tests are shown in Figures 3, 4, 5, and 6. Figures 3 and 5 show the TRI-CARB reading in counts per minute (CPM) versus time. The maximum of these curves indicated the time required for complete mixing and the discontinuity following the maximum represents the inclusion of the charcoal holder into the system. Figures 4 and 6 are semilog plots of CPM vs time. From the slope of these straight lines the half life can be computed. These values of 1.80 hr and 1.95 hr are in excellent agreement with the accepted value of 1.83 hr.

There appeared to be almost no mixing effect when the charcoal holder was switched into the system. The volumes of the system with and without the charcoal holder were 970cc and 929cc respectively and on switching the

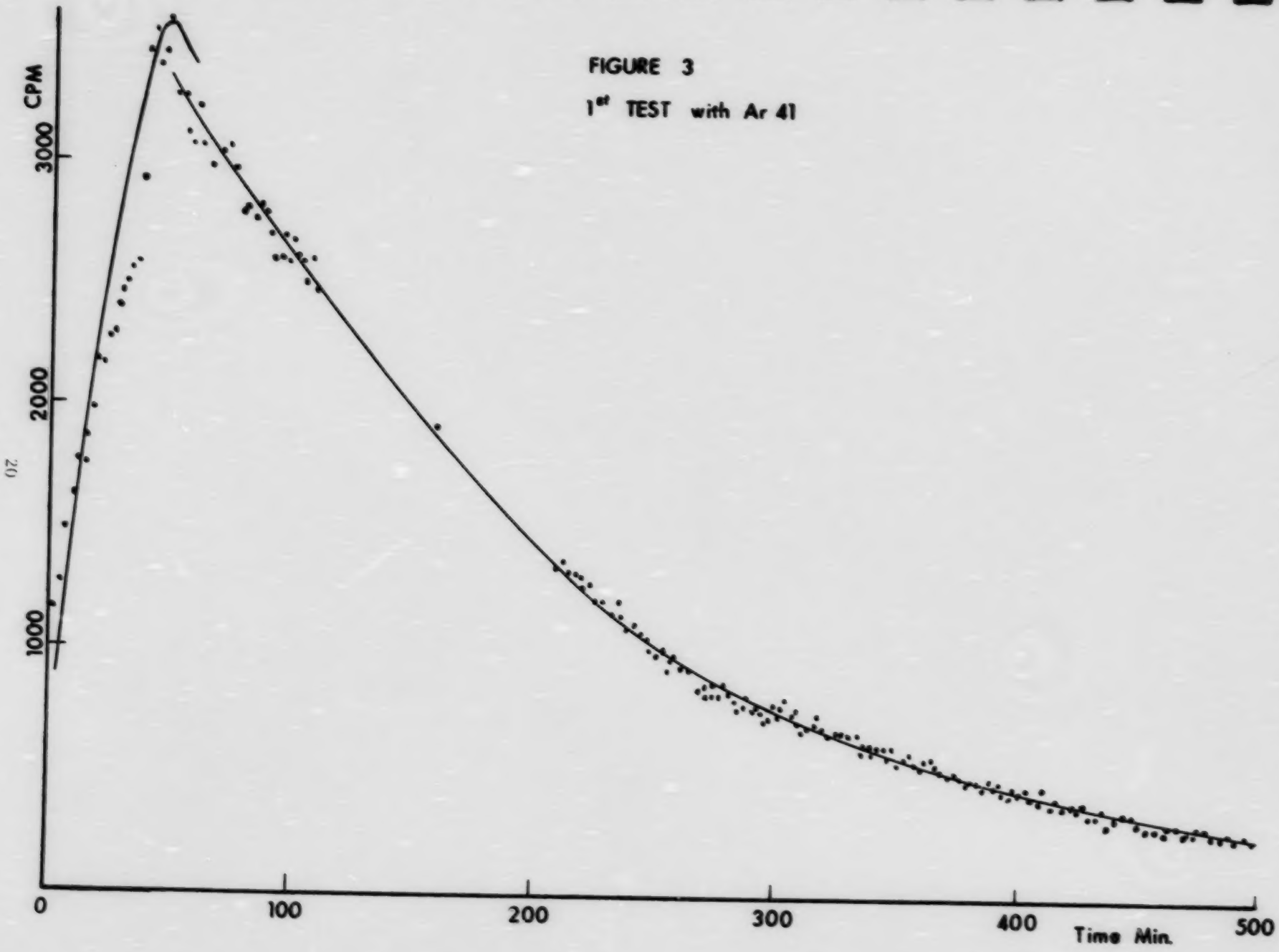

FIGURE 3

1st TEST with Ar 41

FIGURE 4

1ST TEST WITH Ar 41

HALF LIFE : 1.95 hr.

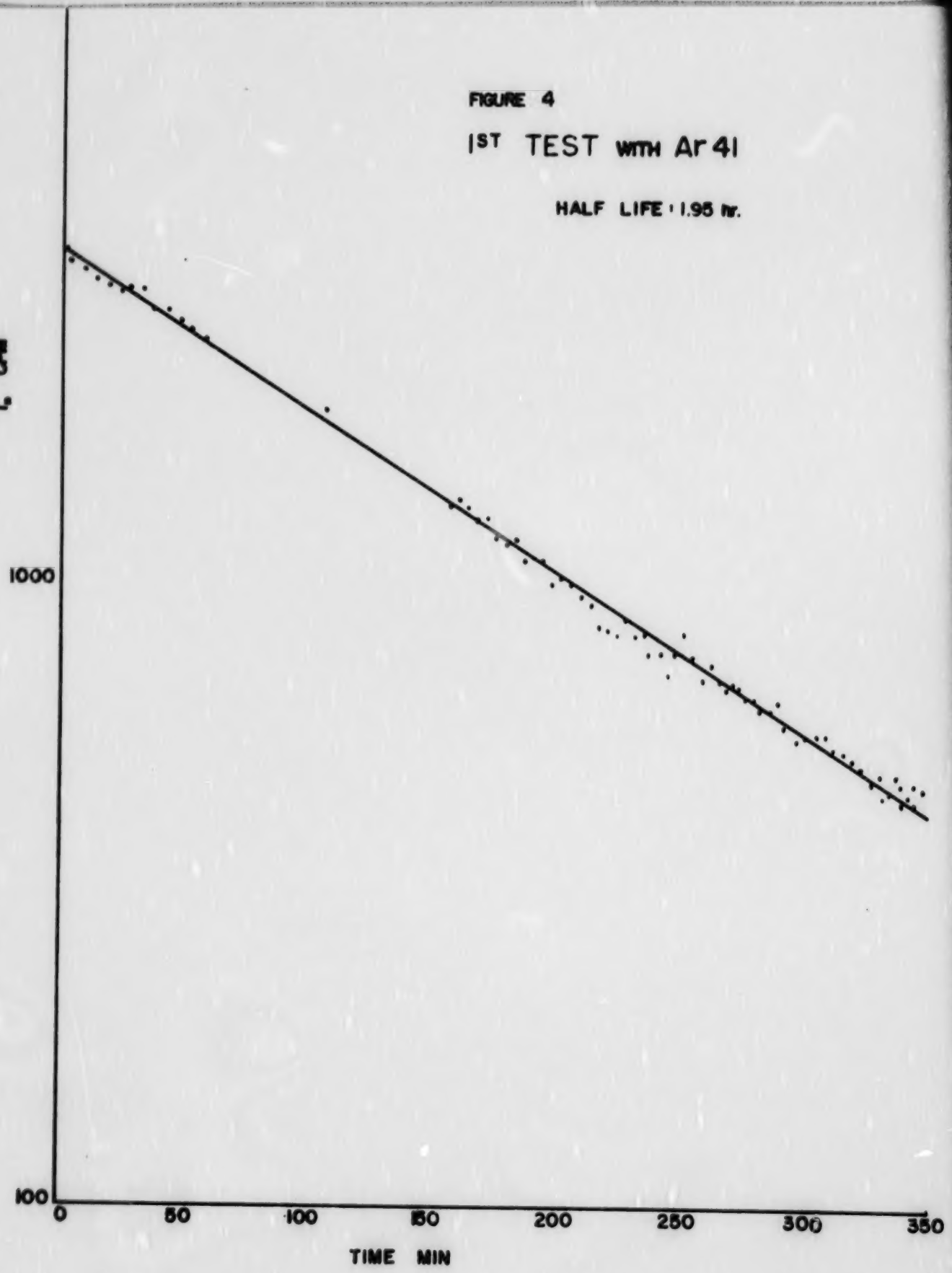

FIGURE 5

2nd TEST with Ar 41

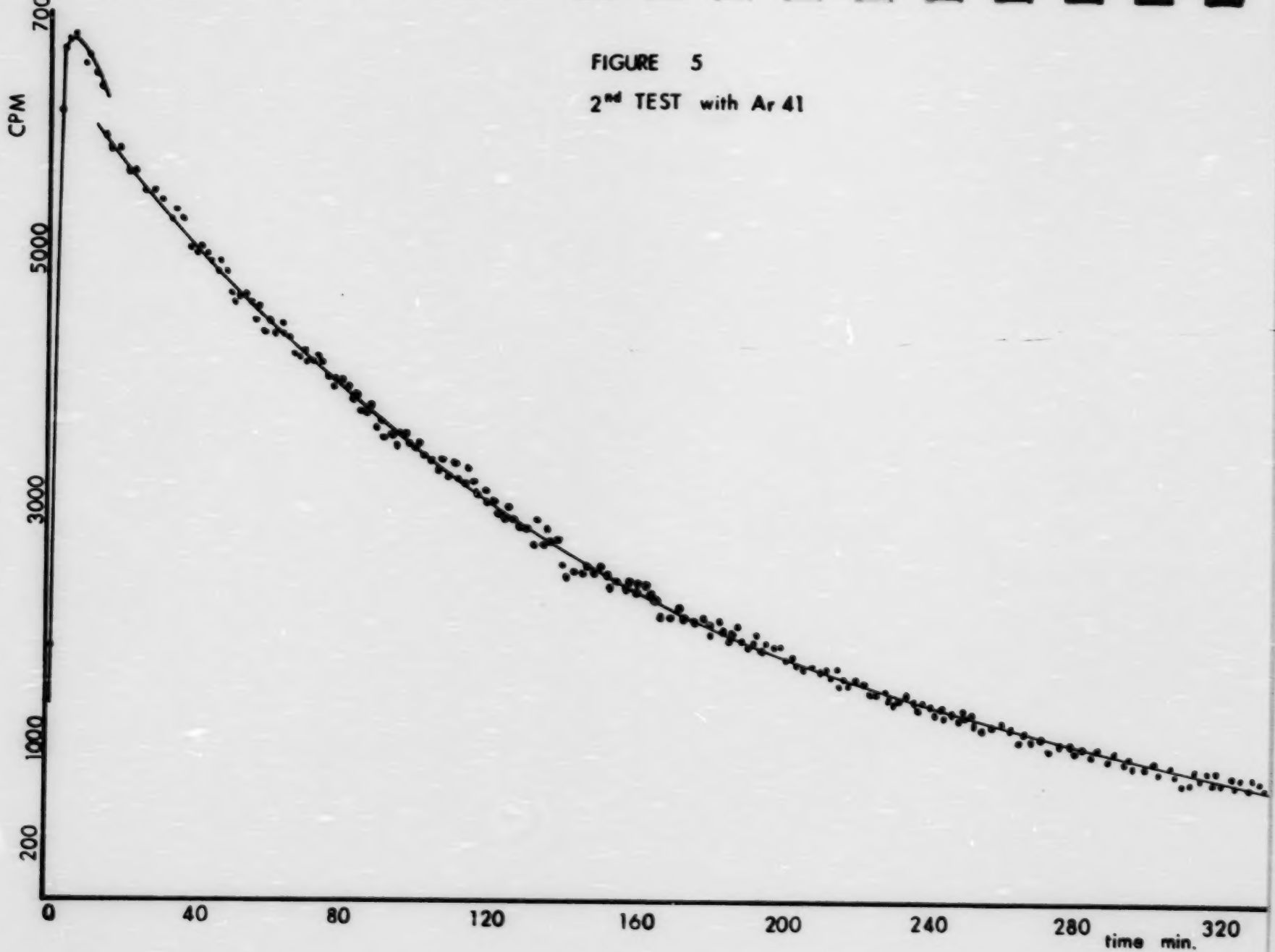

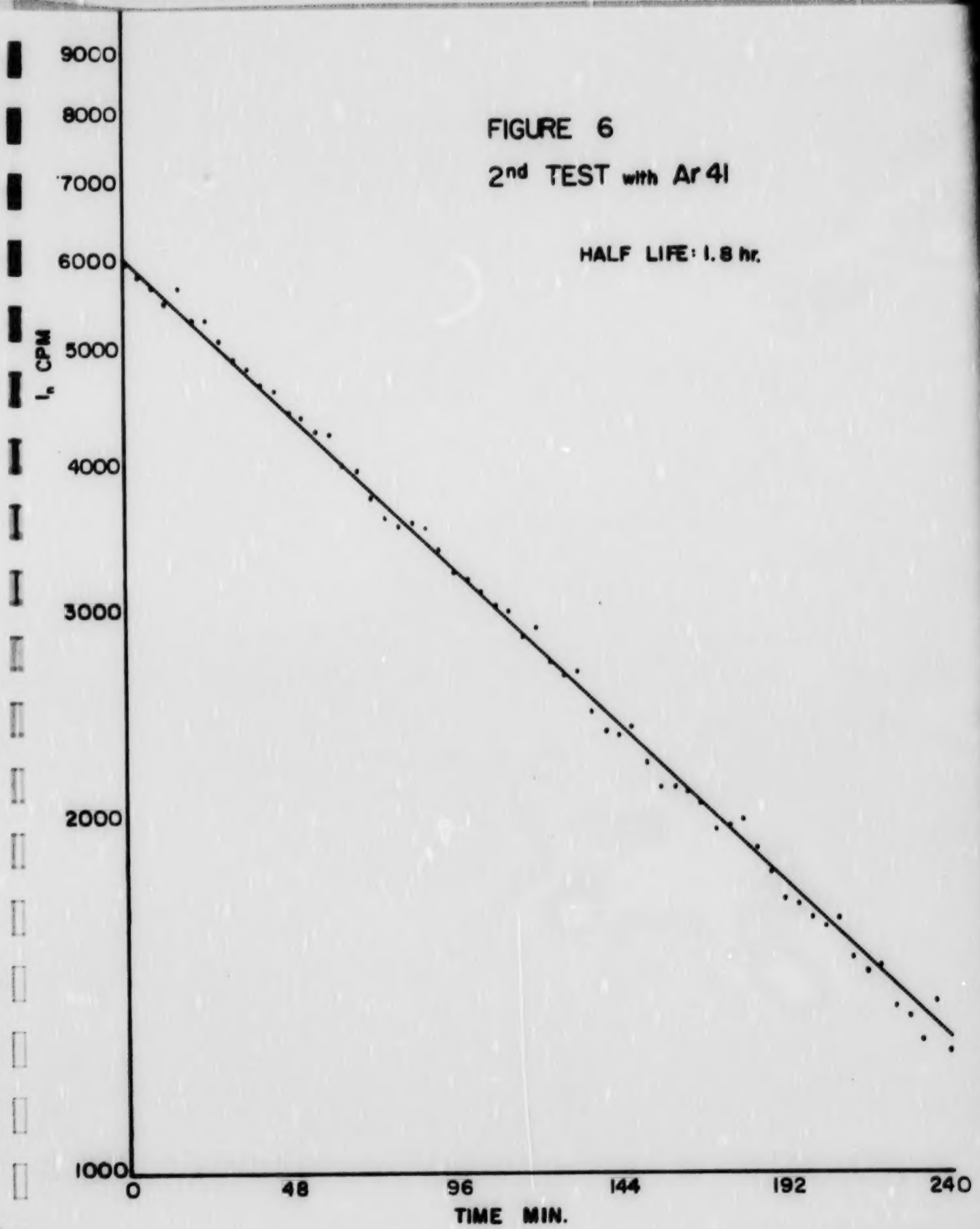

FIGURE 6

2nd TEST with Ar 41

HALF LIFE: 1.8 hr.

charcoal holder into the system one would expect a dilution of the radioactivity in the proportion to the ratio of these volumes (i.e., 929/970 = .948). Readings taken from Figures 3 and 5 gave the following results:

$$\text{First test} \qquad \frac{(CPM)_1}{(CPM)_2} = \frac{3380}{3560} = .952$$

$$\text{Second test} \qquad \frac{(CPM)_1}{(CPM)_2} = \frac{6060}{6360} = .956$$

The above results indicated that this mixing effect was negligible and provided further indication, along with the half life determination, that reliable data could be obtained from the TRI-CARB system.

Ethylmercaptan Tests

Having confirmed that the TRI-CARB system and the circulation system were performing as expected with the ^{41}Ar, the first experiment using ethylmercaptan was attempted. Sulfur 35-tagged mercaptan was used for this test.

After the ethylmercaptan was added the gas was circulated through the Packard TRI-CARB flow cell (at this point the cold trap and charcoal holder are isolated) and readings were taken over a 2 1/2 hour period. The detector readings during this period are shown in Figure 7 as region I. The response in region I indicates loading (adsorption and or absorption) of anthracene with ethylmercaptan and was an unexpected event.

After this circulation period the charcoal holder was switched into the system and adsorption of ethylmercaptan was observed to occur. Region II of Figure 7 shows the detector reading during this period. Because of the loading of the anthracene the adsorptive action of the charcoal was overshadowed at lower concentrations.

The exact nature of the anthracene loading process is not known although it was found that the ethylmercaptan was tightly bound to the anthracene. After the test run the anthracene crystals were removed from the flow cell and allowed to stand in an open beaker for three days. A sample of the anthracene was then dissolved in toluene and the level of radioactivity was determined with a scintillation counter. This measurement showed that a large quantity of ethylmercaptan remained and indicated that the "loading" process is characterized by strong attractive forces.

FIGURE 7

TEST with ETHYL MERCAPTAN

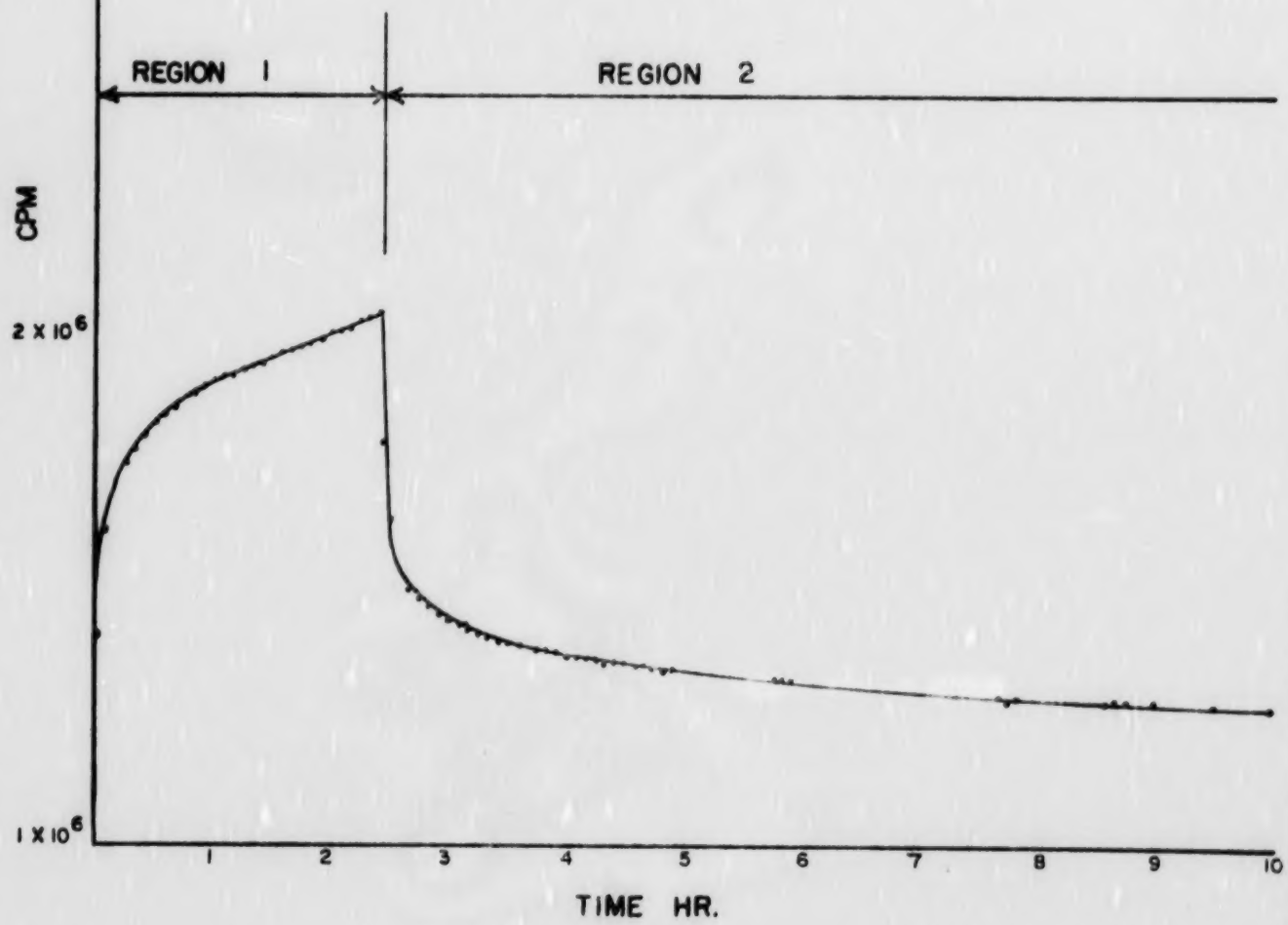

When the plexiglass flow cell was removed from the circulation system, emptied of anthracene, repacked with fresh anthracene, and then replaced in the TRI-CARB system with no gas flow, a high count rate was observed. This indicated that ethylmercaptan was adsorbed or absorbed in the walls of the flow cell.

In an attempt to eliminate or reduce the loading, a flow cell fabricated from Kel-F plastic and packed with Lithium glass bead scintillators was installed. Tests with ^{41}Ar showed this to be a very efficient detection system, however a test with ^{35}S-tagged ethylmercaptan again revealed that loading had occurred.

Because it appeared that the loading phenomenon could not be eliminated, efforts were then directed toward controlling it. This would be attempted by removing the radioactive mercaptan from the flow cell, the Lithium glass bead scintillators, and the inside surfaces of the adsorption system and then presaturating these parts with non-radioactive mercaptan. Previous tests had shown that the mercaptan is very strongly adsorbed and it was believed that once the system had been presaturated, or loaded, that no further loading would occur when the radioactive mercaptan was introduced. Because adsorptive forces are temperature dependent, it was reasoned that increasing the operating temperature of the flow cell from the specified value of 5°C to room temperature should serve to decrease the extent of loading on the flow cell.

Considerable difficulty was encountered in attempting to remove the loaded radioactive mercaptan. Heating the Lithium glass bead scintillators under vacuum for several hours reduced the amount of loaded mercaptan, but when these beads were packed in the flow cell a very high background count was obtained. After some experimentation, a sizeable reduction in background count was obtained by replacing the Lithium glass bead scintillators with new beads, soaking the Kel-F flow cell in toluene and keeping the entire adsorption system under vacuum (less than 5 mm Hg) for approximately a week. These rather drastic measures reduced the background count to about 1300 cpm with air circulating through the adsorption system. Although this is about six times the background count obtained for the original test of this flow cell, the count remained constant for about an hour and the decision was made to proceed with the presaturation step. Non-radioactive mercaptan was introduced into the system and the gas was circulated for almost an hour. The circulating gas was then routed through a liquid nitrogen-cooled trap

for several hours in order to remove any unadsorbed non-radioactive mercaptan. No sign of condensation was observed in the trap indicating that all of the charged mercaptan was adsorbed on the various parts of the system. During this presaturation period the TRI-CARB readings were observed in increase slightly therefore the measurements were extended for several more hours.

The TRI-CARB readings during the presaturation period are shown on Figure 8. These readings have been corrected for the background count of 1300 cpm. The increase in the TRI-CARB output with time prior to introduction of the radioactive mercaptan is difficult to explain. The only possible explanation seems to be that all of the radioactive material was not removed from the interior surfaces of the circulating system during the cleaning process and that some of this material was displaced by the non-radioactive mercaptan. This exchange process would be expected to occur rather slowly as observed.

As can be seen from Figure 8, the Tri-CARB readings showed signs of leveling off after about seventeen hours. At that time a test with radioactive ethylmercaptan was started using the previously described operating procedure. The TRI-CARB output during this test is shown on Figure 8 and on a different time scale on Figure 9. Figure 9 shows that a state of equilibrium appears to occur approximately 45 minutes after the charcoal is switched into the system.

Because of the apparent exchange of radioactive and non-radioactive mercaptan presaturation of the system was not considered feasible. Since the loading phenomenon could be neither eliminated nor controlled it was decided to abandon this experimental approach and investigate the possibility of using other experimental approaches.

FIXED-BED ADSORPTION STUDIES

The fixed-bed approach was chosen because it is a well established technique and would allow kinetic and equilibrium data to be determined under essentially the same conditions as prevail in industrial adsorbers. The method consists of passing a fluid stream of a constant composition at a constant flow rate through a fixed bed of adsorbent which is initially free of the adsorbate. The effluent fluid concentration is monitored and the effluent concentration versus time data is referred to as breakthrough data. A plot of this data is referred to as the breakthrough curve.

FIGURE 8. TEST WITH ETHYLMERCAPTAN.

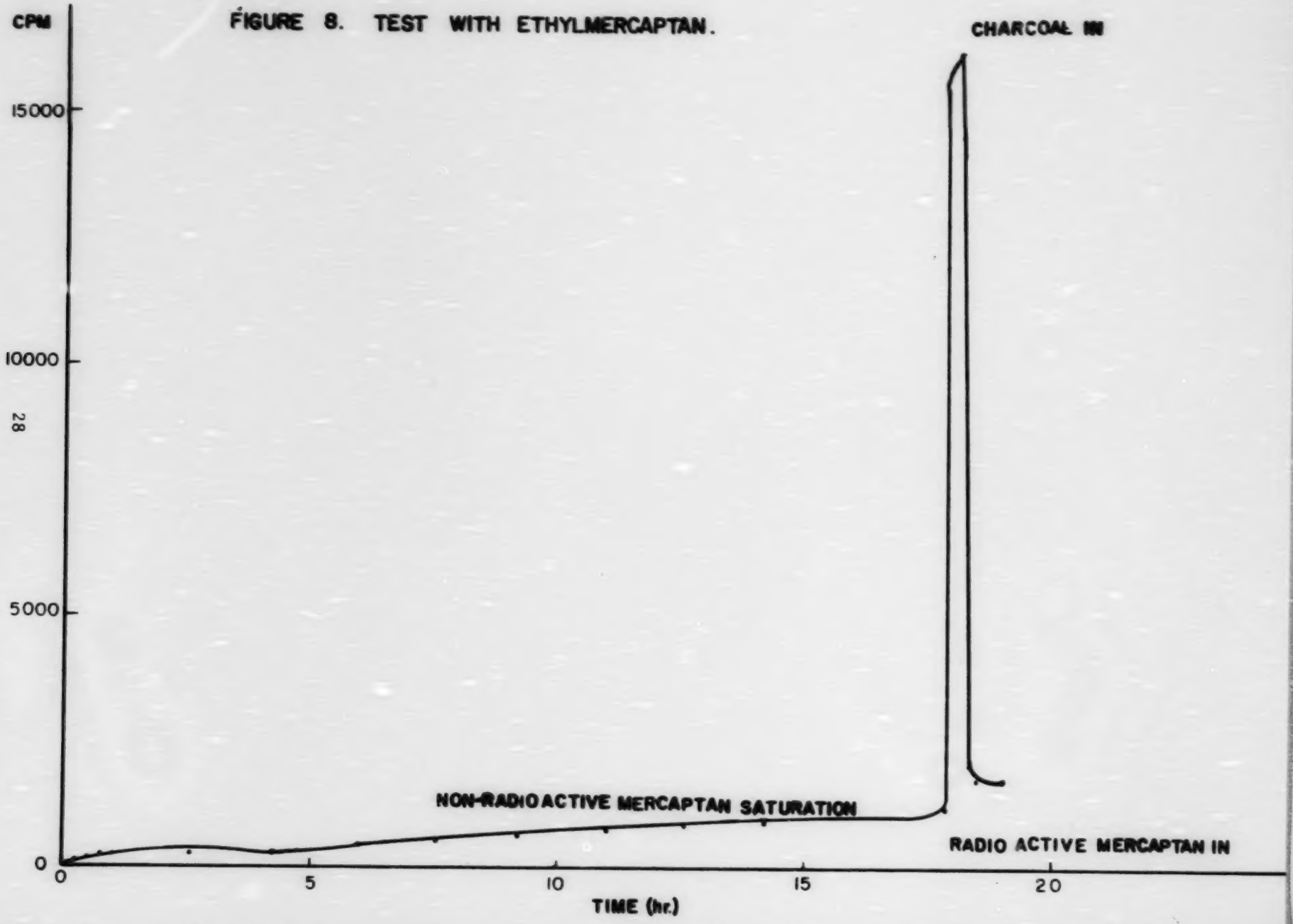

FIGURE 9. TEST WITH ETHYLMERCAPTAN.

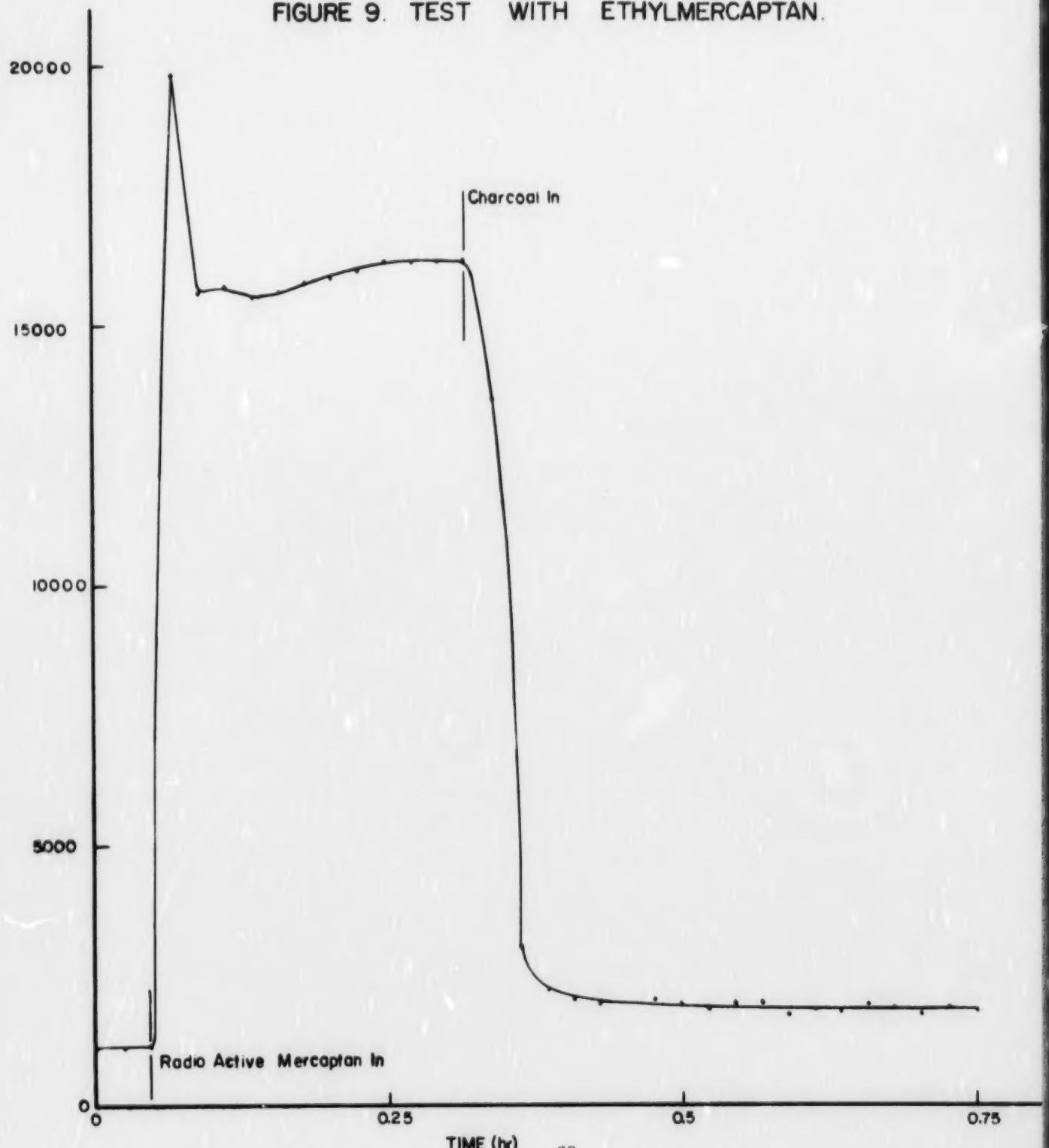

The capacity of the adsorbent can be obtained by a material balance calculation involving integration of the area above the breakthrough curve. This adsorbent capacity is usually the same as the capacity of the adsorbent when in equilibrium with the influent fluid and is customarily taken to be the equilibrium capacity.

A modeling approach is used for a kinetic analysis of fixed-bed adsorption. Here a model is defined as a mathematical expression arrived at through specifying an equilibrium relationship, a rate expression, and appropriate boundary conditions. Many models are possible and the mathematics have been worked out and published for quite a number. In applying the modeling approach one attempts to fit the experimental breakthrough data to a selected model breakthrough equation. This process of curve fitting also permits the evaluation of the model parameters. The validity of a given model is then determined by its ability to fit the experimental breakthrough curves and, additionally, by whether the experimentally determined model parameters are realistic.

Experimental Apparatus

The experimental apparatus used for the fixed-bed studies is sketched on Figure 10. The major parts are: a diffusion cell assembly to generate an influent gas of the desired concentration, flowmeters to regulate the flow rate of the influent gas into the charcoal bed, and a gas chromatograph equipped with a gas sampling valve to analyze both influent and effluent gas streams.

Diffusion Tube Assembly - The use of a diffusion tube to generate gas mixtures containing organic vapors in the parts-per-million range in air has been described by Altshuller and Cohen (2). Our diffusion tube assembly, shown on Figure 11, is patterned after their design and consists of a long capillary tube connected to a liquid reservoir and open to a mixing chamber at the top. Liquid in the capillary tube diffuses from the liquid-gas interface to the upper end of the capillary tube at a rate given by the well known diffusion equation

$$\text{rate} = \frac{DPS}{R_g TL} \ln \frac{P}{P-p} \qquad (55)$$

Gas mixtures of desired concentrations could be prepared by varying the gas flow rate across the upper end of the diffusion tube, or by changing the

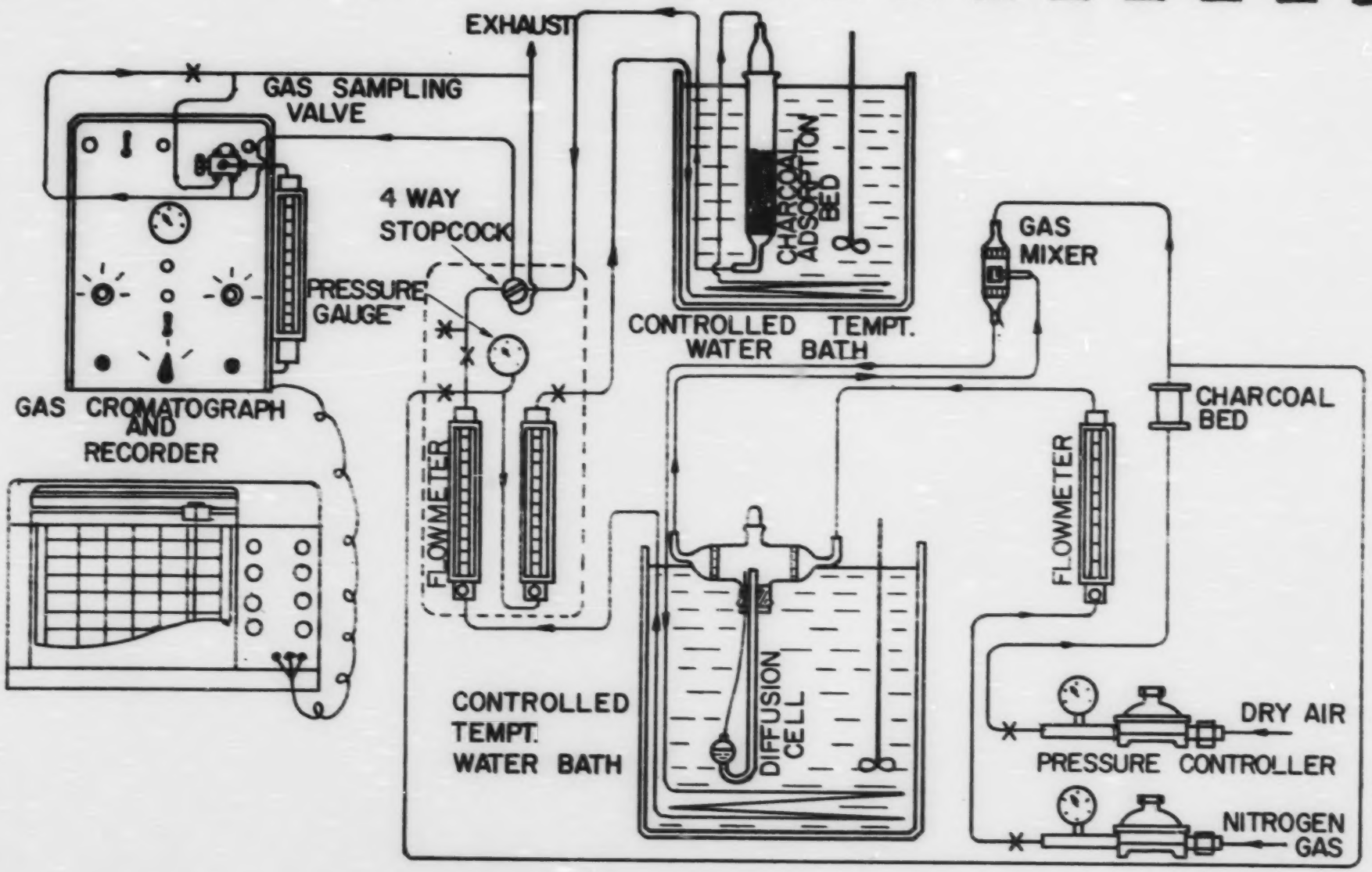

FIG. 10 EXPERIMENTAL ADSORPTION SYSTEM

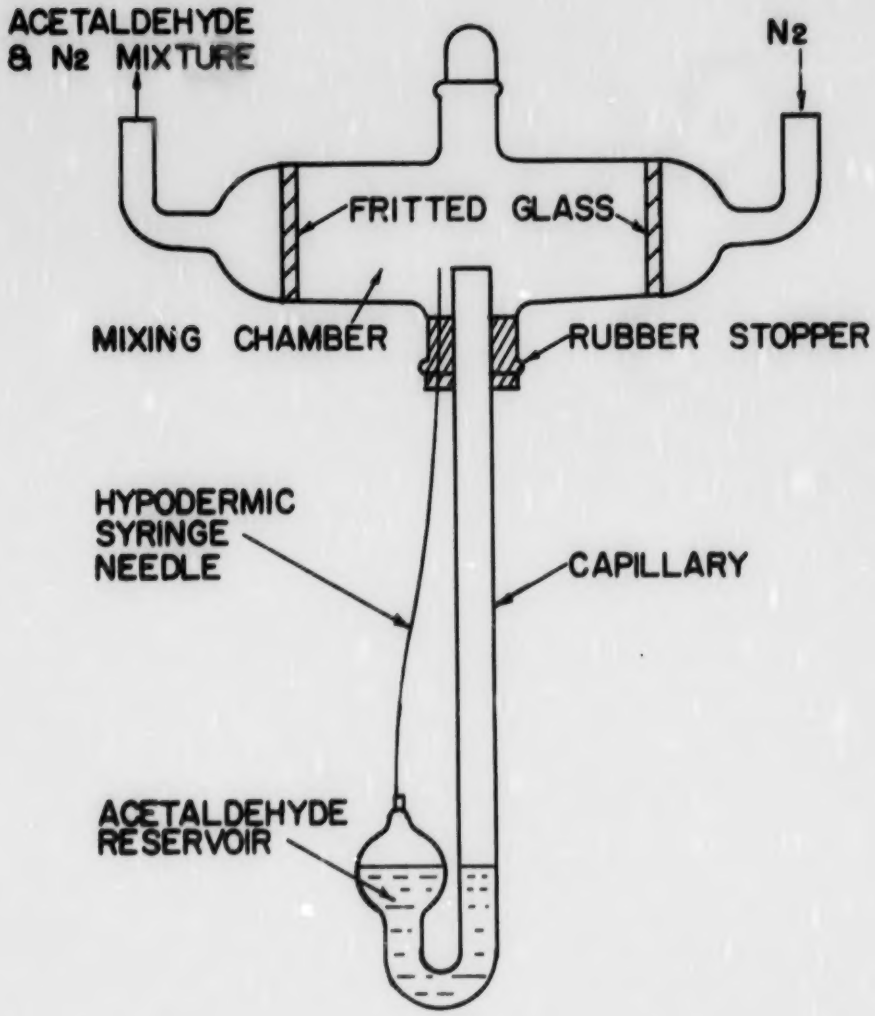

FIG. 11 DIFFUSION TUBE

cross-sectional area of the diffusion tube, or the vapor pressure of the diffusing component which depends only on temperature.

Chromatographic Analysis - In order to establish a calibration curve for chromatographic analyses it was necessary to be able to generate gas mixtures of known composition. Since the air flow rate was easily controlled and measured, it was necessary only to determine the rate of diffusion through the diffusion tube. For this calibration process a straight capillary tube closed at the bottom end was used in the diffusion tube assembly. The diffusion rate was determined by measuring the change in liquid height inside the capillary tube over a measured time interval. The height change, measured by means of a cathetometer, was converted to a volume by means of a previously established calibration. This calibration was established by partial filling of the capillary with mercury followed by weighing on an analytical balance and determination of the mercury column height with the cathetometer. From the volume of liquid evaporated per unit time the diffusion rate was determined from the known liquid density of the diffusing component.

Chromatographic calibration curves were established by determining chromatograms for gas mixtures of several different known concentrations. The calibration curves for ethylmercaptan and acetaldehyde are shown in the appendix.

Fixed-Bed Experimental Procedure

A test was started by filling the diffusion tube and starting the gas flows until a gas mixture of the desired composition could be maintained. When constancy of the influent gas composition was assured the charcoal holder was charged with a known weight of charcoal and the flow rate of influent gas through the charcoal bed was regulated with the flowmeters. Chromatographic analyses of influent and effluent streams were taken as the test progressed.

Fixed-Bed Adsorption Studies with Acetaldehyde

Preliminary tests showed that the acetaldehyde concentration of the gas mixture produced by the diffusion tube assembly could not be maintained constant but continually decreased. This was believed due to an oxidation process occurring at the liquid-gas interface and nitrogen was substituted for air as the flowing gas. With nitrogen flowing a constant diffusion rate was observed, however, it was necessary to mix the small stream from the diffusion tube assembly with air. This was done in the mixer shown on Figure 12.

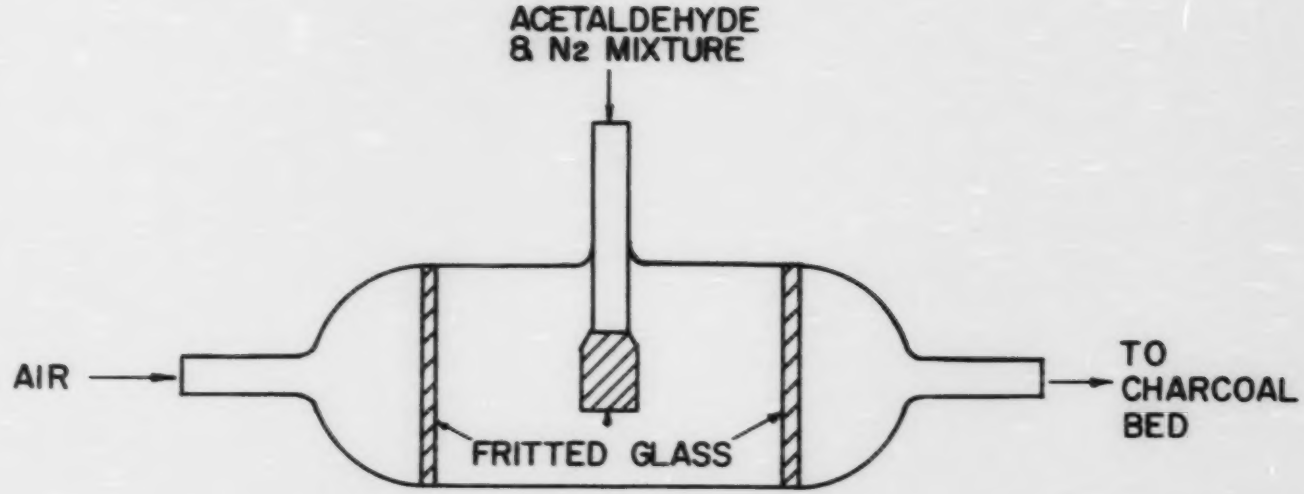

FIG. 12. GAS MIXER

As shown in Figure 10 after leaving the mixer gas flowed through several feet of tubing before reaching the flowmeters. It is believed that thorough mixing occurred. The flow of nitrogen was much smaller than the air flow so that when mixed with air only a small change in the oxygen to nitrogen ratio occurred and the diluent gas could be regarded for all practical purposes, as air.

Breakthrough data were taken with an influent stream containing 28 parts per million of acetaldehyde in air. Tests were made using various influent flow rates, bed depths, bed heights, and charcoal particle sizes. Pittsburgh PCB charcoal, derived from coconut shells, was used in all tests and the adsorption temperature was maintained at 30°C for all tests.

Static Equilibrium Tests

These tests were made so that the equilibrium capacity of the charcoal could be determined and also because knowledge of the equilibrium relationship is helpful in carrying out the modeling studies with the breakthrough data. Flasks of 3 liters capacity were initially filled with known mixtures of acetaldehyde and air. Known weights of charcoal were then added and the flasks were set aside at a controlled temperature of 30°C. After two weeks the gas in the flasks was analyzed. To confirm the attainment of equilibrium the gas was analyzed again several days later. The two analyses were identical which indicated the existance of a state of equilibrium. A material balance calculation allowed the determination of the amount of acetaldehyde adsorbed on the charcoal in equilibrium with the final acetaldehyde concentration in the gas phase. To check for error due to possible adsorption of acetaldehyde onto the wall of the flask no charcoal was placed in one of the flasks. The acetaldehyde concentration within this flask was not observed to change significantly indicating no adsorption on the flask wall.

FIXED-BED CATALYTIC STUDIES

Before catalytic oxidation was discovered, or even expected, the ethylmercaptan - air system was chosen for the study of fixed-bed adsorption. The results of several such tests could only be explained in terms of a chemical reaction involving oxygen and ethylmercaptan which is catalysed by charcoal. Because of these tests the fixed-bed catalytic study phase of the project was initiated.

Experimental Apparatus

The experimental apparatus was essentially the same as that used for the fixed-bed adsorption studies and shown on Figure 10 with the exception that it was not necessary to use a nitrogen flow through the diffusion tube and therefore the gas mixer was not required. Because considerably less charcoal was needed for these studies than for the fixed-bed adsorption studies it was necessary to mix the charcoal particles with glass beads in order to obtain sufficient bed depth to insure good flow patterns through the bed. Usually, equal volumes of charcoal and glass beads were used to form the bed. Concentrations of ethylmercaptan in the influent and effluent streams were again determined chromatographically.

Experimental Procedure

The experimental procedure is very similar to that followed in the fixed-bed adsorption studies; the bed is fed with an influent stream of constant composition at a constant flow rate and the concentration of the effluent stream is monitored. A total of 13 fixed-bed tests were made during the study of ethylmercaptan oxidation on Pittsburgh BPL charcoal catalyst. The variables studied ranged from 20 to 125 PPM influent ethylmercaptan concentration, 3-40 cm/sec superficial velocity, and 3-14 gm charcoal per cm^3 of ethylmercaptan fed/min. All except three of these tests were made with 14 mesh charcoal and the remaining tests were made with 8 mesh charcoal.

Identification of Reaction Products

Several attempts were made to collect and identify reaction products by mass spectrographic analysis. Attempts using a liquid nitrogen trap on the effluent stream were largely unsuccessful because oxygen and water, present in large quantities in the collected sample, did not allow the detection of species which may have been present in much smaller quantitites. One test was made with an acetone-dry ice trap to avoid condensing oxygen, but the quantity of water present in the sample again obscured the analysis. Moderate success was achieved when a liquid nitrogen trap was connected to the chromatograph so that the flow from the chromatograph could be diverted through the trap when the "product" was scheduled to appear. Although a fair mass spectrogram was obtained, the presence of air and water limited the degree of resolution. It is believed that the air entered the system through stopcocks on the trap which were not of the high vacuum variety and the water had condensed out of

the nitrogen carrier gas used for the chromatograph. Installation of high vacuum stopcocks and drying of the carrier gas prior to its entering the chromatograph should produce much better samples.

DISCUSSION

ACETALDEHYDE ADSORPTION STUDY

By applying the previously discussed procedure breakthrough data were obtained at 30°C for fixed-beds of Pittsburgh PCB charcoal fed with a constant influent concentration of 28 PPM of acetaldehyde in air. The effect of bed length, superficial velocity, and charcoal particle size was studied. The ranges of these variables were: 8 to 46 cm bed length, 10, 12, and 14 mesh charcoal particle size, and 8-40 cm/sec superficial velocity. The range of superficial velocities used coincides with the range customarily used for design of commercial fixed-bed adsorption systems; Barnebey (3) states that this later range is 35 to 75 ft/min (18 to 38 cm/sec). The experimental breakthrough curves are shown in the appendix and the salient features of each test are tabulated in Table 1.

Charcoal Capacity

The charcoal capacity was determined both from the static equilibrium tests and from the breakthrough curves.

Static Equilibrium Tests - Nine equilibrium data points have been obtained using the Static Equilibrium Method described previously. These data, listed in Table 2, allow the plotting of a smooth isotherm curve in the range of 0 to 35 ppm of acetaldehyde in air. This plot is shown on Figure 13.

Attempts were made to fit the isotherm data to Langmuir and Freundlich isotherm equations. If the Langmuir equation is followed, a plot of gas concentration divided by equilibrium capacity versus gas concentration should be a straight line. Such a plot is shown on Figure 14 where it can be seen that a reasonably good fit to a straight line occurs. As a test for conformity of the data to the Freundlich isotherm equation, one plots log of equilibrium capacity versus log of gas concentration. If a straight line can be drawn on such a plot the data can be said to fit the Freundlich isotherm equation. Figure 15 shows a log-log plot of the isotherm data. It could be said that the data fit a straight line reasonably well and therefore also can be represented by the Freundlich isotherm equation.

Regeneration studies - The regeneration of once-used Pittsburgh PCB charcoal was carried out in a vacuum oven at a temperature of 120°C and

TABLE 1. RESULTS OF FIXED-BED TESTS WITH ACETALDEHYDE ADSORBED ON PITTSBURGH PCB CHARCOAL

Influent Concentration: 28 ppm of acetaldehyde in air
Temperature: 30°C

RUN No.	CHARCOAL SIZE (mesh)*	BED WEIGHT (GRAMS)	BED DIAMETER (INCHES)	BED LENGTH (INCHES)	INFLUENT FLOW RATE (cc/min)	SUPERFICIAL VELOCITY (cm/sec)	BREAK TIME (min)	CHARCOAL CAPACITY (gm/gm)
2	14	2.0	59/64	0.5	1610	6.2	9	0.00192
3	14	4.0	59/64	1.0	1300	5.0	36	0.00192
4	14	2.0	59/64	0.5	1610	6.2	6	0.00189
5	14	3.45	5/8	2.0	400	3.4	270	0.00407
6	14	3.49	5/8	2.0	700	5.9	150	0.00377
7	14	3.45	5/8	2.0	1000	8.4	70	0.00303
8	14	8.0	59/64	2.0	1524	5.9	145	0.00269
9	14	8.0	59/64	2.0	1524	5.9	130	0.00365
10	14	8.0	59/64	2.0	879	3.4	270	0.00368
11	14	5.2	5/8	3.0	700	5.9	255	0.00381
12	14	5.2	5/8	3.0	400	3.4	515	0.00389
13	14	5.2	5/8	3.0	1000	8.4	380	0.00793
14	14	5.2	5/8	3.0	1000	8.4	400	0.00812
15	14	3.45	5/8	2.0	1000	8.4	80	0.00320
16	14	5.2	5/8	3.0	1425	12.0	90	0.00289
17	14	5.2	5/8	3.0	1188	10.0	140	0.00405
18	14	6.1	5/8	4.0	1425	12.0	310	0.00858
19	14	8.3	5/8	5.375	1950	16.4	270	0.00751
20	14	6.8	5/8	4.5	1950	16.4	270	0.00884
21	14	4.54	5/8	3.0	1950	16.4	120	0.00759
22	14	7.56	5/8	5.0	1425	12.0	510	0.00872
23	14	6.05	5/8	4.0	1000	8.4	210	0.00585
26	14	16.5	5/8	8.0	4700	39.5	300	0.00977
29	14	37.5	5/8	18.0	1950	16.4	1100	0.00722
30	14	37.5	5/8	18.0	2970	25.0	738	0.00740
31	14	37.5	5/8	18.0	4150	35.0	375	0.00650
32	14	37.5	5/8	18.0	3560	30.0	468	0.00700
38	10	102	1	18.0	4750	16.4	884	0.00580
39	12	58	3/4	18.0	2750	16.4	1040	0.00610

*U.S. Standard Seive Size

TABLE 2. RESULTS OF STATIC EQUILIBRIUM TESTS WITH ACETALDEHYDE AND PITTSBURGH PCB CHARCOAL AT 30°C

Test No.	Equilibrium Concentration (PPM of Acetaldehyde)	Charcoal Capacity (gm/gm)
1	24.0	0.00718
2	20.0	0.00592
3	21.5	0.00653
4	15.5	0.00582
5	35.0	0.00869
6	28.5	0.00839
7	5.5	0.00406
8	3.0	0.00247
9	1.5	0.00125

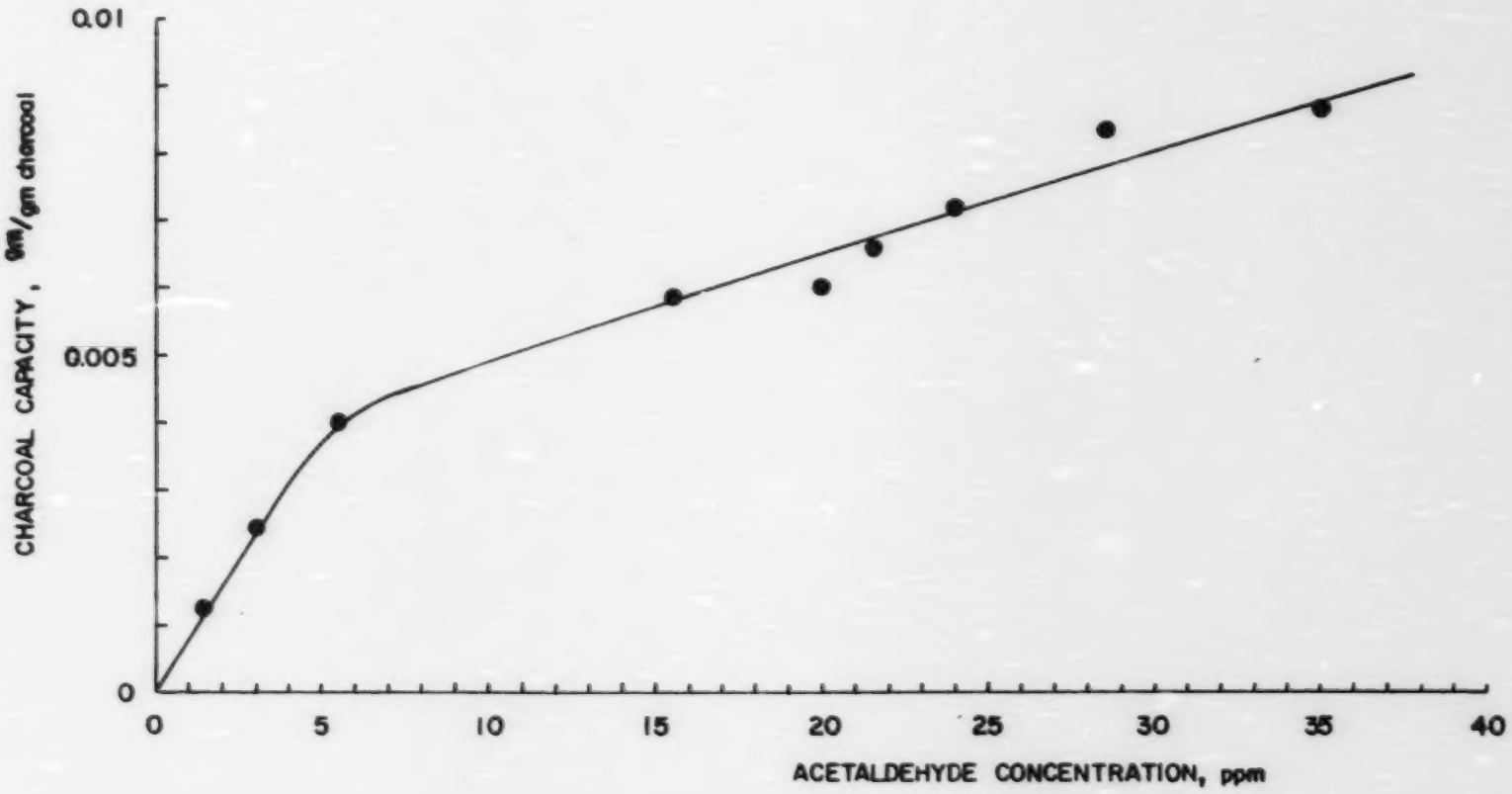

FIG. 13 . STATIC EQUILIBRIUM DATA FOR ACETALDEHYDE ON PITTSBURGH PCB CHARCOAL AT 30 °C

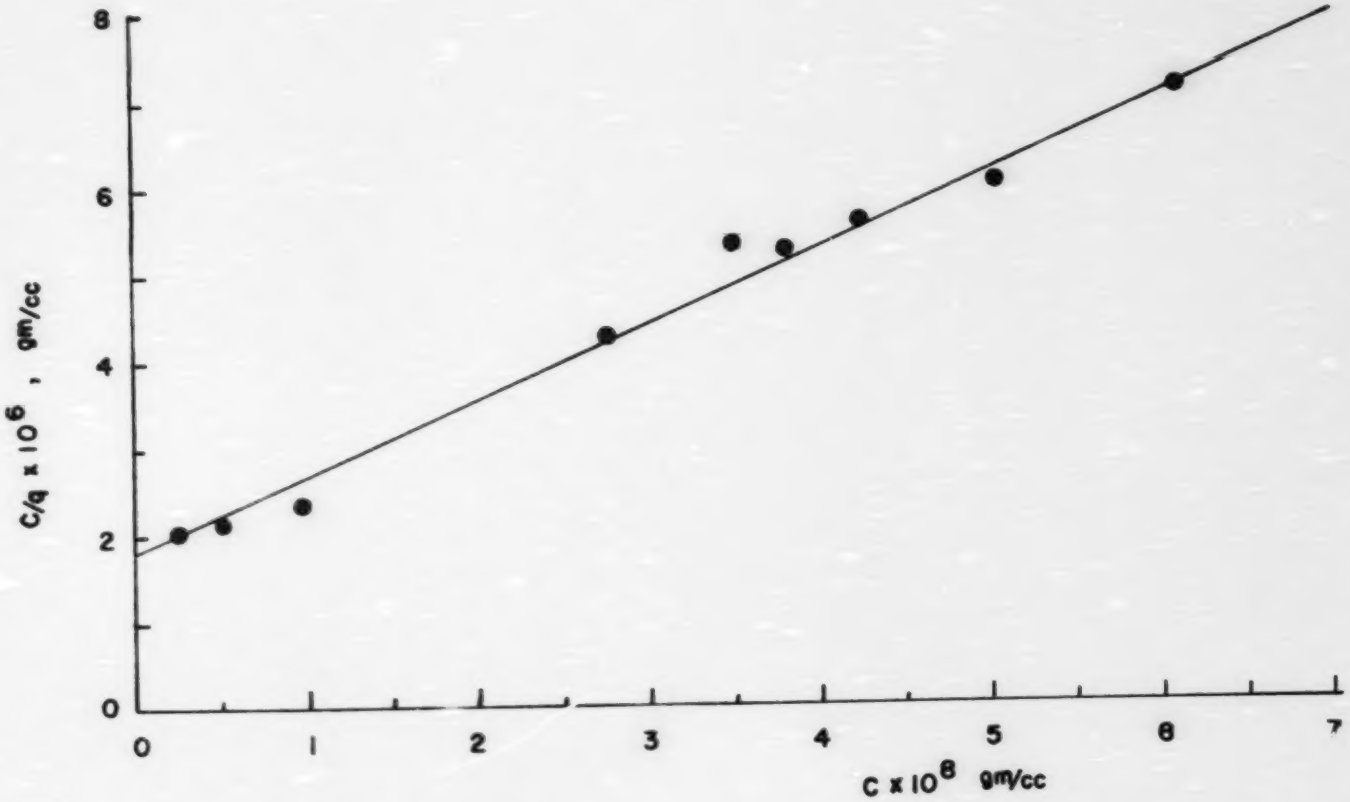

FIG. 14 . EQUILIBRIUM DATA FOR ACETALDEHYDE ON PITTSBURGH PCB CHARCOAL IN LINEAR FORM

FIGURE 15 TEST OF THE FREUNDLICH ISOTHERM EQUATION

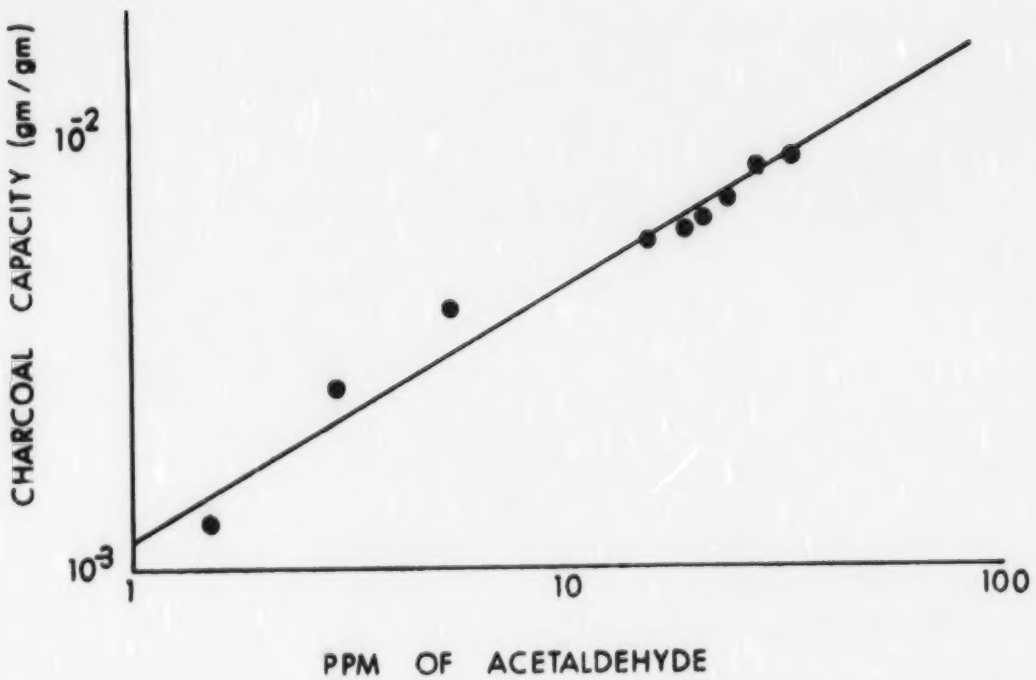

a vacuum of 20 inches Hg. Charcoal regenerated under these conditions for 25 hours was used for a fixed-bed test where a significantly lower capacity was observed. The charcoal was then subjected to an additional 100 hours of regeneration at the above specified conditions and again used for a fixed-bed test. A sizeable increase in capacity was observed although it was somewhat lower than that found from fixed-bed tests with virgin charcoal. The charcoal was then subjected to an additional 245 hours of regeneration. This charcoal showed a fixed-bed capacity in the range of the virgin charcoal and was judged to be completely regenerated.

Fixed-bed tests - Examination of Table 1 reveals that although the influent concentration is the same for all tests (28 PPM) the charcoal capacity is not constant. This was an unexpected development because we had found no mention in the literature of any study where adsorbent capacities were reported to be inconsistent. This discrepancy was disconcerting and a major part of our efforts were devoted toward resolving it. We felt that if we were unable to predict the capacity of a charcoal bed there was very little chance of developing a procedure for design of charcoal beds.

The inconsistency in charcoal capacity is not believed due to experimental technique because it was observed that there is little scatter in the experimental data points and a smooth breakthrough curve can be drawn in all cases. Further, several tests were duplicated and these duplicate breakthrough curves were found to superimpose quite well.

Two different diameter beds were used and it was found that for identical superficial velocities the breakthrough curves and hence the charcoal capacities were identical. The fact that the breakthrough behavior was not found to depend upon bed diameter is not surprising because for all bed diameters investigated the ratio of bed to particle diameter was greater than 8, the generally accepted minimum value for packed beds.

Most of the tests were made to elucidate the effect of bed length and superficial velocity upon charcoal capacity. Although no distinct relationship among these variables was found, we can state that for a constant superficial velocity the charcoal capacity increases with increasing bed length, but approaches a value of about 0.0088 gm/gm. as an upper limit. It is significant that this upper limit is very close to the estimated equilibrium capacity of charcoal as read from Figure 13.

The dependence of capacity on bed length is believed due to two factors; flow patterns within the charcoal bed and the very slow rate of mass transfer between the gas phase and the solid phase when solid-phase saturation is approached. Although the existence of the first effect can be experimentally demonstrated, it is believed that the second effect is the major factor.

In an attempt to determine the effect of bed depth on flow patterns pressure drops across beds of Pittsburgh PCB charcoal (14 - 16 mesh) of various depths were determined at several air flow rates. The bed was formed inside a 16 mm O.D. glass tube fitted with a coarse fritted glass disc in the bottom for distribution of the incoming air. This is the same size of tube and type of fritted glass disc as was used in our fixed-bed studies. Pressure changes across the fritted glass disc and charcoal bed were determined with a pressure transducer. The pressure transducer was not standarized because only relative readings were deemed necessary.

The results are plotted on Figure 16 as relative pressure units versus bed depth at each superficial velocity. One would expect these data to plot a single straight line for each velocity if flow patterns were independent of bed length. This seems to be the case for U = 17 cm/sec and U = 21.25 cm/sec, however, at lower velocities this expected linearity is not found until a bed depth of 3 or 4 inches is reached. This would indicate that flow patterns within the bed do change as bed depth changes.

Changes in charcoal capacity could result from changes in flow patterns when some of the channels and void spaces in the bed did not receive an active flow of gas and became stagnant. The charcoal in these stagnant sections of the bed would adsorb at an extremely slow rate because the adsorbate would reach the adsorbent surface only after diffusing through stagnant air in these channels. The time required for this diffusion to the adsorbent surface could be large compared with the time required to obtain the breakthrough data and thus it would appear that the capacity of the charcoal in the bed was less than the equilibrium capacity.

When the adsorption rate is controlled by a solid phase resistance the rate is known to slow considerably as the solid phase approaches saturation. This type of resistance is characterized by a breakthrough curve which rises rapidly at low values of c/c_o and flattens out as higher values of c/c_o are approached. An examination of Figures A-1 through A-13 reveals

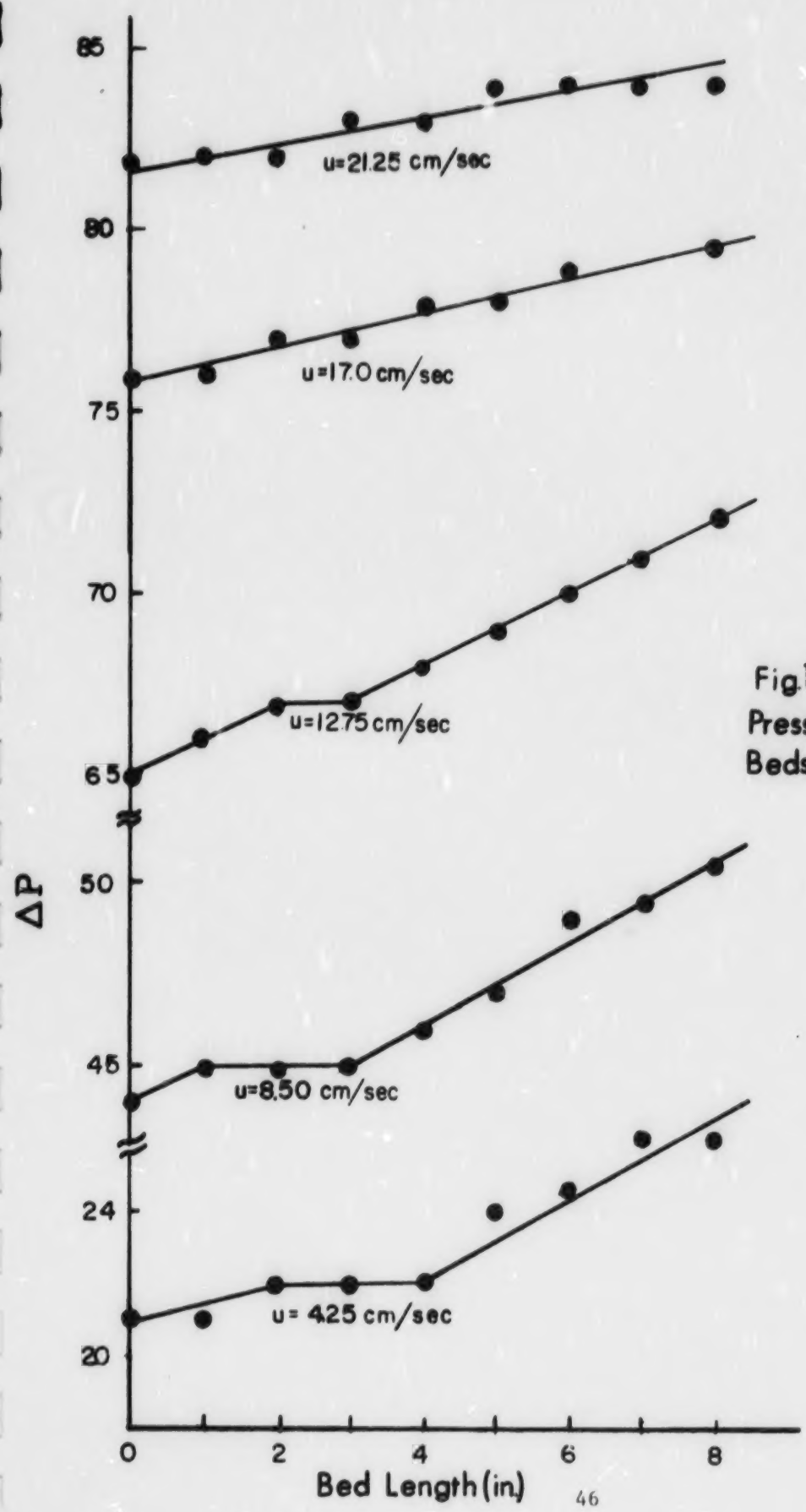

Fig.16
Pressure Drop Through
Beds of Charcoal

that all of our breakthrough curves exhibit this characteristic shape and therefore postulation of the solid-phase resistance controlling the rate of adsorption seems quite reasonable.

If the charcoal bed is short then the exhaustion point occurs after only a small quantity of fluid has passed through the bed. Although the charcoal in the bed still has the potential to adsorb, the rate is quite low and gas flowing through the bed has a short contact time with the solid. With this short contact time and the low rate of adsorption the gas composition changes very little and the bed gives the appearance of exhaustion. If the contact time is lengthened by lengthening the packed bed a detectable gas composition change is possible even with low rate of adsorption. Theoretically, if the bed is long enough the capacity determined from the breakthrough curve should be the equilibrium capacity of the adsorbent. From the results of our static equilibrium studies the capacity of a charcoal bed in equilibrium with an acetaldehyde-air mixture containing 28 ppm of acetaldehyde is about 0.0084 gm/gm. This agrees quite well with the maximum value of the charcoal capacity calculated from the breakthrough curves of about 0.0088 gm/gm.

Modeling Study

The objective of the modeling study is to establish the rate mechanism and to determine the dependence of the parameters in the rate expression upon the system variables so that the design of adsorption systems for odor removal can be accomplished. By fitting a selected model breakthrough equation to the experimental breakthrough curve, the evaluation of the model parameters is possible. The validity of a given model is then determined by its ability to fit the experimental breakthrough curve and also by whether the experimentally determined model parameters are realistic. With design as our prime objective, we want fairly simple models whose parameters have physical significance and can be readily estimated. The four model equations developed in the Theory Section of this report were applied to the experimental breakthrough data. Because of the inconsistency of the charcoal capacity found for beds of depths less than three inches, only the tests mady with bed depths three inches or greater were used for the modeling study.

All of the four model equations contain as parameters the number of transfer units, the separation factor, and the distribution ratio. The

number of transfer units is defined by equations 20, 26, 33, and 49, the separation factor is defined by either equation 15 or 16 and the distribution ratio, D, appears in equation 18 which defines the through-put parameter Z and is defined as

$$D = \frac{q_o^* W}{C_o v \varepsilon} \tag{56}$$

The separation factor and the distribution ratio are seen to be expressable in terms of the equilibrium data and it is normally expected that they can be evaluated if the equilibrium data are known. In our first attempt to fit the model equations to the experimental breakthrough data we evaluated these parameters from our equilibrium data shown on Figure 13. We were unable to obtain a reasonable fit and therefore decided to use the separation factor as evaluated from our equilibrium data (R = 0.28), but regard the distribution ratio as a parameter to be obtained from the curve fitting process. When used in this empirical manner, D will be denoted by D_e and called the effective distribution ratio.

All model equations were fitted to the experimental breakthrough data with a least-squares procedure. Because of the extreme "tailing off" exhibited by most of our breakthrough curves, the upper portion of the experimental breakthrough curve was not used in the curve fitting process. Figures A-1 through A-13 show a comparison of the experimental breakthrough curve and the various model equations which were fitted to the breakthrough data. The parameters obtained from fitting each of the four model breakthrough equations are listed in Tables 3 through 6 and are plotted versus the residence time, $v\varepsilon/F$, in Figures 17 through 24.

Inspection of Figures A-1 through A-13 reveals that of the four model equations the particle-phase diffusion (or solid diffusion) model fits the breakthrough curves over the widest range of effluent concentration. All model equations fit rather well in the region from about 5 to 17 PPM, however for most tests the solid diffusion model fits over the wider range 0 to 17 PPM.

Particle-phase Diffusion Model - Figure 17 shows that the effective distribution ratio can be considered constant. Even though this average value is only a fraction of the value which one calculates from the equilibrium

TABLE 3. PARAMETERS OBTAINED FROM MODEL EQUATION FOR PARTICLE-PHASE DIFFUSION MODEL

Run No.	ve/F sec	Effective Distribution Ratio D_{ep}	N_p
APC-14	0.677	62,386	5.00
APC-18	0.595	57,990	4.00
APC-19	0.592	59,179	3.60
APC-20	0.515	54,441	4.80
APC-21	0.303	59,020	3.00
APC-22	0.747	68,341	4.60
APC-26	0.556	54,002	6.30
APC-29	1.471	53,159	15.00
APC-30	0.966	58,127	10.00
APC-31	0.691	47,780	5.25
APC-32	0.745	51,179	5.98
APC-38	1.239	52,872	10.00
APC-39	1.401	54,577	11.00

TABLE 4. PARAMETERS OBTAINED FROM MODEL EQUATION FOR PORE DIFFUSION MODEL

Run No.	ve/F sec	Effective Distribution Ratio D_{epore}	N_{pore}
APC-14	0.677	60,746	3.081
APC-18	0.595	55,543	2.373
APC-19	0.592	54,146	2.384
APC-20	0.515	55,441	2.355
APC-21	0.303	53,650	1.985
APC-22	0.747	63,739	3.349
APC-26	0.556	54,009	3.188
APC-29	1.471	52,624	10.990
APC-30	0.966	56,130	8.827
APC-31	0.691	44,064	10.040
APC-32	0.745	48,199	8.768
APC-38	1.239	50,385	10.769
APC-39	1.401	54,321	6.782

TABLE 5. PARAMETERS OBTAINED FROM EXTERNAL DIFFUSION MODEL EQUATION

Run No.	ve/F sec	Effective Distribution Ratio D_{ef}	N_f
APC-14	0.677	53,000	5.026
APC-18	0.595	47,457	4.164
APC-19	0.592	46,644	3.363
APC-20	0.515	45,252	4.081
APC-21	0.303	44,281	2.685
APC-22	0.747	57,431	4.807
APC-26	0.556	47,915	7.466
APC-29	1.471	50,954	26.261
APC-30	0.966	54,125	13.320
APC-31	0.691	42,703	11.806
APC-32	0.745	46,454	13.846
APC-38	1.239	48,960	11.331
APC-39	1.401	51,341	16.796

TABLE 6. PARAMETERS OBTAINED FROM REACTION KINETICS MODEL EQUATION

Run No.	ve/F sec	Effective Distribution Ratio D_{eR}	N_R
APC-14	0.677	57,607	7.85
APC-18	0.595	52,437	6.28
APC-19	0.592	52,703	5.35
APC-20	0.515	50,097	7.35
APC-21	0.303	51,485	4.59
APC-22	0.747	62,651	8.33
APC-26	0.556	50,719	11.11
APC-29	1.471	51,801	32.07
APC-30	0.966	55,901	18.52
APC-31	0.691	44,284	17.71
APC-32	0.745	47,919	21.33
APC-38	1.239	50,847	20.83
APC-39	1.401	52,677	21.35

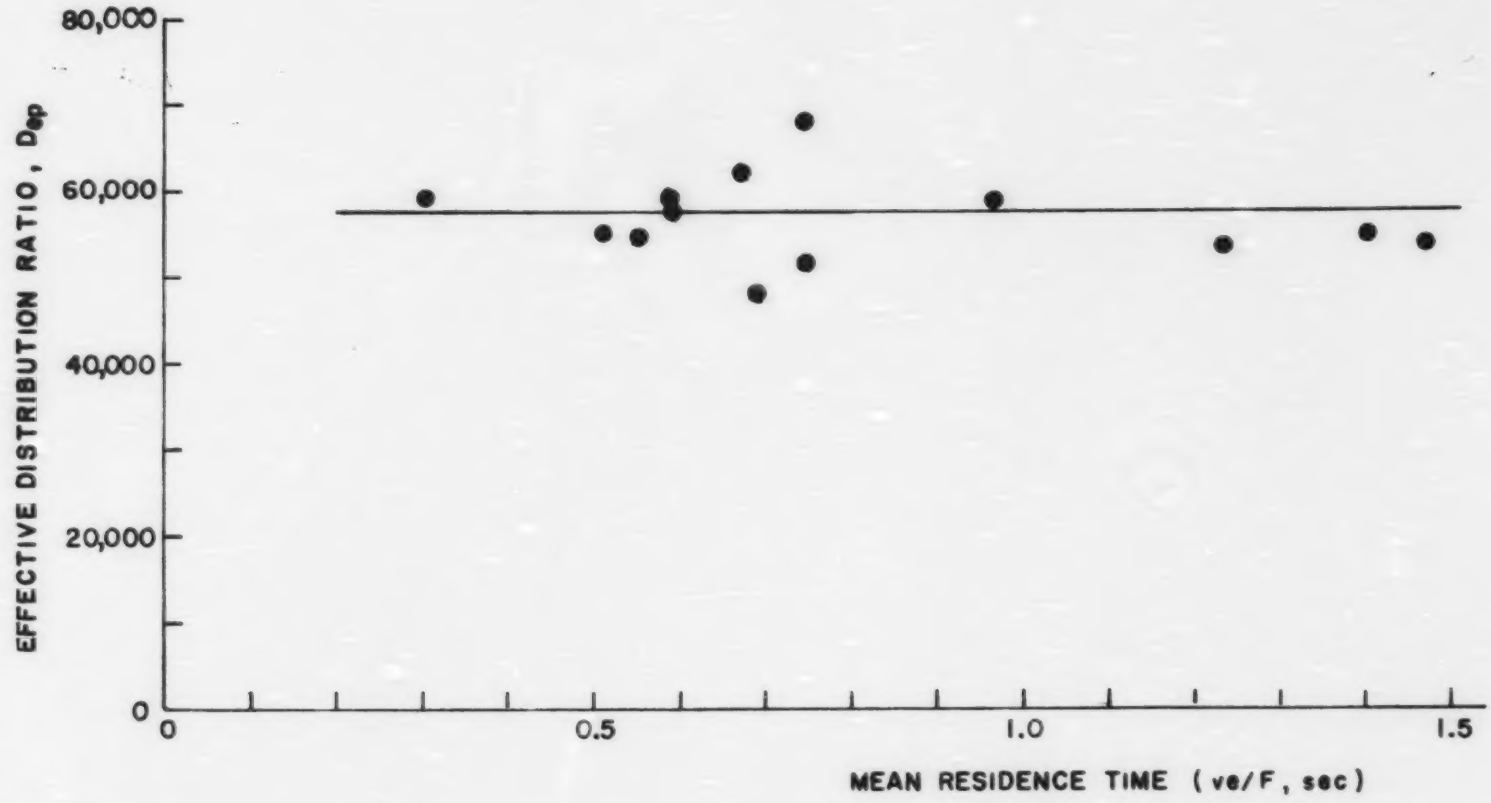

FIG. 17 . RELATION BETWEEN MEAN RESIDENCE TIME AND EFFECTIVE DISTRIBUTION RATIO FOR PARTICLE-PHASE DIFFUSION MODEL. AVERAGE VALUE OF D_{ep}=57,865

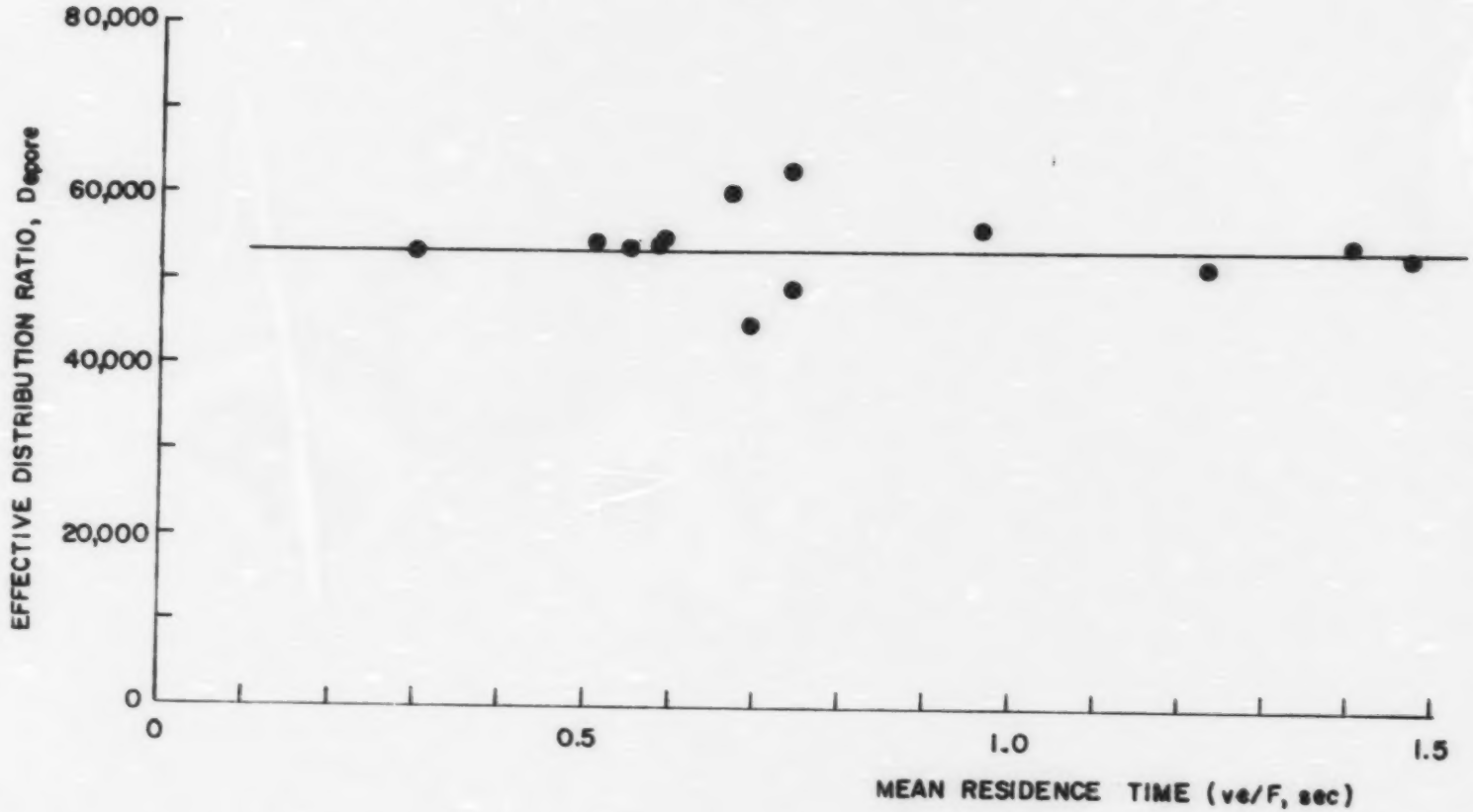

FIG. 18 . RELATION BETWEEN MEAN RESIDENCE TIME AND EFFECTIVE DISTRIBUTION RATIO FOR PORE DIFFUSION MODEL
AVERAGE VALUE OF D_{epore} = 53,210

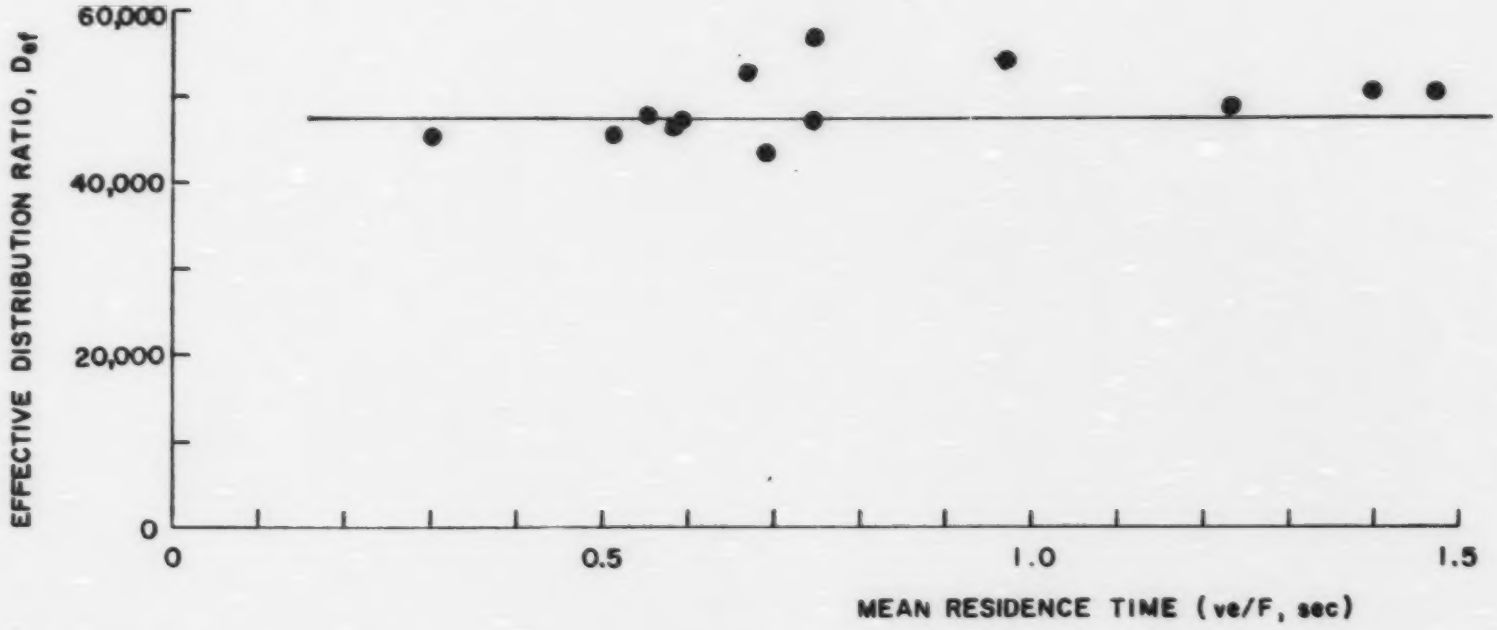

FIG. 19 . RELALATION BETWEEN MEAN RESIDENCE TIME AND EFFECTIVE DISTRIBUTION RATIO FOR EXTERNAL DIFFUSION MODEL AVERAGE VALUE OF D_{ef} = 47,607

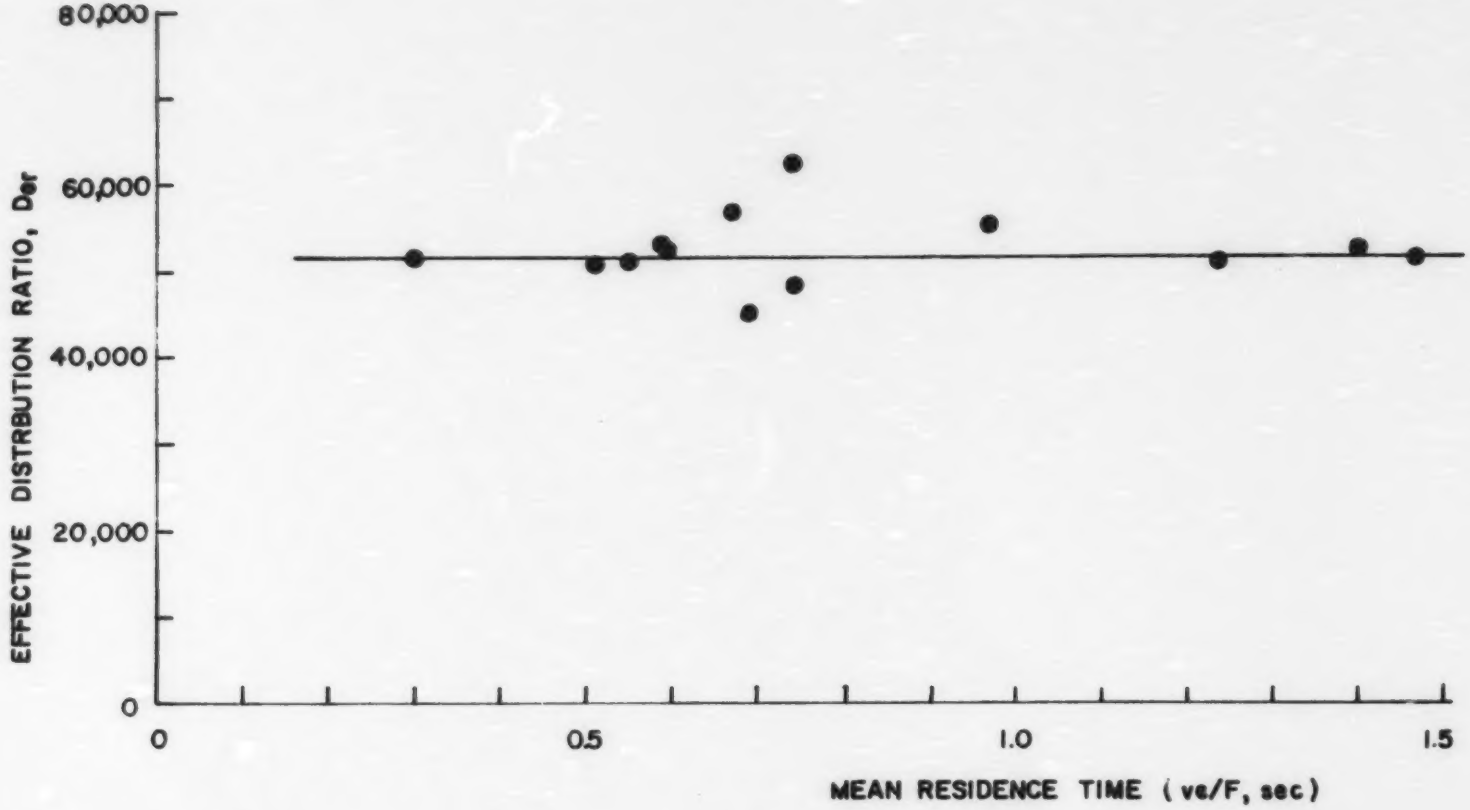

FIG. 20 . RELATION BETWEEN MEAN RESIDENCE TIME AND EFFECTIVE DISTRIBUTION RATIO FOR REACTION KINETICS MODEL AVERAGE VALUE OF D_{er} = 51,520

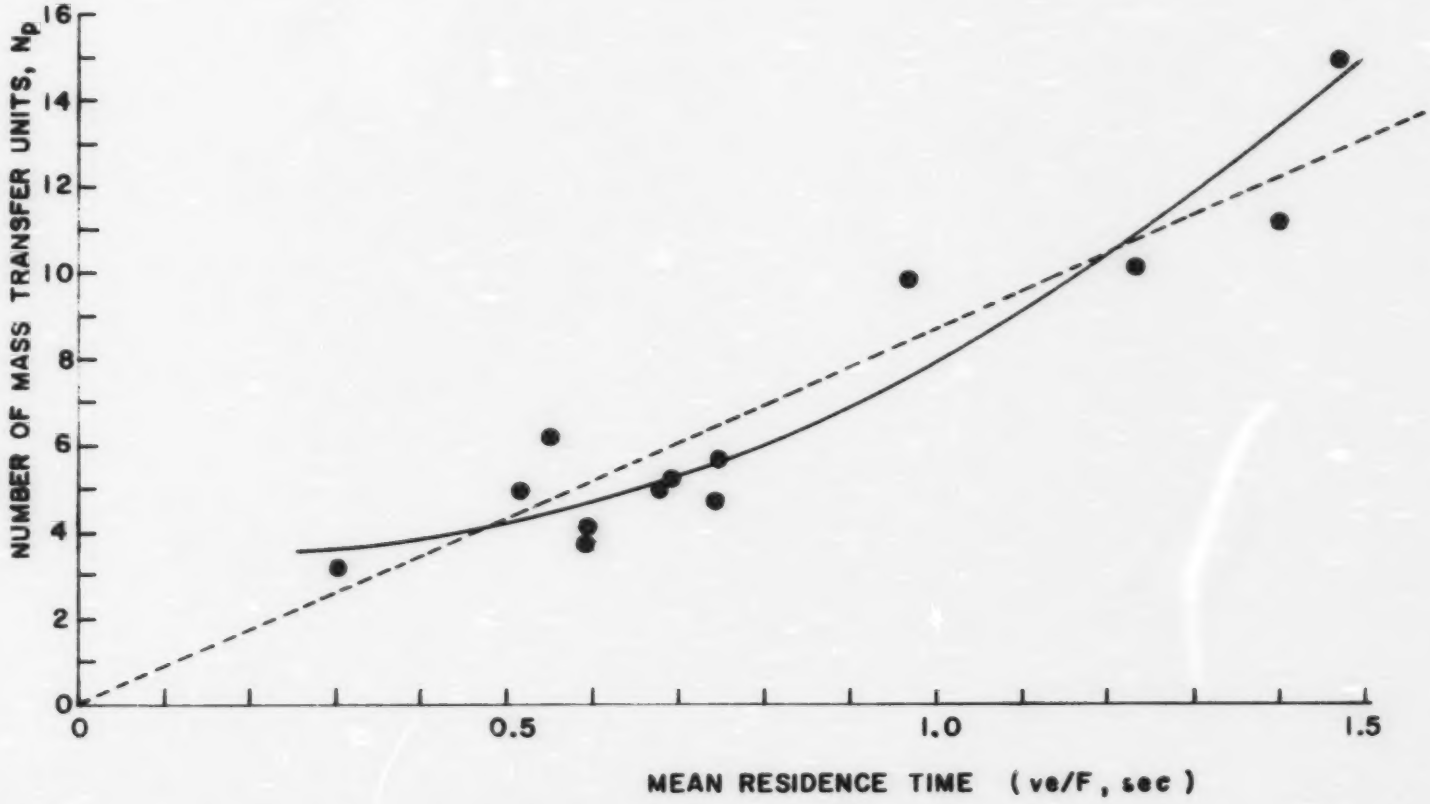

FIG. 21 . NUMBER OF MASS TRANSFER UNITS VERSUS RESIDENCE TIME FOR PARTICLE-PHASE DIFFUSION MODEL

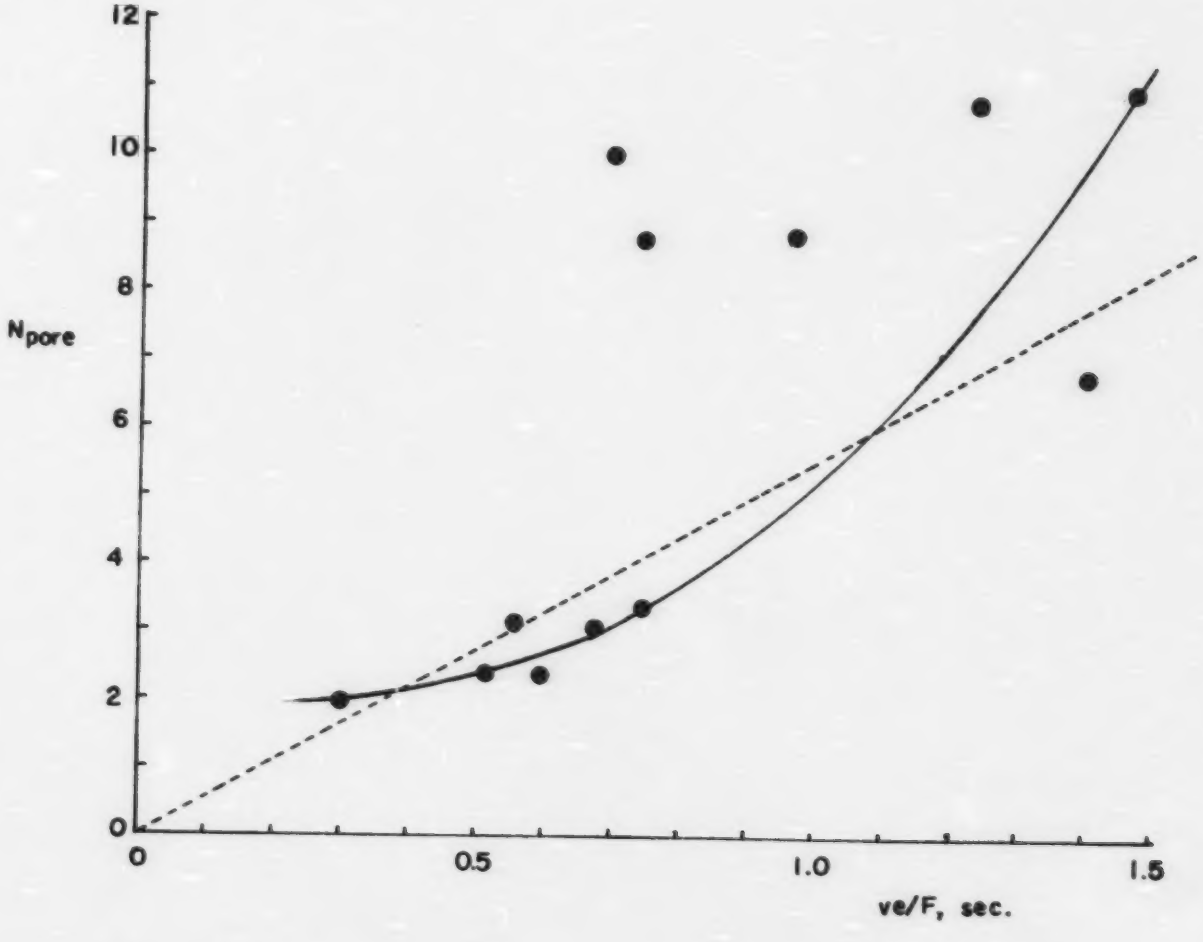

FIG. 22 . NUMBER OF MASS TRANSFER UNITS VERSUS RESIDENCE TIME FOR PORE DIFFUSION MODEL

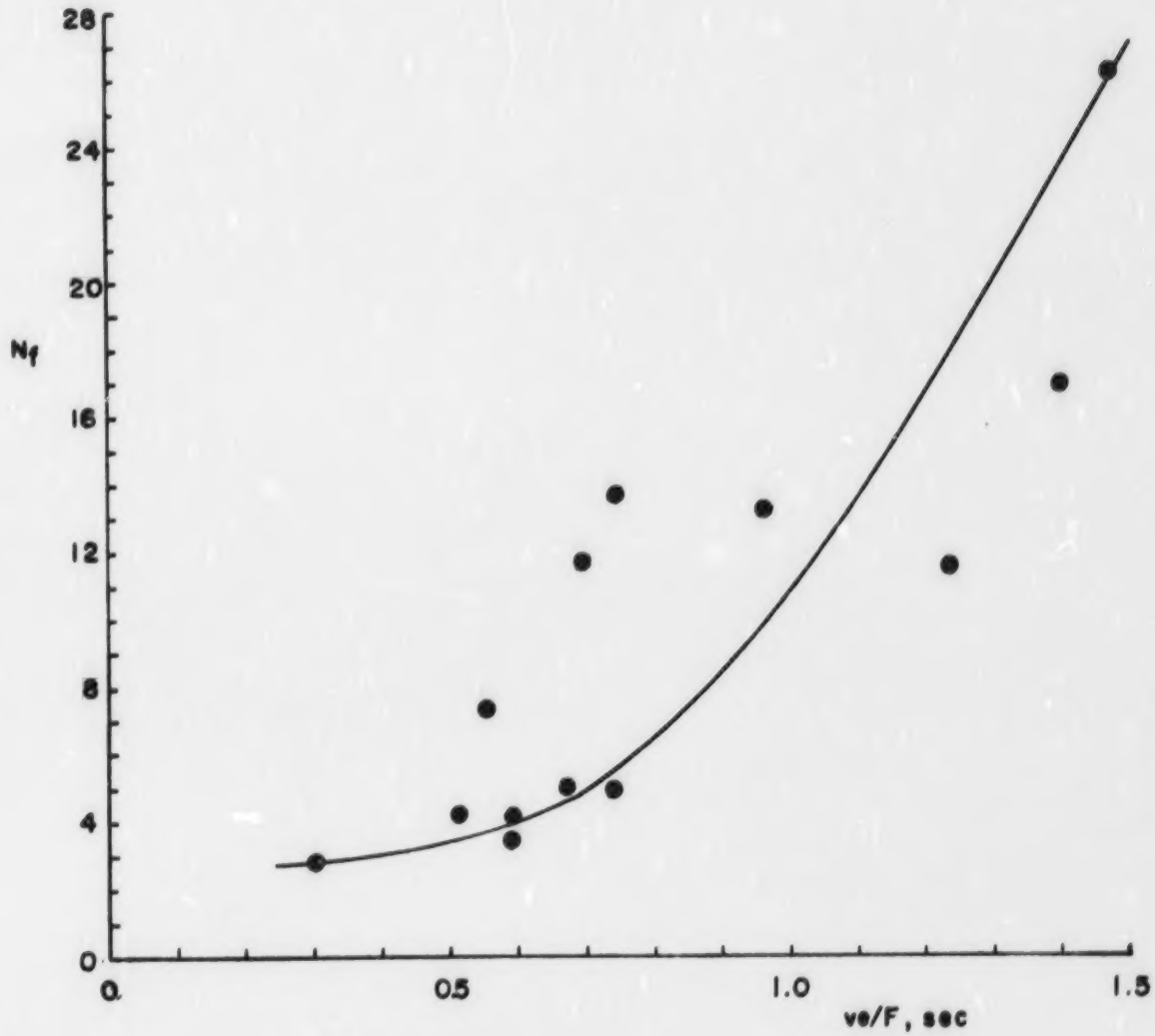

FIG. 23 . NUMBER OF MASS TRANSFER UNITS VERSUS MEAN RESIDENCE TIME FOR EXTERNAL DIFFUSION MODEL

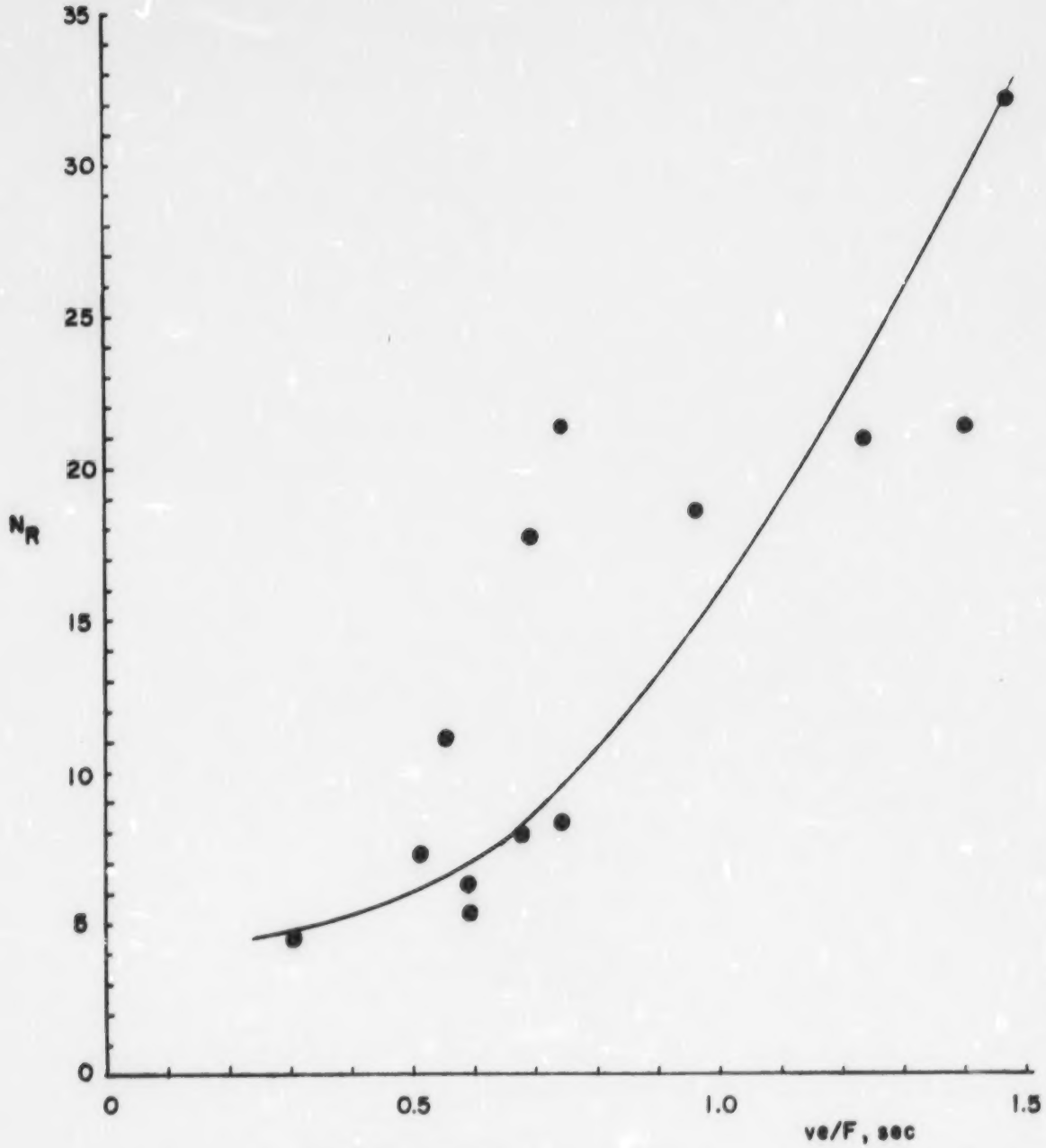

FIG. 24 . NUMBER OF MASS TRANSFER UNITS VERSUS RESIDENCE TIME FOR REACTION KINETICS MODEL

data, the constancy of the parameter is expected and in this respect it can be said that the parameter behaves realistically.

The particle-phase mass transfer coefficient, k_p, is not expected to depend upon superficial velocity or the residence time, $v\epsilon/F$, and therefore equation 26 predicts that N_p should be a linear function of $v\epsilon/F$. The plot of this parameter, Figure 21, shows a reasonably good linear relationship, however, the solid curve appears to fit the data somewhat better. In a qualitative sense this parameter also behaves realistically.

Using smoothed values of the two parameters as obtained from the solid curves on Figures 17 and 21 the breakthrough times (time when $C = 0.05\ C_o$) were back-calculated breakthrough times agreed with the experimental values to within 10 percent; N_p values obtained from the smooth curve on Figure 21 gave better results than values obtained from the linear relationship. A comparison of these experimental and calculated results is shown on Figure 25 and details of the calculation procedure are given in the appendix.

Pore Diffusion Model - As shown by Figure 18, the effective distribution ratio is constant as expected. Although the effective distribution coefficient is considerably smaller than the value calculated from equilibrium data, it at least shows qualitatively realistic behavior.

Because k_{pore} is expected to be independent of $v\epsilon/F$, a plot of N_{pore} versus $v\epsilon/F$ should be linear. Figure 23 shows that while there is considerable scattering to the data a linear relationship is not unreasonable. However, it was found that parameters obtained from the solid curve gave better results for the back calculation of breakthrough times. In addition to this qualitative evaluation it is possible to estimate the pore diffusivity and hence calculate values of N_{pore} corresponding to the conditions of each breakthrough curve. Wheeler (4) has derived the following equation for the calculation of pore diffusivity

$$D_{pore} = \frac{D_f x_p}{2} \left\{1 - Exp\left\{- \frac{4\ \bar{r}_p}{3\ D_f} \left(\frac{8 R_g\ T}{M}\right)^{0.5}\right\}\right. \qquad (57)$$

From the values of the internal void fraction, x_p, and average pore radius, $\bar{r}_p$, supplied by the Calgon Corporation (5) for Pittsburgh PCB charcoal the pore diffusivity, D_{pore}, was calculated. This value was then used to calculate N_{pore} via equations 47 and 49. Values of N_{pore} so calculated

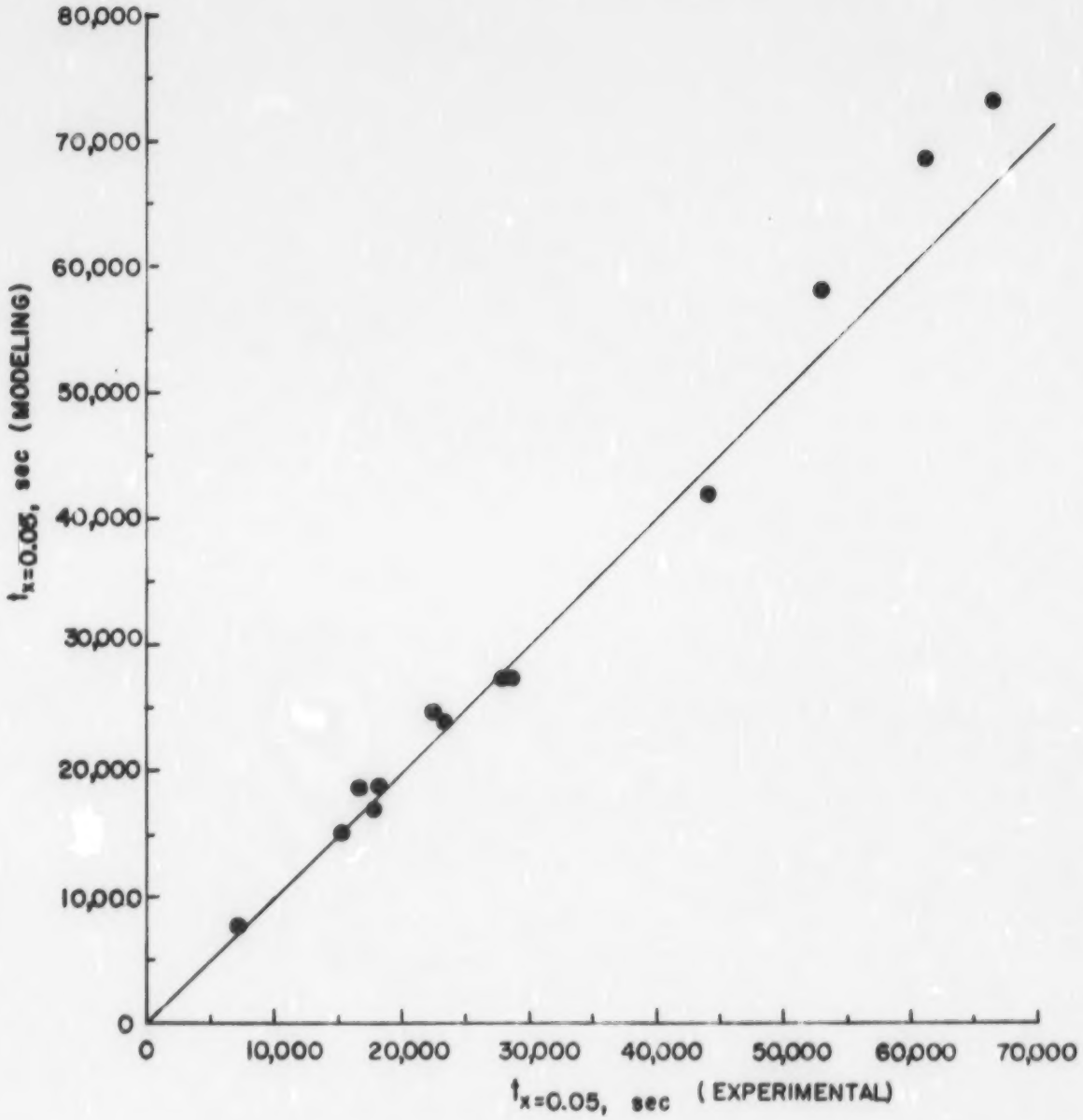

FIG. 25 . COMPARISON OF PARTICLE-PHASE MODELING BREAK-TIMES WITH EXPERIMENTAL VALUES

are compared with the N_{pore} values obtained from the modeling study in Table 7 where it is seen that the agreement is remarkably good.

Results of the back-calculation of breakthrough times using smoothed parameters from Figures 18 and 22 are shown on Figure 26. Again the back-calculated values agree with experimental values to within 10 percent.

Fluid-phase Diffusion Model - Figure 19 shows that the effective distribution ratio is again constant and hence qualitatively realistic.

Because the fluid-phase mass transfer coefficient will be a function of superficial velocity and hence not constant, no simple dependence of N_f upon v_e/F is expected. However, it is possible to estimate the mass transfer coefficient and hence calculate N_f for the conditions of each breakthrough curve. The correlation recommended by Wilke and Hougen (6) was used to estimate $k_f a$ and N_f was calculated via equation 20. The comparison of these estimated N_f values with those obtained from the model study is shown in Table 8 where it is seen that only fair agreement is obtained.

The back-calculation procedure was carried out with smoothed parameters from Figures 19 and 23 again obtaining agreement within ten percent with the experimental values. A comparison is shown on Figure 27.

Reaction Kinetics Model - As shown on Figure 20 the effective distribution ratio shows the same behavior as was found with the other model equations.

It has been shown that the number of reaction units, N_R, can be interpreted as being dependent upon both solid-phase and fluid-phase resistances. For this reason it is not expected that N_R will show a simple dependence on superficial velocity or v_e/F. That this is indeed the case can be seen from Figure 24. Thus, there appears to be no criterion by which N_R can be judged to be realistic except to say that N_R shows the same range of values as does N_p and N_f. This is to be expected if N_R is visualized as arising from the addition of resistances in series.

FIXED-BED CATALYTIC STUDY

The results of fixed-bed tests made with Pittsburgh BPL and PCB charcoal and ethylmercaptan are tabulated in Table 9 and a plot of conversion versus W/F for Pittsburgh BPL charcoal is shown on Figure 28. All data were taken at atmospheric pressure and a temperature of 30°C.

TABLE 7. COMPARISON OF CALCULATED N_{pore} VALUES WITH MODELING VALUES

Run No.	d_p mm	Pe	Calculated N_{pore}	Modeling N_{pore}
APC-14	1.41	11.61	3.59	3.00
APC-18	1.41	16.54	2.95	2.68
APC-19	1.41	22.63	2.94	2.68
APC-20	1.41	22.63	2.41	2.40
APC-21	1.41	22.63	1.61	2.00
APC-22	1.41	16.54	3.66	3.26
APC-26	1.41	54.54	2.42	2.55
APC-29	1.41	22.63	13.29	10.95
APC-30	1.41	34.47	8.73	4.85
APC-31	1.41	48.20	6.24	3.04
APC-32	1.41	41.36	7.27	3.25
APC-38	2.00	32.80	7.20	7.90
APC-39	1.68	27.55	10.04	10.00

TABLE 8. RESULTS OF CALCULATED N_f VALUES COMPARED WITH THE MODELING N_f

Run No.	D_{mm}^{P}	P_e	Calculated N_f	Modeling N_f
APC-14	1.41	11.61	6.35	4.6
APC-18	1.41	16.54	6.22	3.9
APC-19	1.41	22.63	7.22	3.9
APC-20	1.41	22.63	5.92	3.4
APC-21	1.41	22.63	3.95	2.6
APC-22	1.41	16.54	7.71	5.6
APC-26	1.41	54.54	9.17	3.7
APC-29	1.41	22.63	32.65	26
APC-30	1.41	34.47	26.34	9.9
APC-31	1.41	48.20	22.20	4.9
APC-32	1.41	41.36	24.00	5.6
APC-38	2.00	32.80	21.22	18
APC-39	1.68	27.55	27.15	23.3

TABLE 9. RESULTS OF FIXED-BED TESTS WITH ETHYLMERCAPTAN AND PITTSBURGH BPL CHARCOAL

Run No.	Charcoal Type	Charcoal Size (mesh)	Charcoal Weight (gm)	Influent Flow Rate (cc/min)	Influent Concentration (PPM)	Conversion %	Superficial Velocity (cm/sec)	W/F ($\frac{\text{gm charcoal}}{\text{cc of reactant/min}}$)
M-1	BPL	14	1.0	720	20	100	2.7	69
M-2	BPL	14	1.0	4700	20	77.5	39.5	10.6
M-3	BPL	14	1.0	4700	20	82.5	39.5	10.6
M-4	BPL	14	0.5	4700	20	30.0	39.5	5.3
M-5	BPL	14	1.0	4700	20	80.0	26.6	10.6
M-6	BPL	14	0.75	2800	60	70.0	15.8	4.46
M-7	BPL	14	1.0	2800	60	61.6	15.8	5.95
M-8	BPL	14	0.5	2800	60	41.7	15.8	2.97
M-9	BPL	14	1.0	2800	25	83.0	15.8	14.3
M-10	BPL	14	1.0	2800	45	70.0	15.4	7.93
M-11	BPL	14	1.0	1250	125	69.0	7.05	6.40
M-12	BPL	8	2.0	4700	20	86.5	20.6	21.3
M-13	BPL	8	1.0	4700	20	78.0	20.6	10.6
M-14	BPL	8	1.0	4000	50	59.0	17.5	5.00
4	PCB	-	2.0	710	27	100	—	104

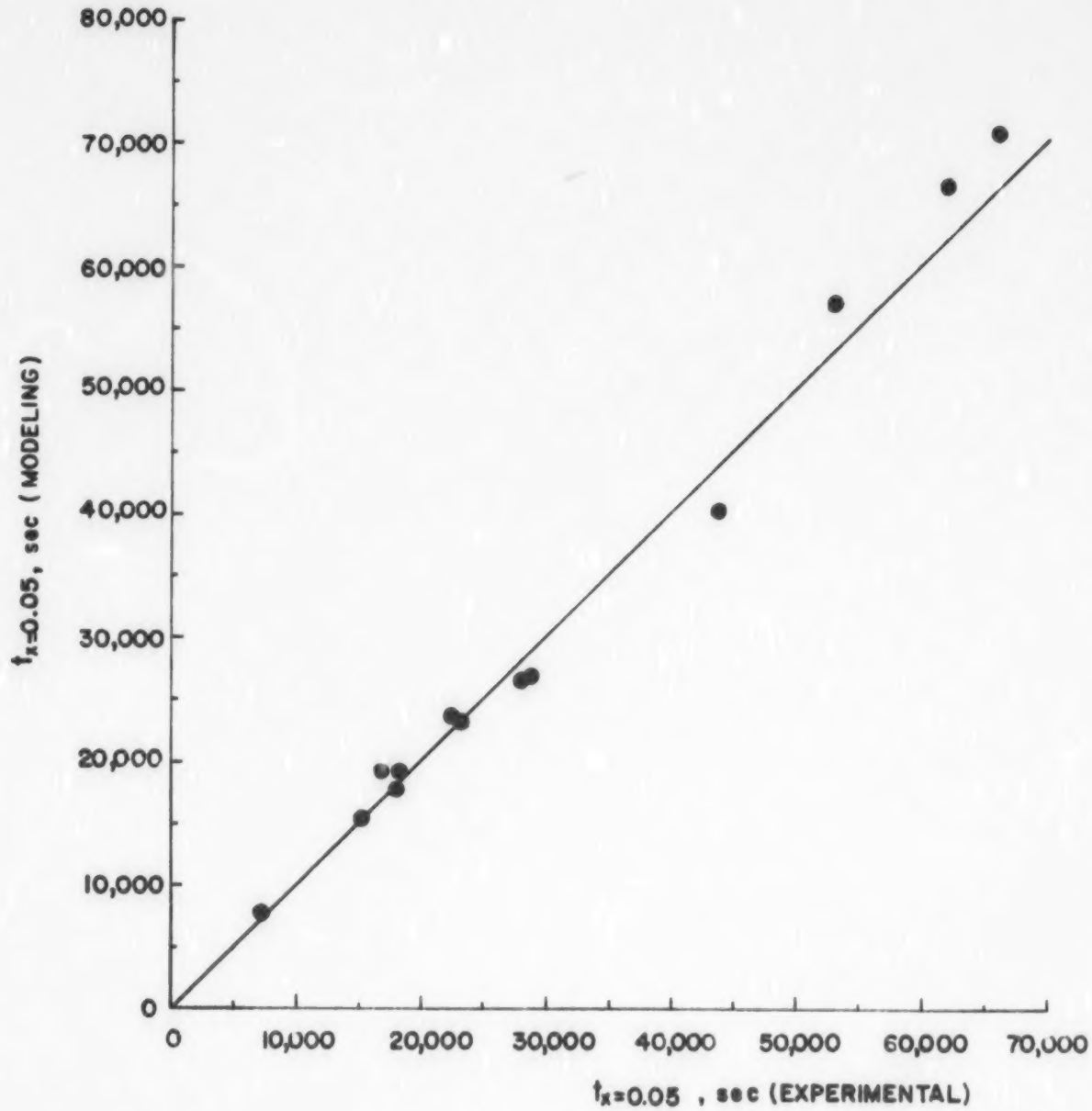

FIG. 26 . COMPARISON OF PORE DIFFUSION MODELING BREAK-TIME WITH EXPERIMENTAL VALUES

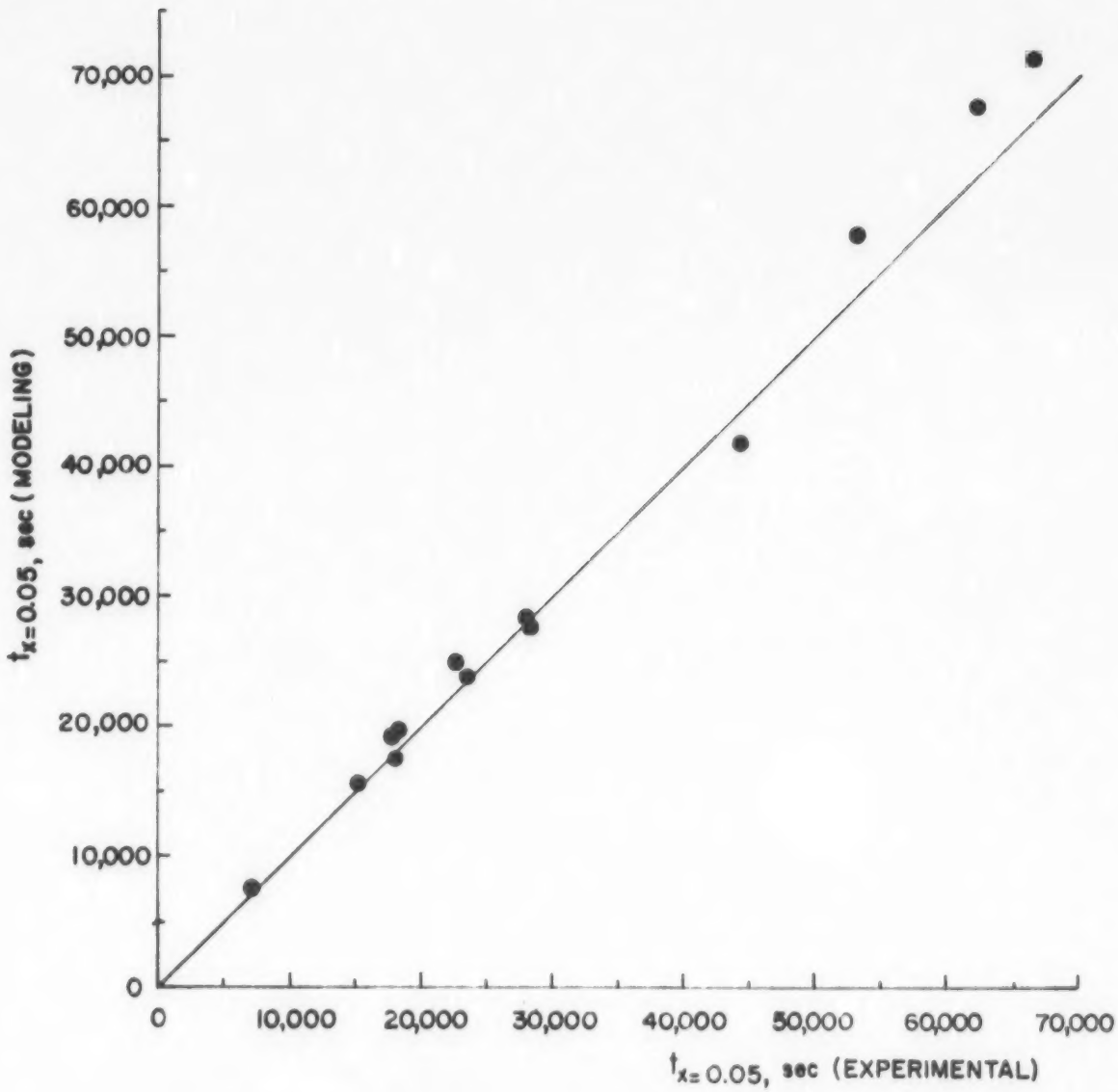

FIG. 27 . COPARISON OF EXTERNAL DIFFUSION MODELING BREAK-TIMES WITH EXPERIMENTAL VALUES

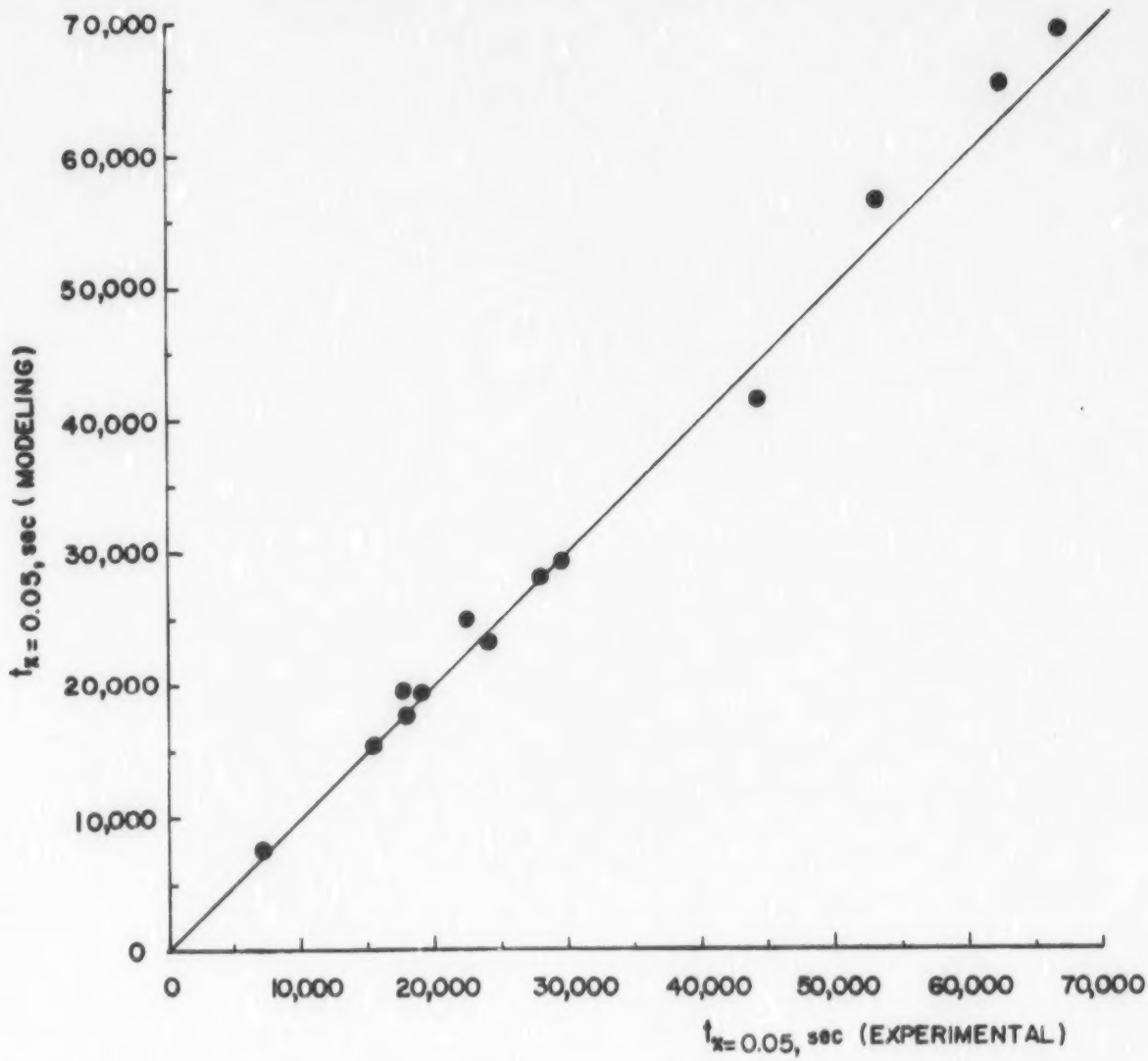

FIG. 28 . COMPARISON OF REACTION KINETICS MODEL BREAK-TIME DATA WITH EXPERIMENTAL VALUES

The data from a typical fixed-bed test are plotted on Figure 29. As shown on the figure, the effluent concentration of ethylmercaptan quickly attains its steady state value and after considerable time a new peak appears in the chromatographic analysis of the effluent stream. This new peak is believed to represent one or more reaction products which are apparently adsorbed onto the charcoal and begin to desorb as the charcoal becomes saturated. When saturation is approached, product is observed in the effluent stream with a concentration history closely resembling a conventional breakthrough curve.

Test M-3 was allowed to continue for seven days in order to observe whether the charcoal looses its catalytic efficiency with time; no indication of this was found. For the duration of the test the 1 gram of charcoal had removed 2.15 gram of ethylmercaptan. An extrapolation of published equilibrium data for ethylmercaptan on a similar charcoal in the absence of air (7) indicates that when saturated with respect to our influent stream (20 PPM) each gram of charcoal should adsorb about 0.03 grams of ethylmercaptan. Relative to its equilibrium adsorption capacity it is seen that the charcoal has catalyzed the oxidation of a large quantity of ethylmercaptan without loss of catalytic activity.

Mechanism Study

Before the reaction mechanism can be discerned from the fixed-bed data it is necessary to ensure that the reaction is not controlled by either external or internal diffusion.

External Diffusion Test - Tests M-2, M-3, and M-5 were all made with a bed containing 1 gram of charcoal and fed at the rate of 4700 cc/min of an influent stream containing 20 PPM of ethylmercaptan in air. Tests M-2 and M-3 were made with a bed geometry which resulted in a superficial velocity of 39.5 cm/sec. These tests showed conversions of 82.5% and 77.5% which indicates the degree of reproducibility obtainable. The test M-5 was made with a bed geometry which resulted in a superficial velocity of 26.6 cm/sec and showed a conversion of 80.0%. Because the conversion found for test M-5 is essentially the average of that found for the other two tests it can be said that a change in superficial velocity did not significantly affect the conversion. Thus external diffusion is not a rate-controlling resistance in this range of superficial velocity.

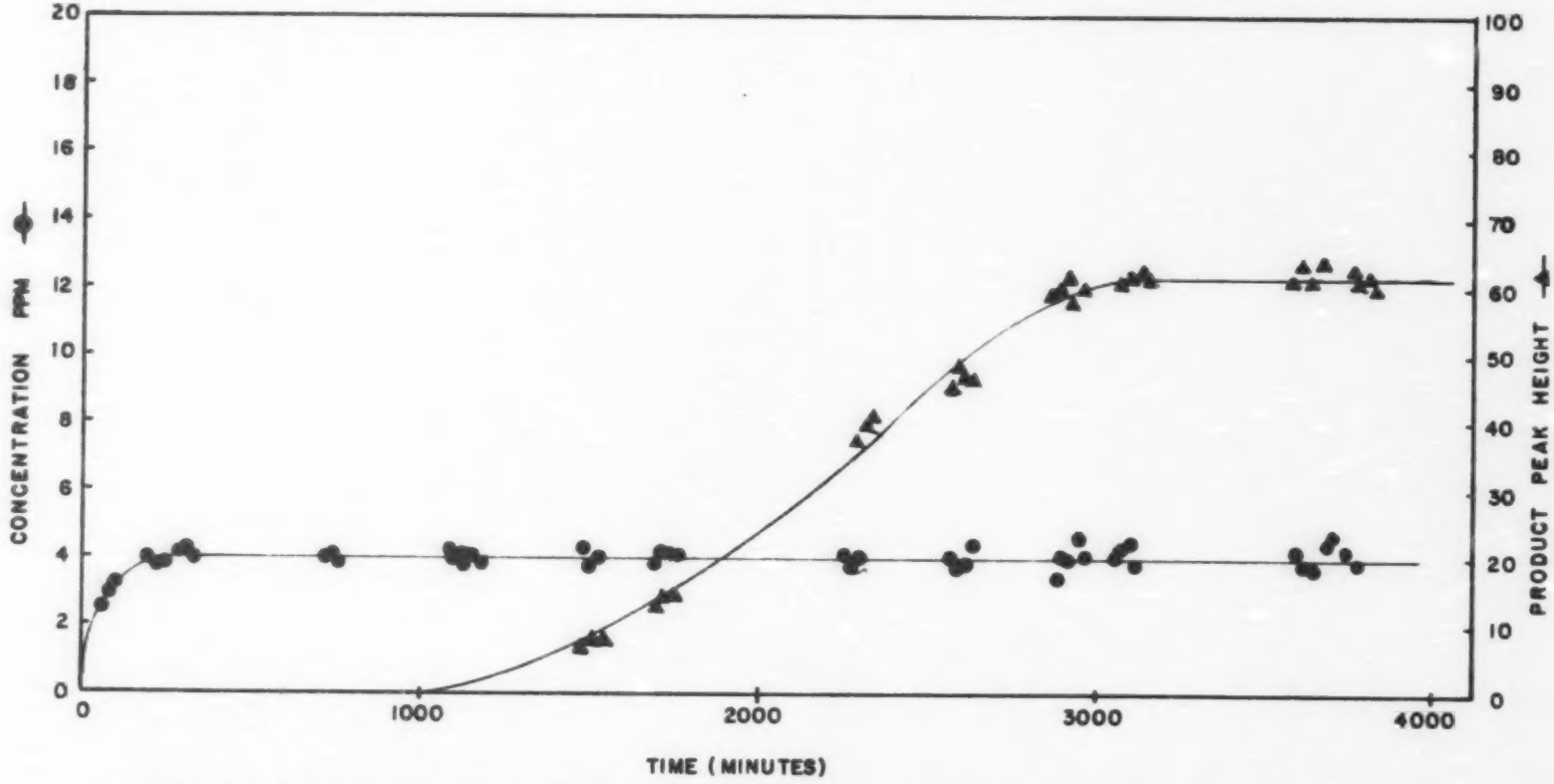

FIGURE 29. TYPICAL EFFLUENT HISTORY CURVES FOR THE CATALYTIC OXIDATION OF ETHYLMERCAPTAN. BY CHARCOAL.

Internal Diffusion Test - As can be seen from Figure 30 all data points fit a single curve when conversion is plotted versus W/F. Included on this plot are three data points representing tests made with 8 mesh charcoal thus indicating that the rate is unaffected by particle size. If internal diffusion were the rate-controlling step, the rate would be expected to depend upon the inverse square of the particle size and therefore a noticeable decrease in conversion should have been observed for the larger particle size. As this is not the case it appears that the rate of reaction is not limited by internal diffusion.

Test for Reaction Mechanism - Table 9 shows that essentially total conversion was found for test M-1; with this information it is not necessary to consider reaction mechanisms involving a reverse reaction term. The integrated reaction equation approach described in the Theory section of this report was used to analyze the data. Several simple reaction mechanisms were tested, but a one-half order reaction was found to best fit the data. For this mechanism the integrated rate equation is given by equation 53 which indicates that a straight line should result from a plot of $C_{Ao}^{1/2}[1-(1-x_A)^{1/2}]$ versus W/V. It is to be further noted that on such a plot the data for all values of C_o should lie on a single straight line passing through the origin. The data are plotted in this fashion on Figure 31 where it is seen that while there is some scattering, with the exception of the 125 PPM data point which lies considerably below the line, these conditions are satisfied. This low conversion found for the 125 PPM point might be due to the extremely low superficial velocity used for this test which could result in the reaction being controlled by external diffusion.

Hougen and Watson (8) have shown that a catalytic reaction one-half order in a reactant can be explained in terms of a mechanism whereby that reactant disassociates on the catalyst before participating in the reaction. Further, the effluent composition history curves for individual tests, such as shown on Figure 29, suggest that the reaction rate is not limited by the number of active sites because the rate of decomposition of reactant is unaffected by the buildup of product on the charcoal. This is probably the reason that the rate can be represented with a simple one-half order expression rather than requiring the more complex forms suggested by the active-site theory.

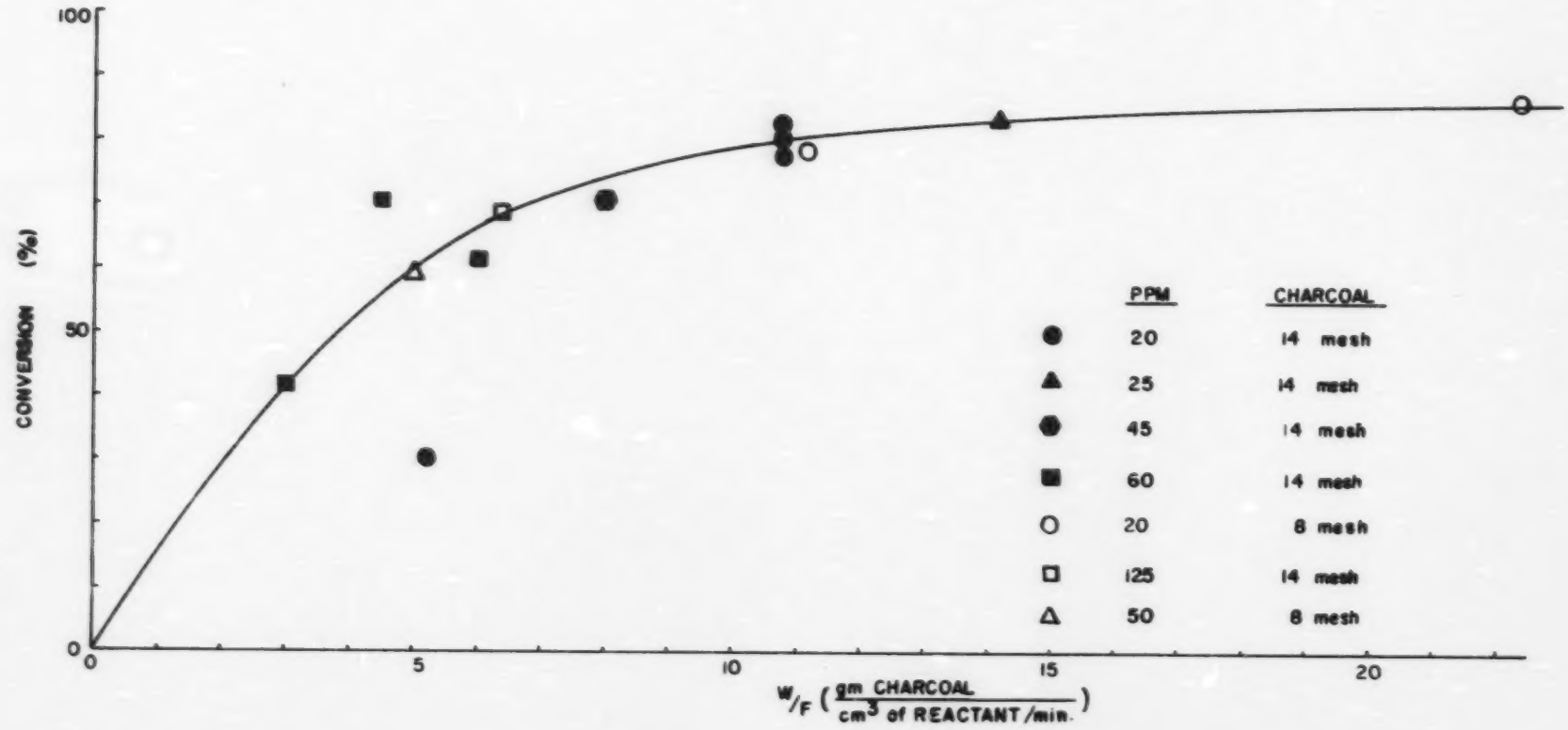

FIGURE 30. A PLOT OF CONVERSION VERSUS W/F FOR FIXED-BEDS OF PITTSBURGH BPL CHARCOAL FED WITH AN INFLUENT STREAM OF ETHYLMERCAPTAN IN AIR.

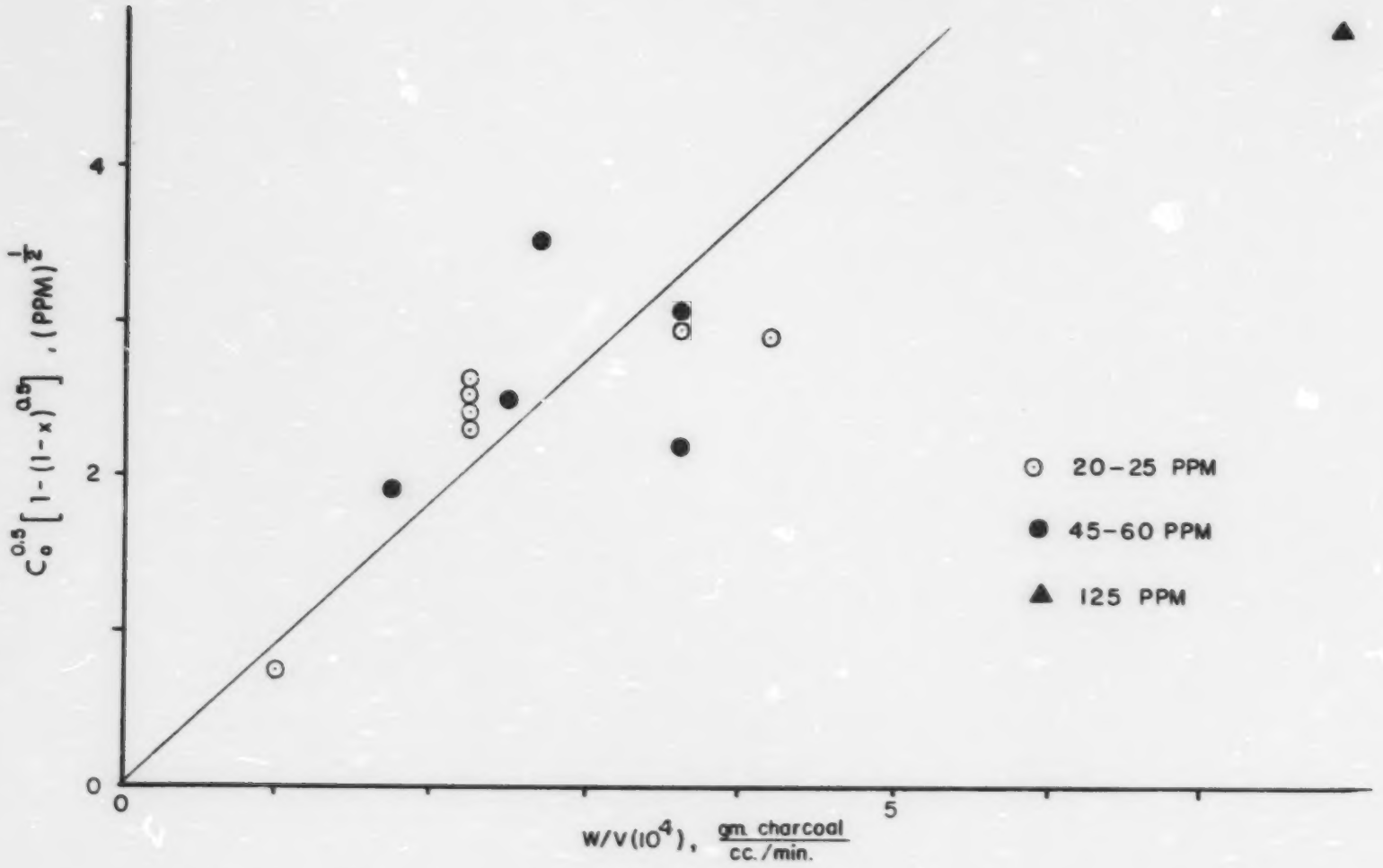

FIG. 31. TEST OF 0.5 ORDER REACTION

The above analysis applies to Pittsburgh BPL charcoal catalyst; the single fixed-bed test made with Pittsburgh PCB charcoal is insufficient to allow a similar evaluation of its catalytic effectiveness. It can only be said that this type of charcoal also possesses catalytic activity.

Reaction Products Identification

The mass spectrogram obtained from the sample which was collected by the trap on the chromatograph showed the presence of diethyldisulfide and some other peaks which could not be identified. Because of uncertainty associated with the other mass spectrographic analyses, diethyldisulfide appears to be the only reaction product we are able to identify. Since disulfides are known to be products of the air oxidation of mercaptans (9,10) the presence of diethyldisulfide in the reaction products is entirely reasonable.

Neutron Activation Analyses of Charcoal

An analysis of trace elements present in charcoal using neutron activation analysis was undertaken with the hope that this information might help explain the catalytic activity. Three types of charcoal were analyzed: Pittsburgh BPL, Pittsburgh PCB, and Barnebey-Cheney AC. The first is a coal-based charcoal and the others are derived from coconut shells. The results, listed in Table 10, were determined by subjecting the charcoal samples to differing degrees of neutron bombardment and determining their spectra after various decay times. It was originally intended to determine the concentration of each element, however before this could be accomplished it became necessary to change detectors and thereby the calibration was lost.

TABLE 10. ELEMENTS PRESENT IN CHARCOAL SAMPLES AS DETERMINED BY NEUTRON ACTIVATION ANALYSIS

Element	Pittsburgh BPL	Pittsburgh PCB	Barnebey-Cheney AC
Sodium	970 ppm	740 ppm	313 ppm
Manganese	288 ppm	224 ppm	140 ppm
Vanadium	119 ppm	0	36 ppm
Potassium	X	X	X
Chlorine	X	X	X
Aluminum	2541 ppm	X	X
Cobalt	X	0	0
Iron	X	X	0
Scandium	X	0	0
Cesium	X	X	---
Rubidium	X	0	---
Barium	X	0	---
Gold	X	0	---
Lanthanum	X	0	---

X denotes the presence of an element

0 denotes the absence of an element

--- indicates that a test was not made

APPLICATION TO DESIGN

ACETALDEHYDE REMOVAL

The operation of a fixed-bed adsorber is cyclic. First, a bed of freshly regenerated adsorbent is contacted with the influent stream containing the adsorbate and operated until the adsorbate concentration in the effluent stream reaches some predetermined level, normally about 5% of the influent value. The bed is then regenerated in preparation for another adsorption cycle. Thus the design of this type of system requires that both the adsorption and desorption behavior be known and understood.

The ultimate design objective would be a priori approach where the mathematical description of the system could be formulated then transformed into useable form from a knowledge of adsorbent properties such as particle size, average pore size and bed porosity, fluid properties such as viscosity and diffusivity, and system variables such as temperature, pressure, and fluid flow rate. In addition to the often intractable mathematics, problems arise because some of the phenomena are often not completely understood nor is the basic physical data available to implement the computations for those phenomena which are understood. Failing in this a priori approach the next best strategy appears to be the modeling approach. Here, small scale experiments with the proposed adsorbate-adsorbent systems are required before sufficient understanding and mathematical description for design purposes are possible.

The original intent of this study was to conduct enough small scale experiments for the acetaldehyde-Pittsburgh PCB charcoal system so that a realistic model could be selected and the model parameters (e.g. distribution ratio, separation factor, and number of transfer units) evaluated and correlated against the pertinent system variables. From our experiments it appears that the solid-phase diffusion model and the pore diffusion model are realistic and could safely be used to design a fixed-bed adsorber operating at 30°C with an influent stream containing 28 PPM of acetaldehyde. While the separation factor is known and the number of transfer units can be estimated, design for other influent concentrations would involve considerable uncertainty about the value of the effective distribution ratio.

The design of an adsorber fed with an influent stream containing 28 PPM of acetaldehyde and operated at 30°C can be accomplished by using the model breakthrough equations with the smoothed parameters or if the conditions are equivalent, by directly employing the experimental data. This is possible because the model equations are written in dimensionless form. Thus, for the same charcoal particle size and superficial velocity the break time obtained from a small, laboratory scale bed would apply for a bed of much larger dimensions providing that the ratio v/F is the same for both.

The design of an adsorber fed with an influent stream containing between 35 and 1 PPM of acetaldehyde and operated at 30°C can be accomplished via the solid-phase diffusion model equation, equation 25, if the effective distribution ratio can be estimated for influent concentrations other than 28 PPM. The distribution ratio is defined by equation 56, however, recall that it was found necessary to use an effective distribution ratio which was determined by fitting the breakthrough data to a model equation. For the solid-phase diffusion model a constant value of 57,865 was found for the influent concentration of 28 PPM. Since w/v$_e$ is expected to be constant for a given charcoal, equation 56 suggests that an effective distribution ratio for other influent concentrations would be

$$D_e = 57{,}865 \left[\frac{q_o^*}{0.0078}\right] \left[\frac{28}{C_o}\right]$$

where q_o^* and C_o represent a point on the equilibrium curve, Figure 13, corresponding to the desired influent concentration, C_o.

The typical adsorption system would probably consist of a set of three fixed-beds: one operating, one regenerating, and one cooling. The required amounts of charcoal corresponding to various removal percentages and influent concentrations are shown in Table 12 for the case where each bed spends one hour on stream and two hours regenerating and cooling. An average superficial velocity of 50 ft/min (reference 3) was used for these calculations. Until the regeneration process is better understood, more detailed calculations do not seem to be justified. However, the data of Table 12 indcate that fixed-bed adsorption appears to be a feasible means of removing acetaldehyde vapor from low concentrations in air.

ETHYLMERCAPTAN REMOVAL

The rate of ethylmercaptan oxidation on charcoal was not found to depend on superficial velocity or on charcoal particle size and therefore a reactor can be designed from equation 53, the integrated rate equation. The value of k determined from the slope of the straight line on Figure 31 is 0.117 $gmole^{1/2}\ cc^{1/2}\ min^{-1}\ gm\ charcoal^{-1}$. With this k we can determine the mass of catalyst required to achieve any conversion at 30°C and for any influent concentration in the range 20 to 125 PPM. In Table 11 are listed the pounds of charcoal required to remove various percentages of ethylmercaptan from 100 cfm of air containing various influent concentrations.

TABLE 11. AMOUNT OF CHARCOAL REQUIRED TO REMOVE VARIOUS PERCENTAGES OF ETHYLMERCAPTAN FROM VARIOUS CONCENTRATIONS IN AIR AT 30°C.

Influent Concentration (PPM)	Pounds of Charcoal per 100 cfm Air		
	90%	95%	99%
25	2.32	2.64	3.06
50	3.26	3.72	4.30
75	4.01	4.56	5.29
100	4.61	5.25	6.09
125	5.15	5.86	6.80

TABLE 12. AMOUNT OF CHARCOAL REQUIRED TO REMOVE VARIOUS PERCENTAGES OF ACETALDEHYDE FROM VARIOUS INFLUENT CONCENTRATIONS IN AIR AT 30°C

Influent Concentration (PPM)	Pounds of Charcoal per 100 cfm Air		
	90%	95%	98%
10	69	81	93
20	75	87	100
28	78	90	102
35	81	93	105

REFERENCES

1. Vermeulen, T., "Separation by Adsorption Methods," Vol. II Advances in Chemical Engineering, edited by T. B. Drew and J. W. Hoopes, Academic Press, New York (1958).

2. Altshuller, A. P. and Cohen, I. R., "Application of Diffusion Cells to the Production of Known Concentrations of Gaseous Hydrocarbons," Analytical Chemistry, 32 802 (1960).

3. Barnebey, H. L., "Activated Charcoal in the Petrochemical Industry," Chemical Engineering Progress, 67 (1971).

4. Wheeler, A., "Reaction Rates and Selectivity in Catalyst Pores," Advances in Catalysis, 2 250 (1951).

5. Manufacturer's Technical Data for Pittsburgh Activated Carbon, The Calgon Corporation.

6. Wilke, C. R., and Hougen, O. A., "Mass Transfer in the Flow of Gases through Granular Solids Extended to Low Modified Reynolds Numbers," Transactions American Institute of Chemical Engineers, 41, 445 (1945).

7. Grant, R. J., Manes, M., and Smith, S. B., "Adsorption of Normal Paraffins and Sulfur Compounds on Activated Carbon," American Institute of Chemical Engineers Journal, 8, 403 (1962).

8. Hougen, O. A., and Watson, K. M., "Chemical Process Principles," Part three, John Wiley and Sons, New York, 1946.

9. Wertheim, E., "Textbook of Organic Chemistry," Blakiston, Philadelphia, 1945.

10. Reid, E. E., "Organic Chemistry of Bivalent Sulfur," Vol. 1, Chemical Publishing Co., 1958.

NOMENCLATURE

a	Surface area per unit volume of packed-bed
A	Quantity of adsorbent
b	Constant
C	Concentration
C_o	Initial concentration
D	Distribution ratio, defined by equation 56
D_f	Diffusivity
dp	Particle diameter
D_p	Particle diffusivity
D_{pore}	Pore diffusivity
F	Feed rate
F_{Ao}	Feed rate of component A
k	Kinetic rate constant
k_f	Fluid-phase mass transfer coefficient
k_p	Particle-phase mass transfer coefficient
k_{pore}	Pore mass transfer coefficient
L	Length
M	Molecular weight
N_f	Number of fluid-phase mass transfer units
N_p	Number of particle-phase mass transfer units
N_{pore}	Number of pore mass transfer units
N_R	Number of reactor units
p	Partial pressure
P	Total pressure
p_o	Upper limit of fluid-phase pressure
q	Concentration of adsorbate in solid phase
$\bar{q}$	Average concentration of adsorbate in solid phase
q_m	Maximum concentration of adsorbate in solid phase
q_o^*	Concentration of adsorbate in solid phase in equilibrium with initial fluid phase adsorbate concentration
r	Radius
r	Rate of chemical reaction

NOMENCLATURE (Continued)

R	Separation factor, defined by equation 15
r_i	Internal particle radius
r_p	External particle radius
$\bar{r}_p$	Average pore radius
R_g	Gas Law Constant
S	Cross sectional area
t	Time
T	Absolute temperature
v	Bed volume
V	Volume of fluid entering bed
V_s	Volume of adsorption system
W	Mass of packed bed
X	Dimensionless fluid-phase concentration
X*	Dimensionless fluid-phase concentration in equilibrium with solid phase
x_A	Conversion of component A in a chemical reaction
x_p	Internal void fraction of particle
Y	Dimensionless solid-phase concentration
Y*	Dimensionless solid-phase concentration in equilibrium with fluid phase
Z	Through-put parameter, defined by equation 5
α_f	Constant in equation 21
α_p	Constant in equation 35
β	Correction factor for addition of resistances
ε	Void fraction of packed bed
ρ_b	Bulk density of packed bed

APPENDIX

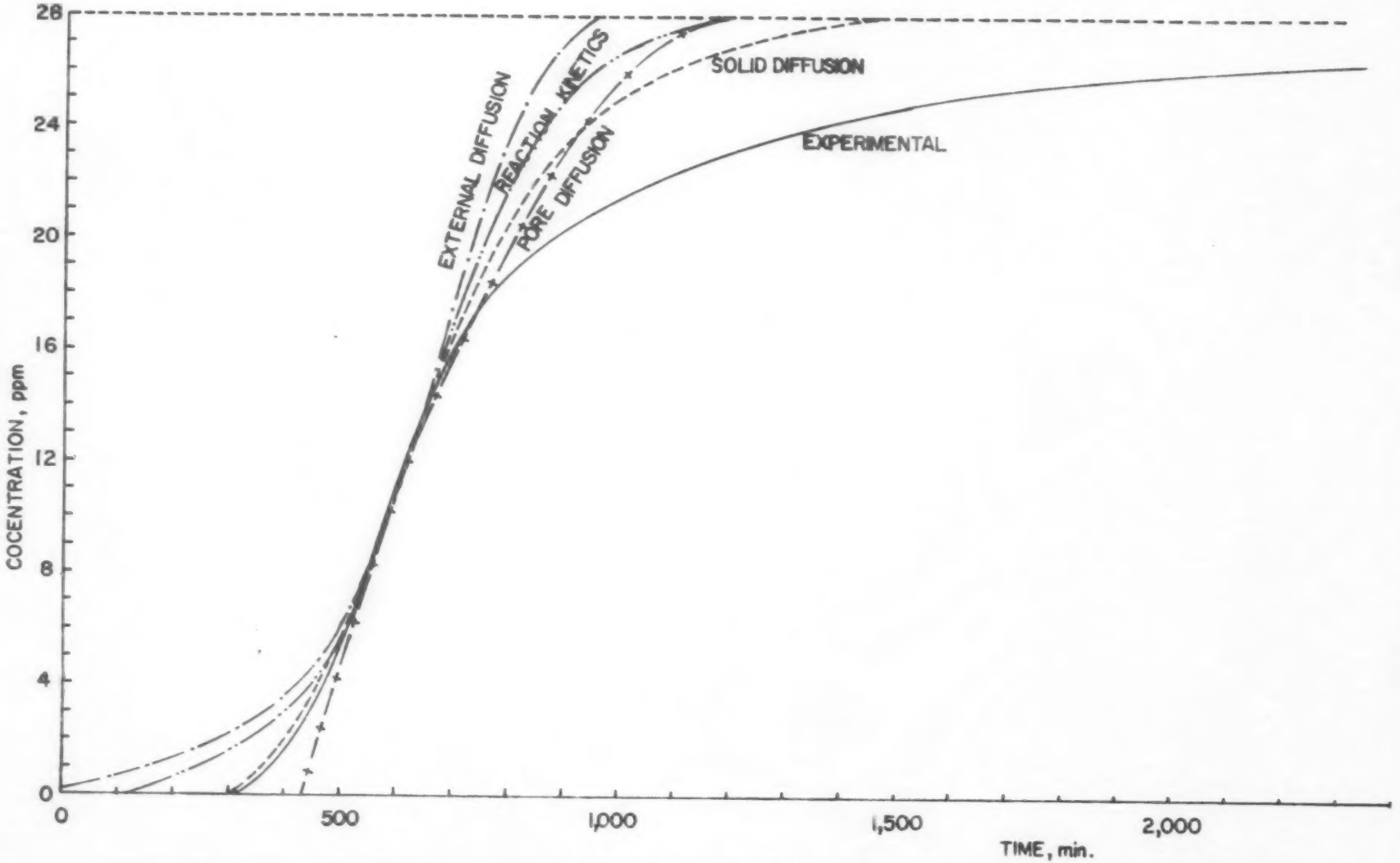

FIG. (A-1). APC-14, FIXED-BED TEST WITH 14 MESH CHARCOAL, 8.56 cm DEEP BED, AND 16.67 cc/sec FLOW RATE COMPARED WITH MODEL BREAKTHROUGH CURVES

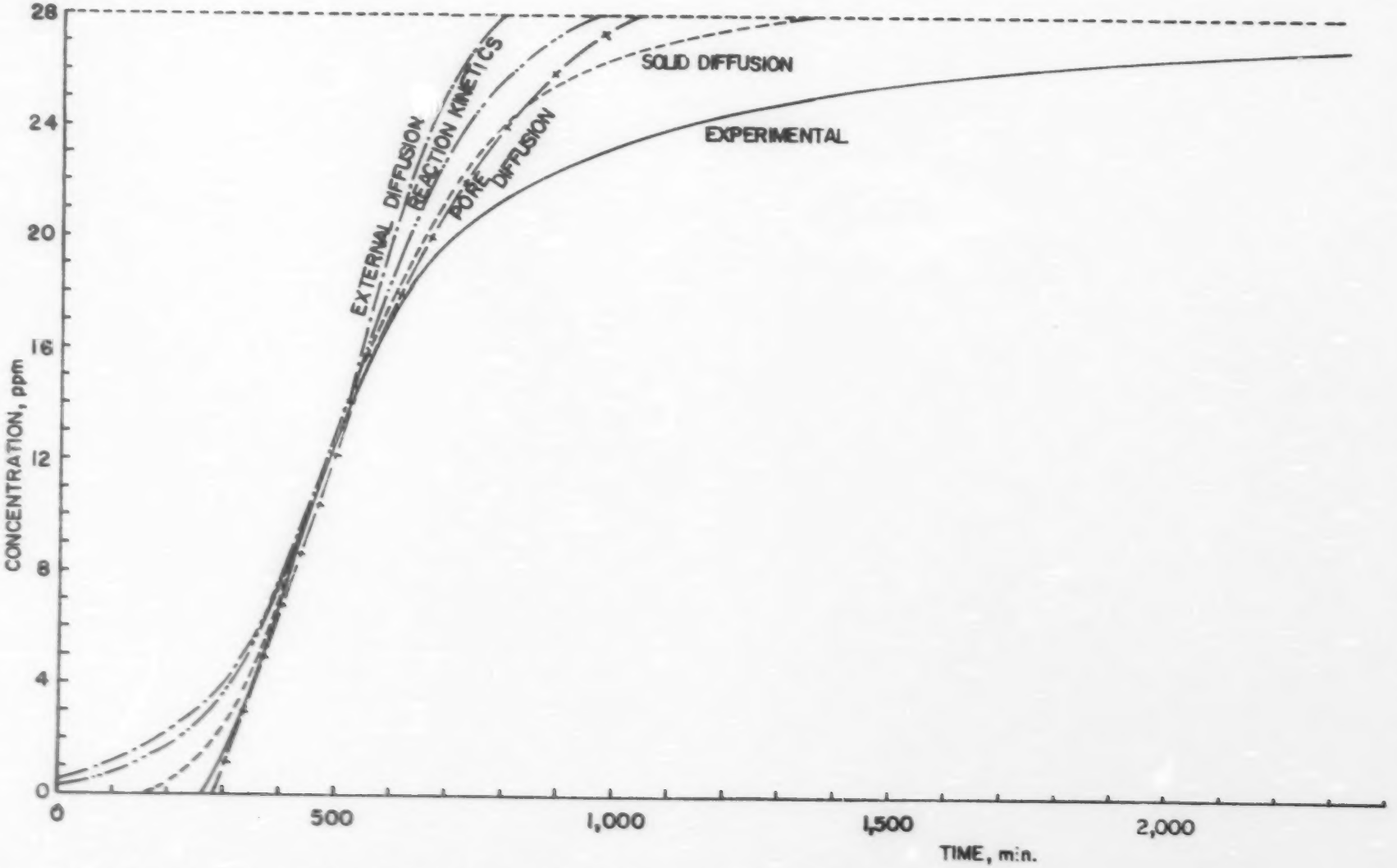

FIG. (A-2). APC-18, FIXED-BED TEST WITH 14 MESH CHARCOAL, 10.16 cm DEEP BED, AND 23.75 $^{cc}/_{sec}$ FLOW RATE COMPARED WITH MODEL BREAKTHROUGH CURVES

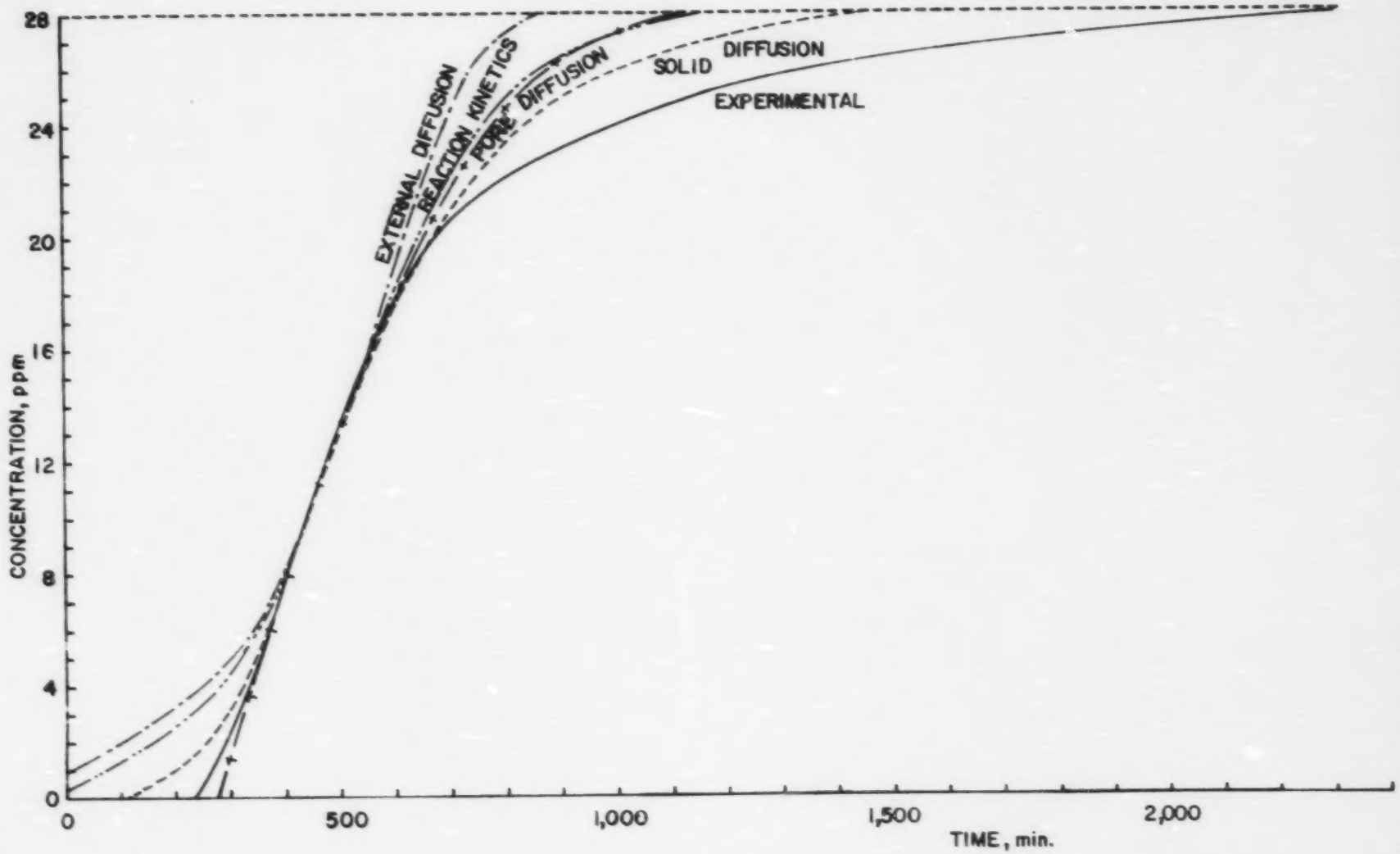

FIG.(A-3). APC-19, FIXED-BED TEST WITH 14 MESH CHARCOAL, 13.82 cm DEEP BED AND 32.5 cc/sec FLOW RATE COMPARED WITH MODEL BREAKTHROUGH CURVES

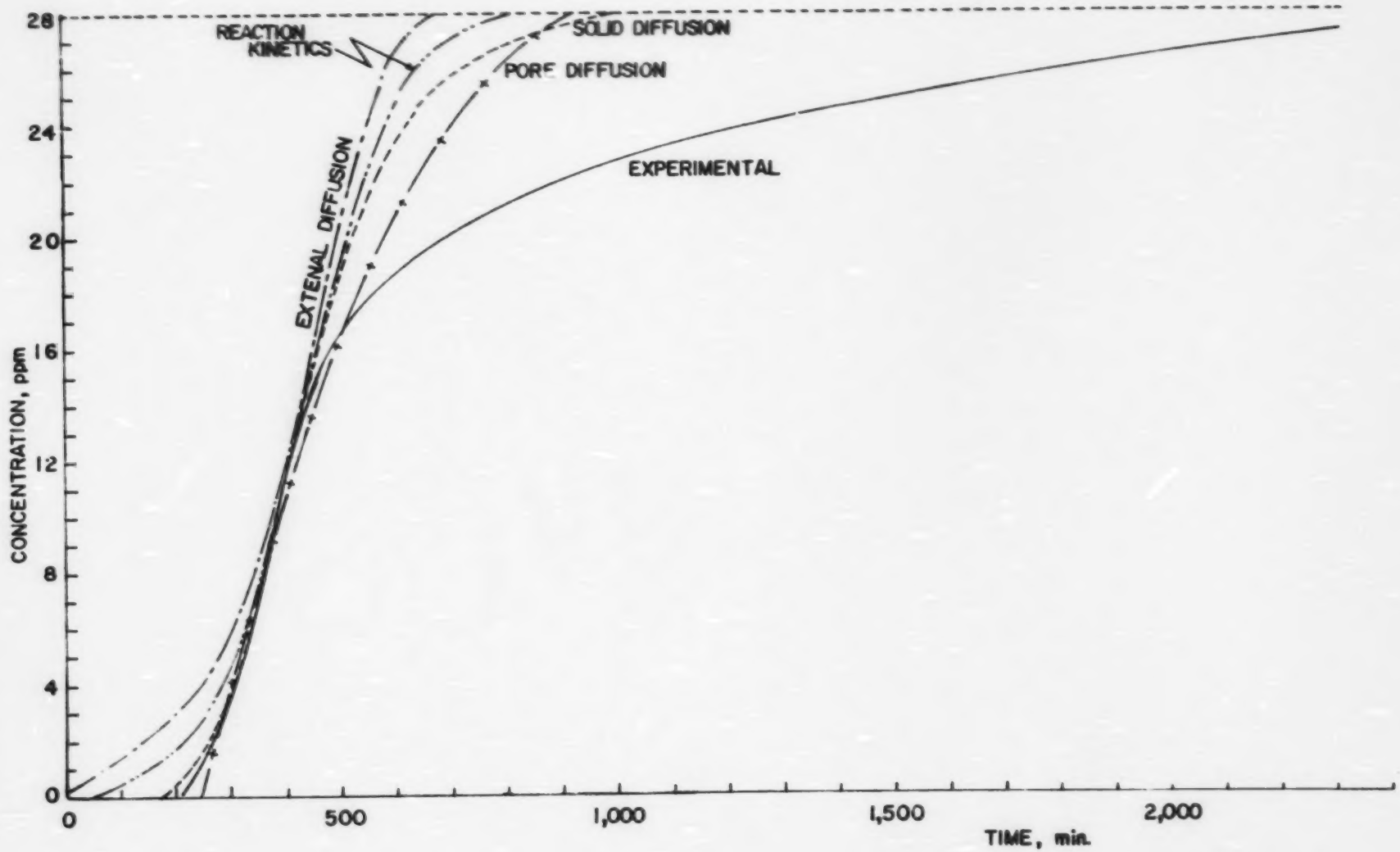

FIG.(A-4). APC-20, FIXED-BED TEST WITH 14 MESH CHARCOAL, 11.33 cm DEEP BED AND 32.5 cc/sec FLOW RATE COMPARED WITH MODEL BREAKTHROUGH CURVES

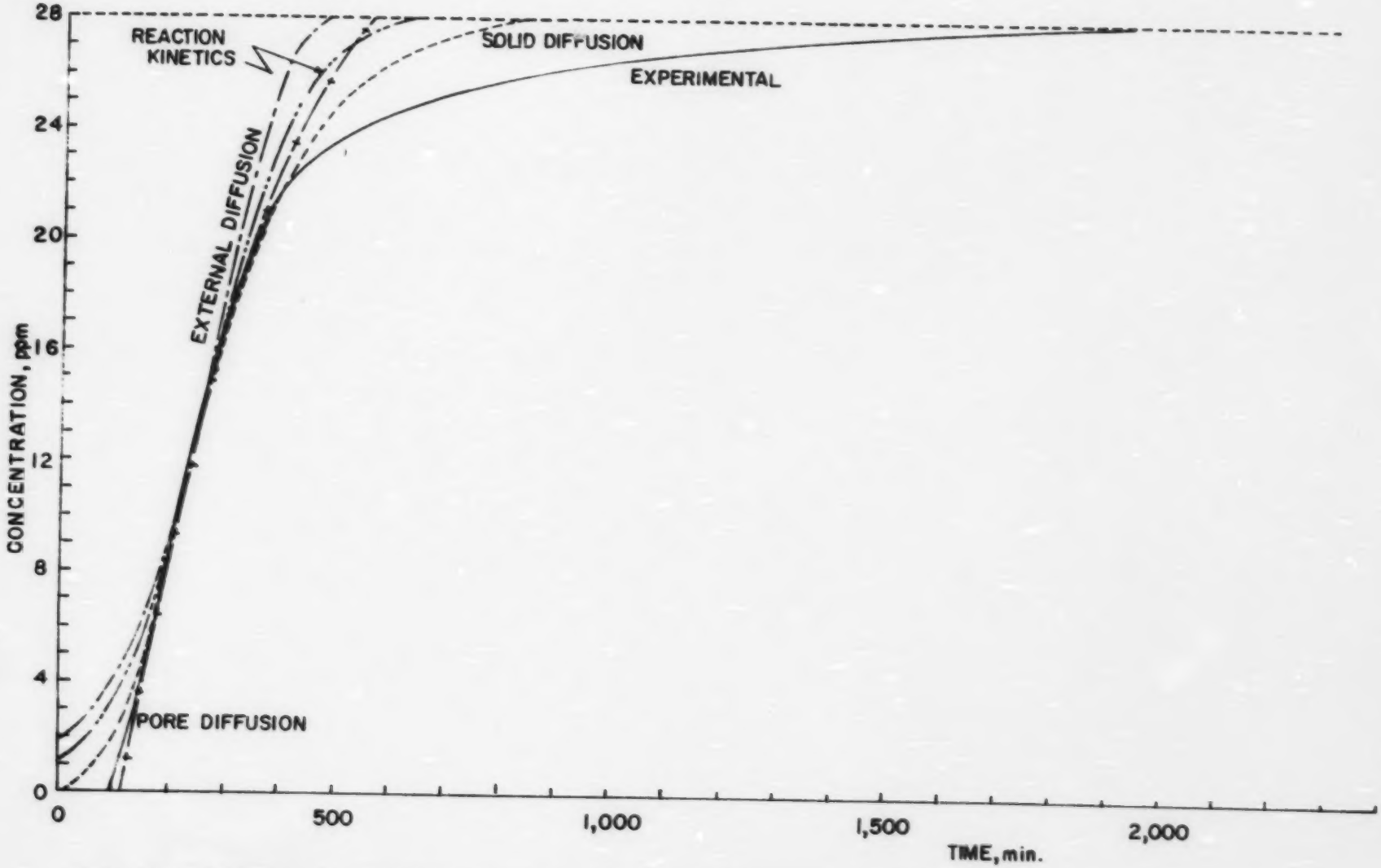

FIG. (A-5). APC-21, FIXED-BED TEST WITH 14 MESH CHARCOAL, 7.56 cm DEEP BED, AND 32.5 cc/sec FLOW RATE COMPARED WITH MODEL BREAKTHROUGH CURVES

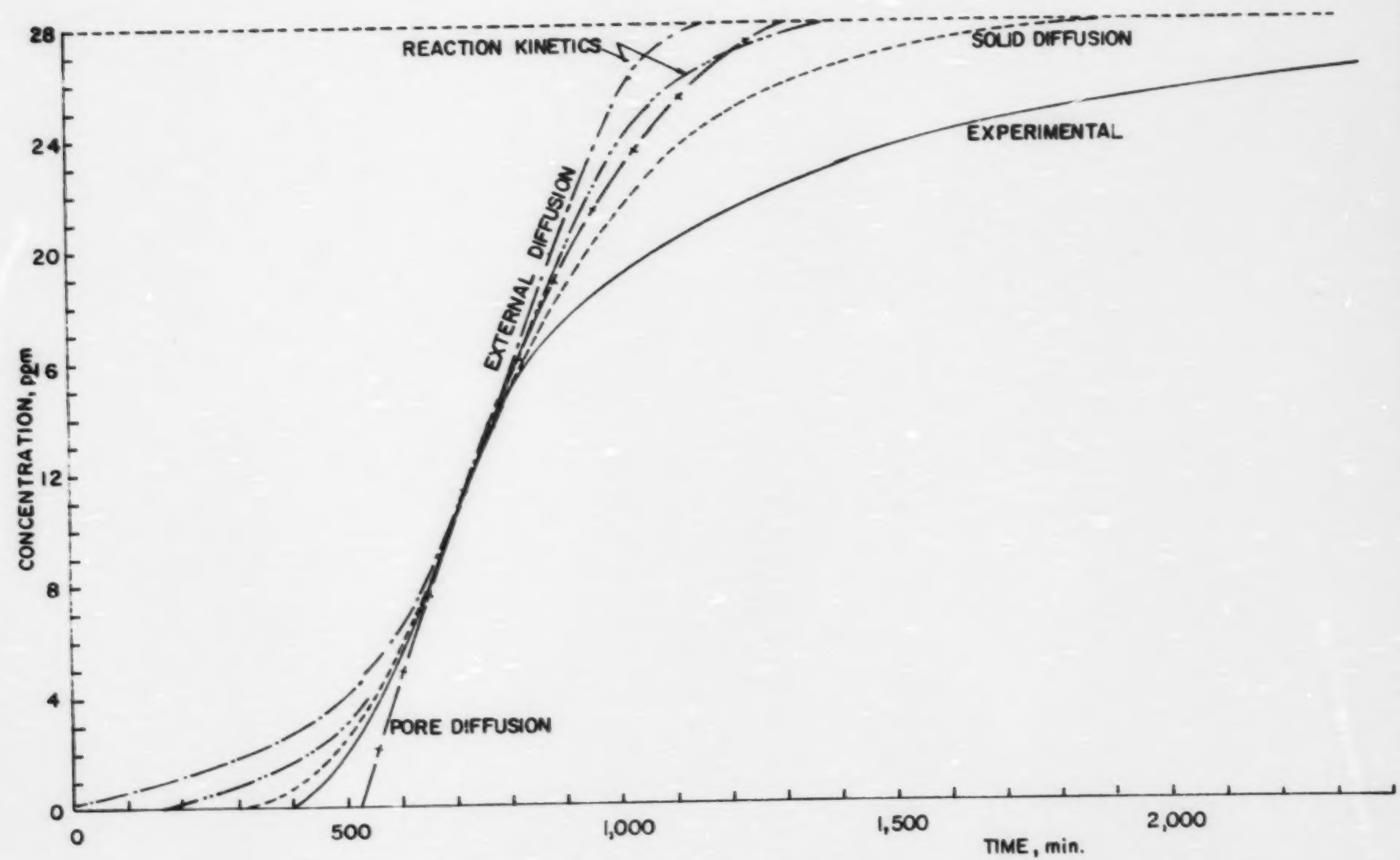

FIG.(A-6). APC-22, FIXED-BED TEST WITH 14 MESH CHARCOAL, 12.59 cm DEEP BED, AND 23.75 cc/sec FLOW RATE COMPARED WITH MODEL BREAKTHROUGH CURVES

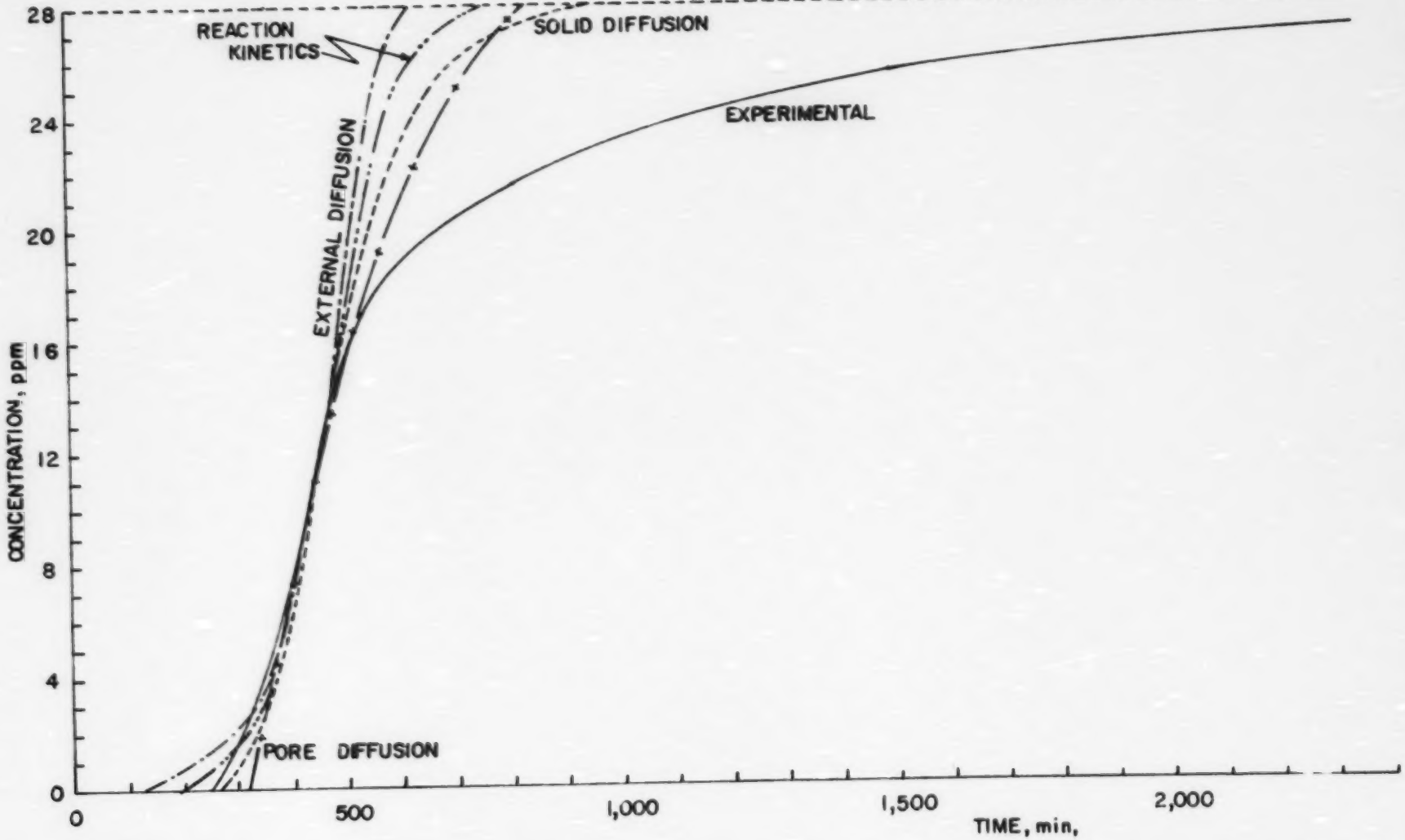

FIG.(A-7). APC-26, FIXED-BED TEST WITH 14 MESH CHARCOAL, 20.32 cm DEEP BED, AND 78.33 cc/sec FLOW RATE COMPARED WITH MODEL BREAKTHROUGH CURVES

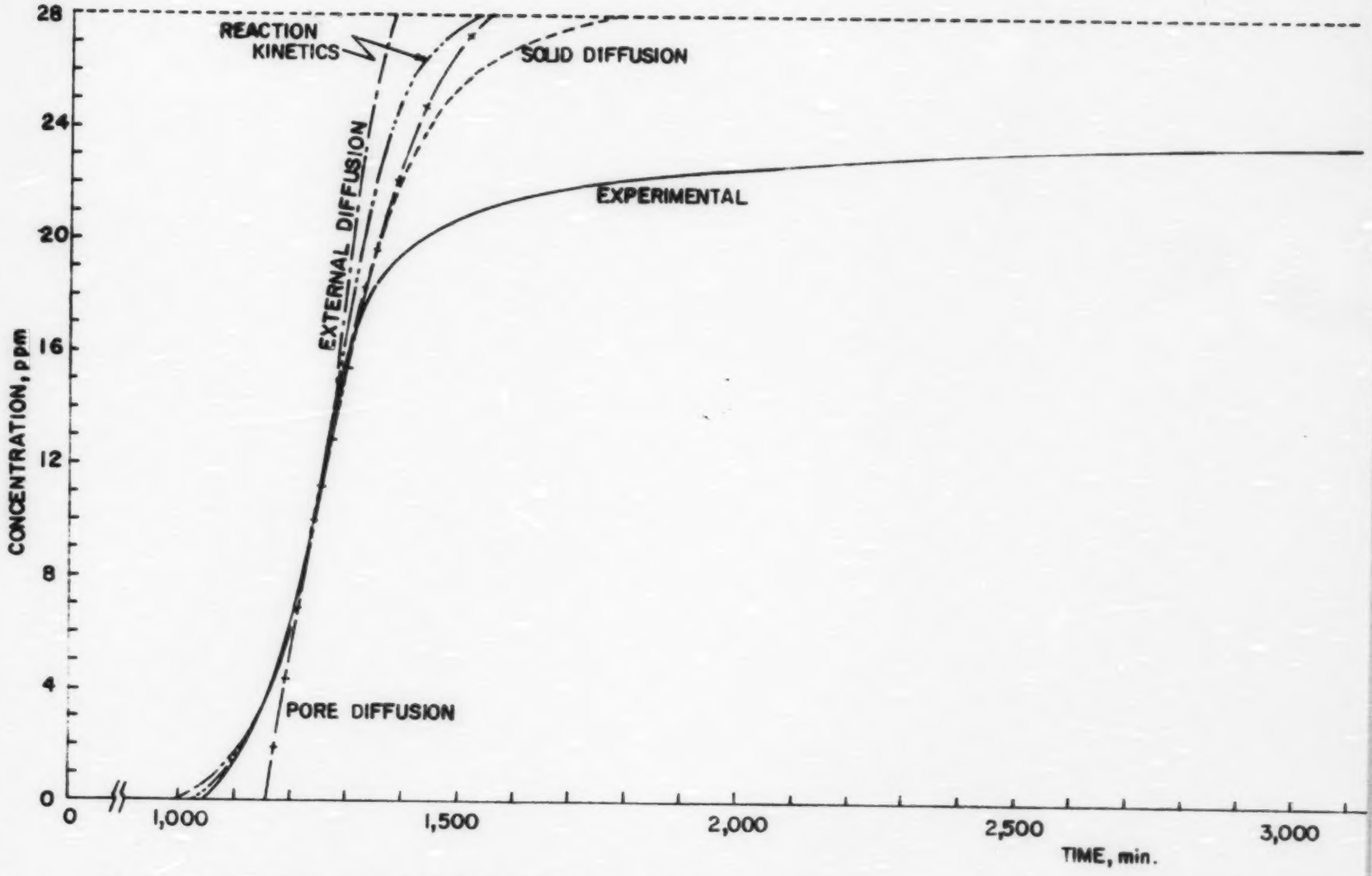

FIG.(A-8). APC-29, FIXED-BED TEST WITH 14 MESH CHARCOAL, 45.72 cm DEEP BED AND 32.5 cc/sec FLOW RATE COMPARED WITH MODEL BREAKTHROUGH CURVES

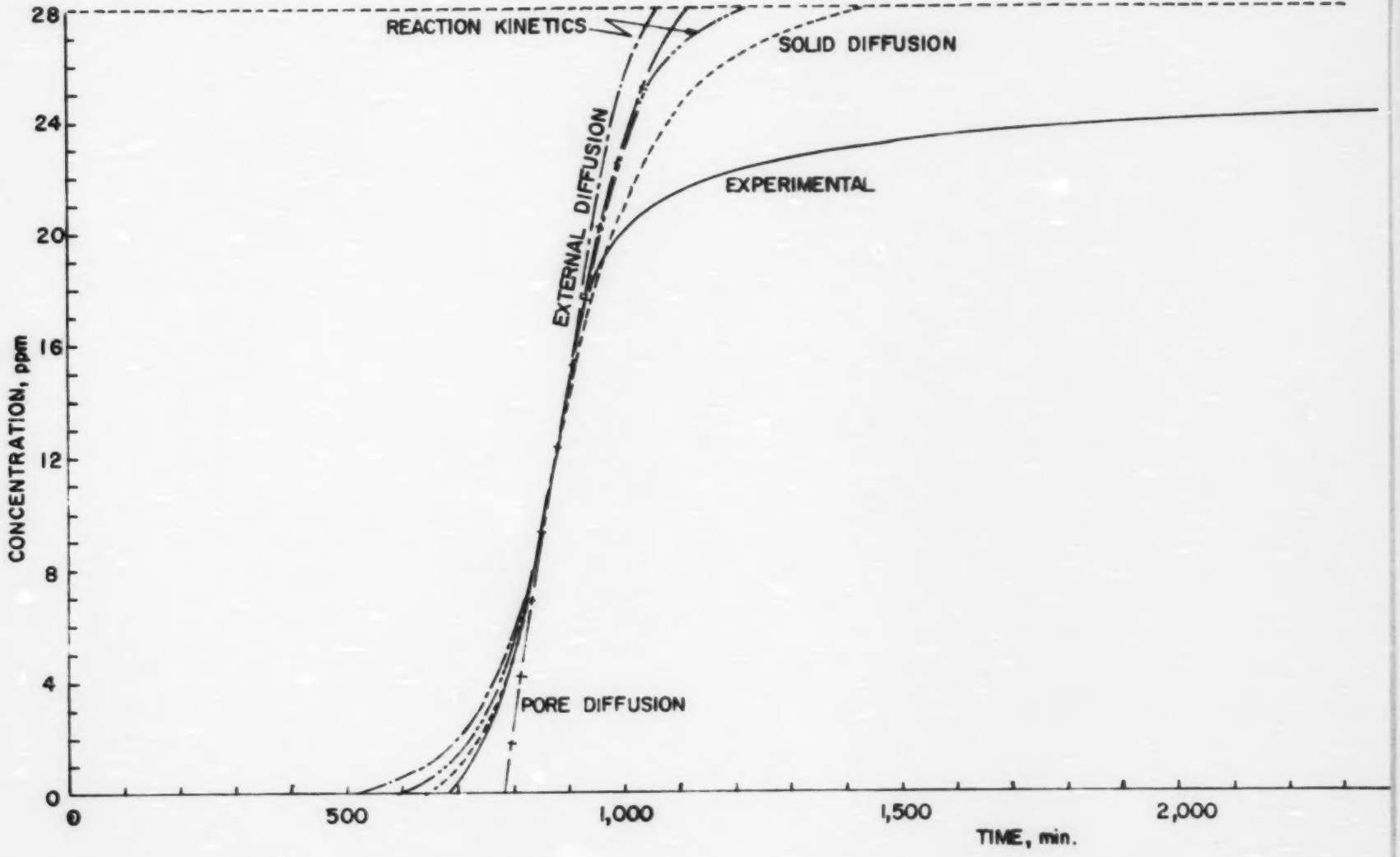

FIG.(A-9). APC-30, FIXED-BED TEST WITH 14 MESH CHARCOAL, 42.72 cm DEEP BED, AND 49.5 $^{cc}/_{sec}$ FLOW RATE COMPARED WITH MODEL BREAKTHROUGH CURVES

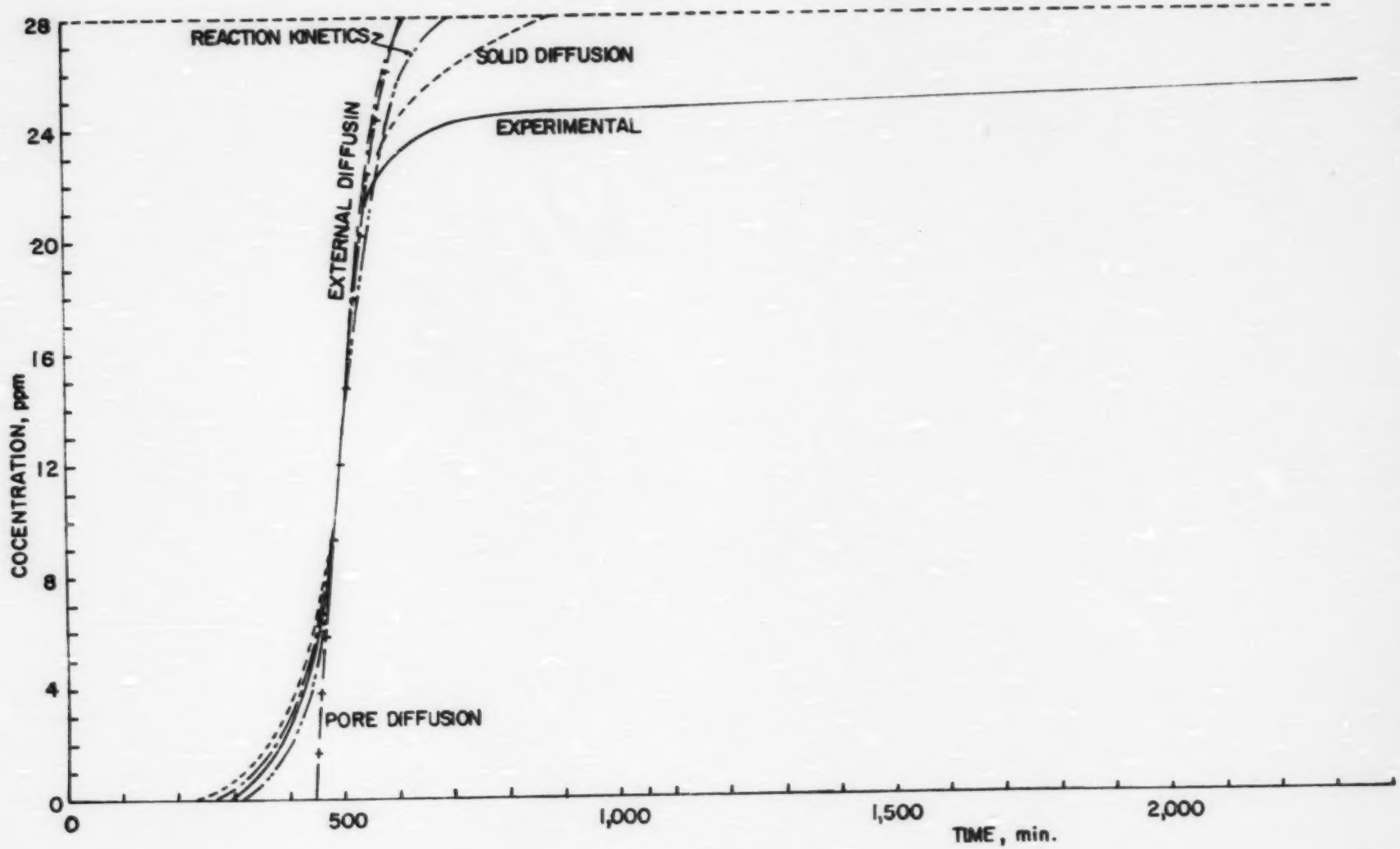

FIG.(A-10). APC-31, FIXED-BED TEST WITH 14 MESH CHARCOAL, 45.72 cm DEEP BED AND 69.22 $^{cc}/_{sec}$ FLOW RATE COMPARED WITH MODEL BREAKTHROUGH CURVES

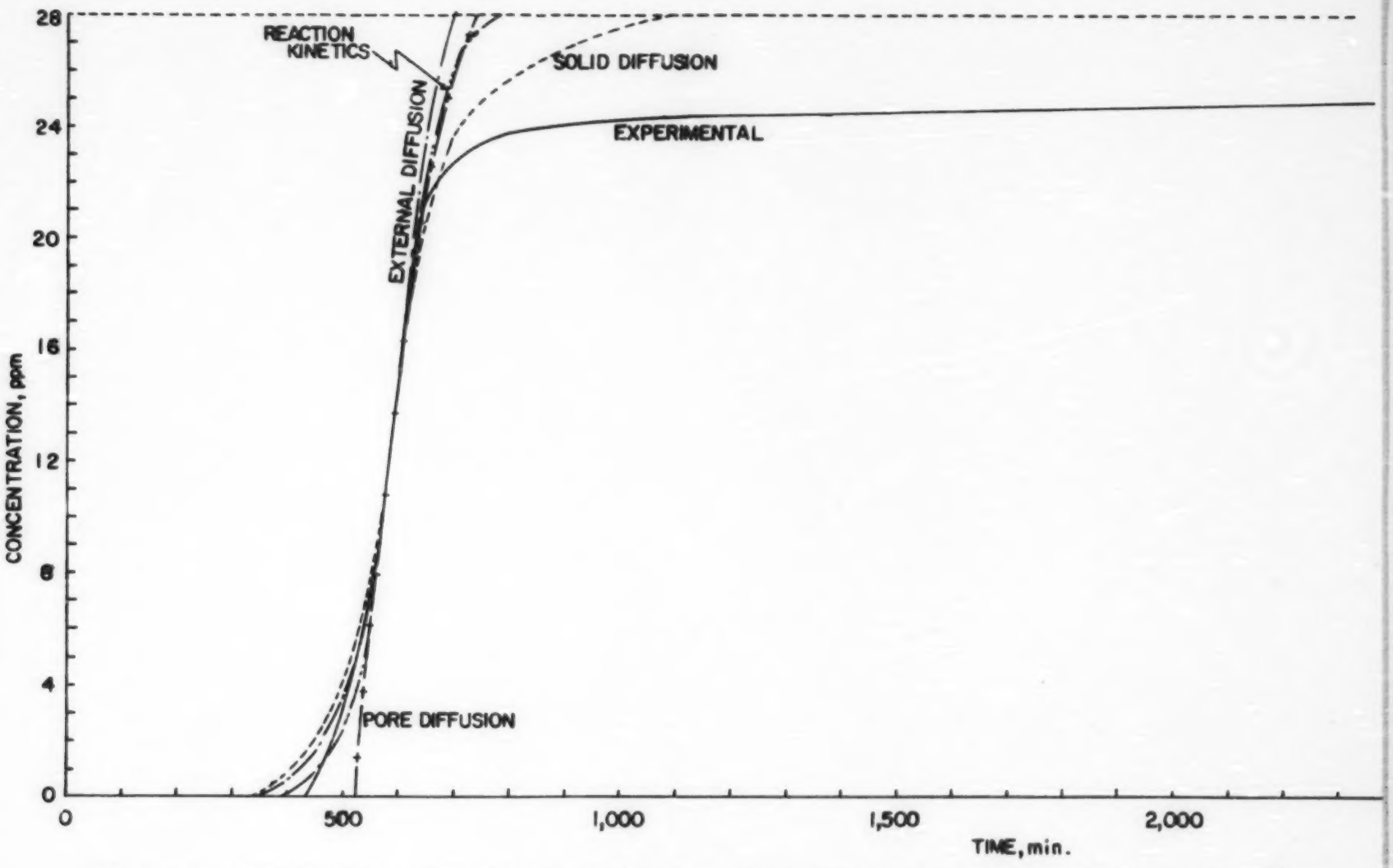

FIG. (A-11). APC-32, FIXED-BED TEST WITH 14 MESH CHARCOAL, 45.72 cm DEEP BED AND 59.4 $\frac{cc}{sec}$ FLOW RATE COMPARED WITH MODEL BREAKTHROUGH CURVES

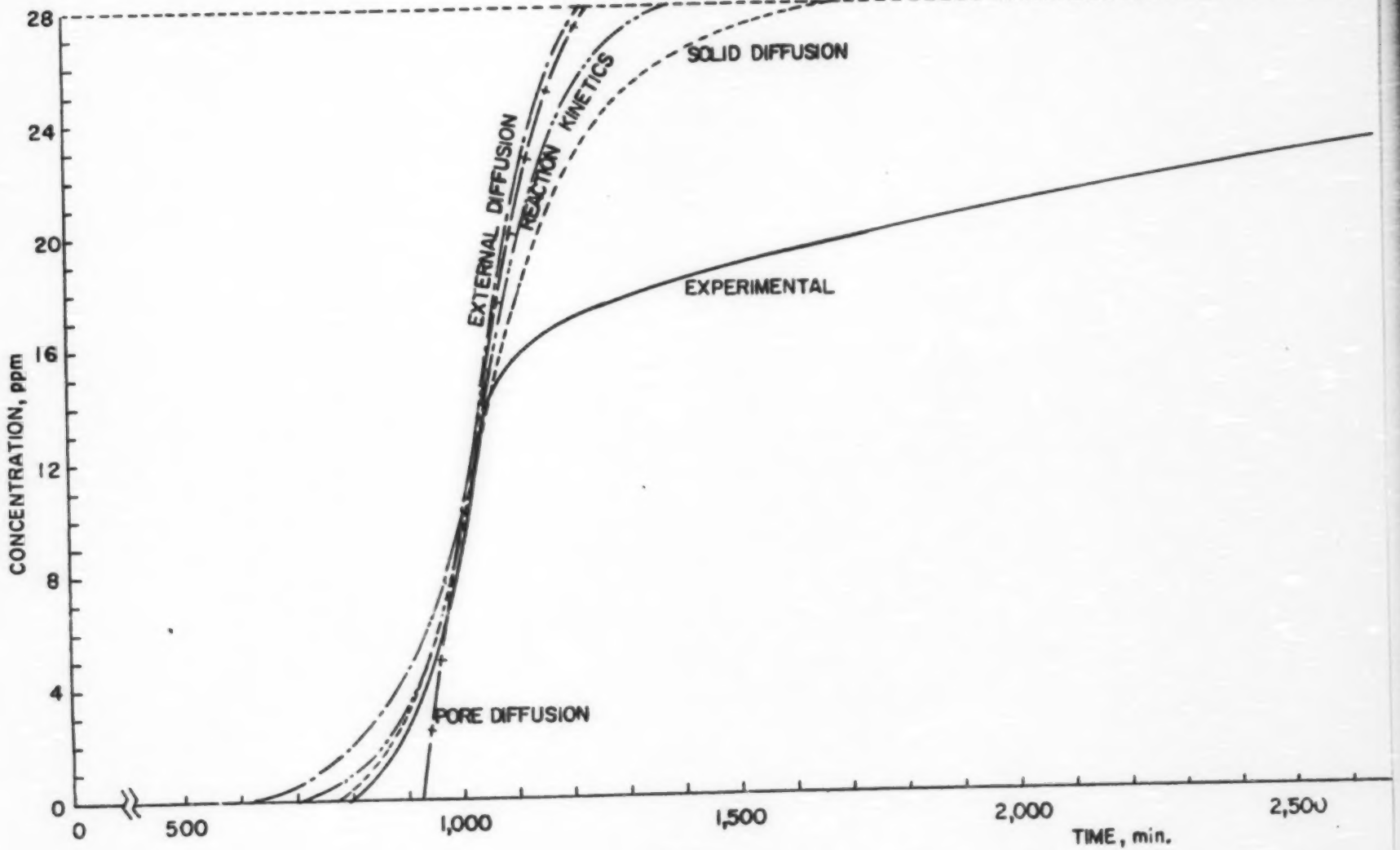

FIG. (A-12). APC-38, FIXED-BED TEST WITH 10 MESH CHARCOAL, 45.72 cm DEEP BED AND 79.35 cc/sec FLOW RATE COMPARED WITH MODEL BREAKTHROUGH CURVES

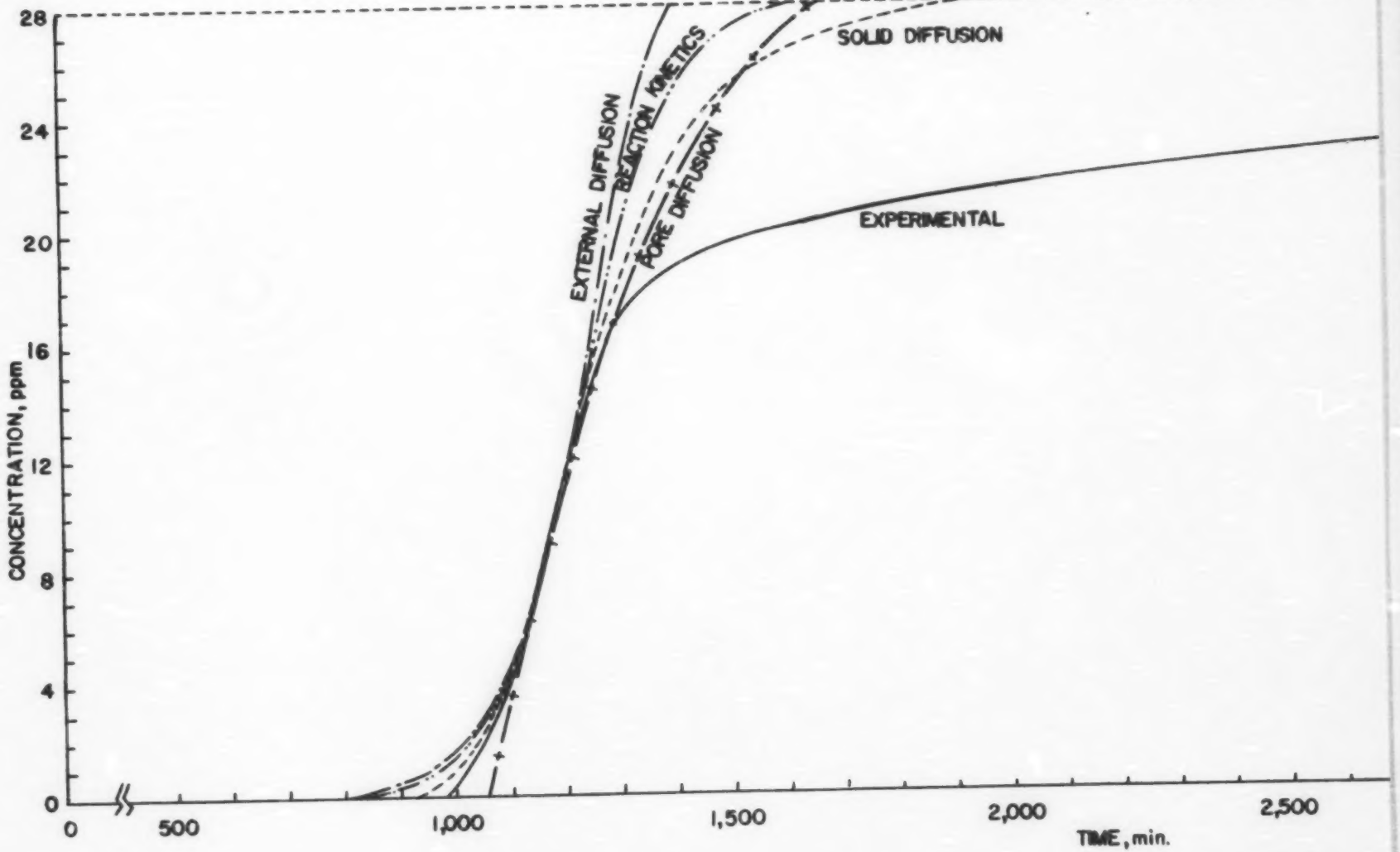

FIG.(A-13). APC-39, FIXED-BED TEST WITH 12 MESH CHARCOAL, 45.72 cm DEEP BED, AND 45.83 cc/sec FLOW RATE COMPARED WITH MODEL BREAKTHROUGH CURVES

FIG. (A-14) GAS CHROMATOGRAPH CALIBRATION CURVE.

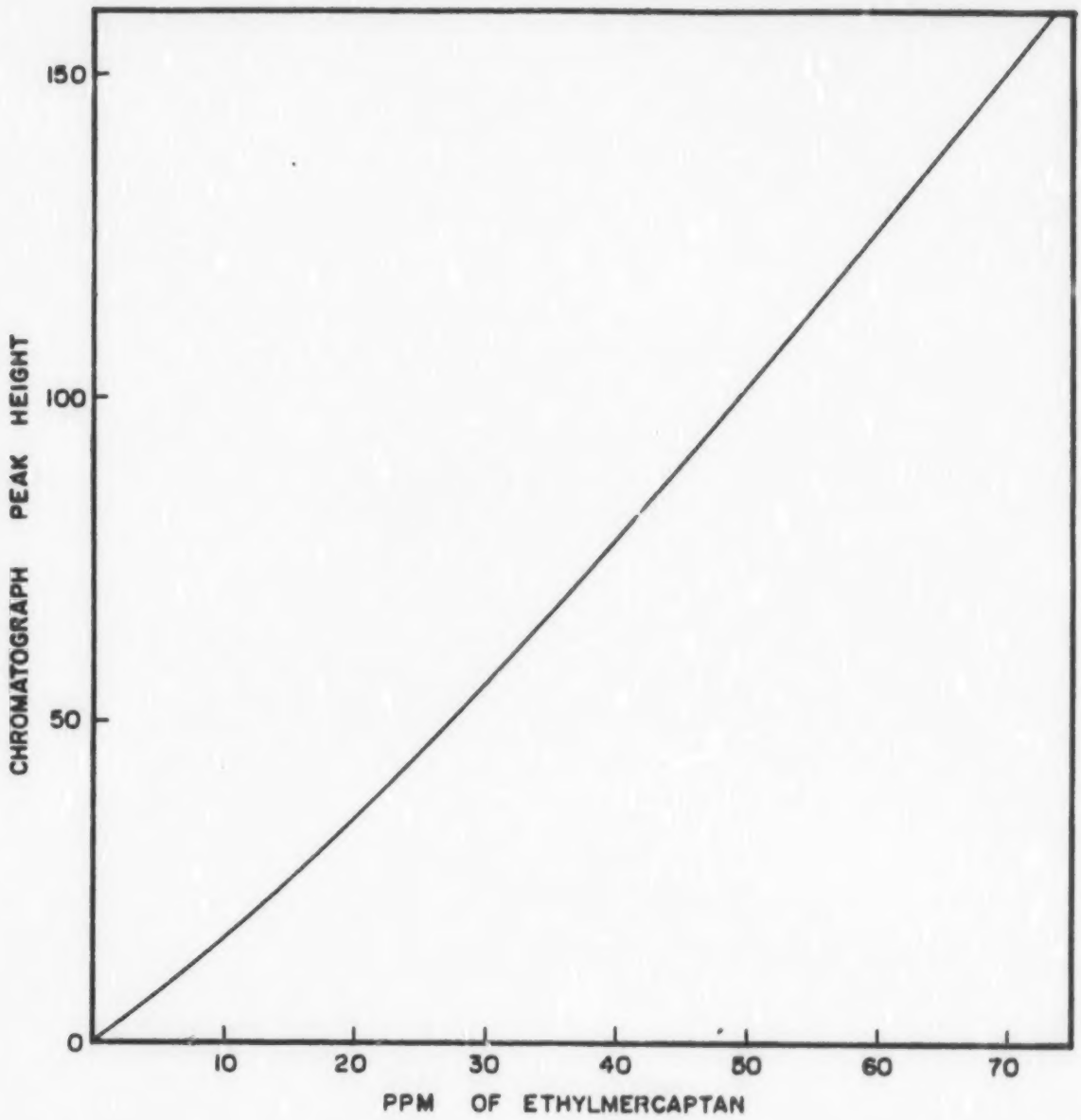

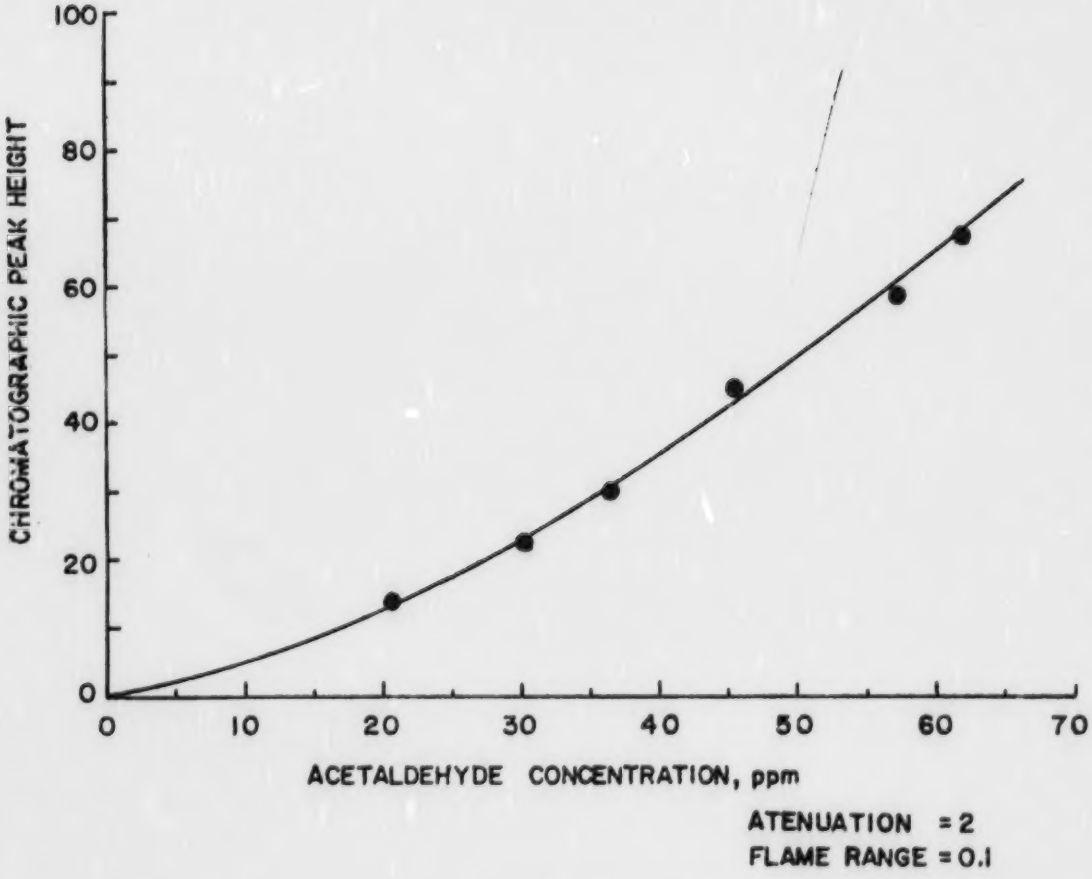

FIG.(A-15). CHROMATOGRAPHIC CALIBRATION CURVE
ACETALDEHYDE